AD-A059 720 BATTELLE COLUMBUS LABS OHIO F/G 11/6
METAL PHYSICS AND TITANIUM-ALUMINUM ALLOYS.(U)
FEB 78 E W COLLINGS AFOSR-75-2786

UNCLASSIFIED AFOSR-TR-78-1240 NL

| OF 2
AD A059720

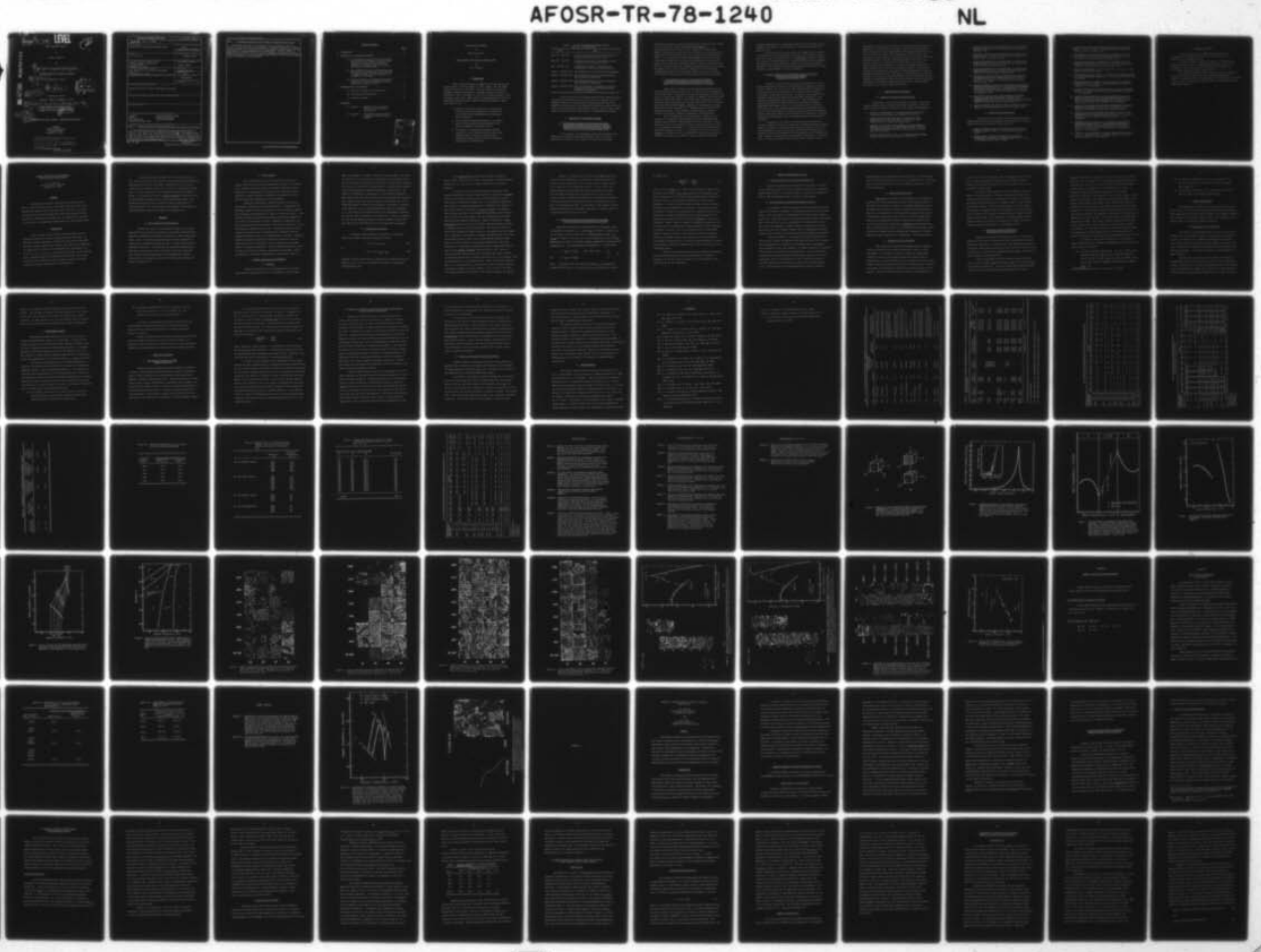


F
9720

(18) AFOSR-TR- (19) 78-1240

LEVEL

(2)

FINAL SCIENTIFIC REPORT

on

Projects Relating

to

(6) METAL PHYSICS AND TITANIUM-ALUMINUM ALLOYS

AIR FORCE OFFICE OF SCIENTIFIC RESEARCH

(11) 24 Feb 78 February 24, 1978

by

(10) E. W. Collings

(12) 116p.

covering the period

January 1, 1975 to December 31, 1977

(9) Final rept. 1 Jan 75-31 Dec 77,

This research was supported by the
Air Force Office of Scientific Research
(AFSC) under Grant No. AFOSR-75-2786

(15)

(16) 2306

(17) A1

"APPROVED FOR PUBLIC RELEASE. DISTRIBUTION UNLIMITED"

BATTELLE
Columbus Laboratories
505 King Avenue
Columbus, OH 43201

407 080

UNCLASSIFIED
SECURITY CLASSIFICATION OF THIS PAGE (When Data Entered)

REPORT DOCUMENTATION PAGE

READ INSTRUCTIONS BEFORE COMPLETING FORM

1. REPORT NUMBER: AFOSR-TR- 78-1240	2. GOVT ACCESSION NO.
3. RECIPIENT'S CATALOG NUMBER	
4. TITLE (and Subtitle): METAL PHYSICS AND TITANIUM-ALUMINUM ALLOYS	5. TYPE OF REPORT & PERIOD COVERED: FINAL 1 Jan 75 to 31 Dec 77
	6. PERFORMING ORG. REPORT NUMBER
7. AUTHOR(s): E. W. Collings	8. CONTRACT OR GRANT NUMBER(s): AFOSR-75-2786
9. PERFORMING ORGANIZATION NAME AND ADDRESS: Battelle Columbus Laboratories, 505 King Avenue, Columbus, OH 43201	10. PROGRAM ELEMENT, PROJECT, TASK AREA & WORK UNIT NUMBERS: 61102F, 2306/A1
11. CONTROLLING OFFICE NAME AND ADDRESS: Air Force Office of Scientific Research/NE, Bldg. 410, Bolling AFB, DC 20332	12. REPORT DATE: February 24, 1978
	13. NUMBER OF PAGES: 116
14. MONITORING AGENCY NAME & ADDRESS (if different from Controlling Office)	15. SECURITY CLASS. (of this report): UNCLASSIFIED
	15a. DECLASSIFICATION/DOWNGRADING SCHEDULE

16. DISTRIBUTION STATEMENT (of this Report)

Approved for public release; distribution unlimited.

17. DISTRIBUTION STATEMENT (of the abstract entered in Block 20, if different from Report)

18. SUPPLEMENTARY NOTES

19. KEY WORDS (Continue on reverse side if necessary and identify by block number)

titanium
aluminum
phase equilibria
titanium-aluminum alloys
iron-nickel-chrome alloys
magnetic properties
structural stability

20. ABSTRACT (Continue on reverse side if necessary and identify by block number)

Paper 1 -- Magnetic Studies of Phase Equilibria in Ti-Al (30-57) at .%) Alloys

Room temperature magnetic susceptibility studies have been made on a series of Ti-Al alloys in the composition range 30-57 at .%Al, quenched from anneals at 900, 1065, 1165, 1215, 1265, 1315, and 1365°C. As a result of this work, an equilibrium partial phase diagram has been constructed, compared with literature data, and discussed with reference to the results of a comprehensive metallographic and microhardness study. (continued on back)

DD FORM 1 JAN 73 1473

UNCLASSIFIED
SECURITY CLASSIFICATION OF THIS PAGE (When Data Entered)

Paper 2 -- Austenitic Stainless Steels as Magnetic Transition Metal Alloys

The magnetic properties of stainless steels are considered within the context of transition metal alloy magnetism. The magnetic properties of binary transition metals are reviewed with particular emphasis on spin glasses and their relationship to superparamagnetism and micromagnetism. Physical property measurements on specific Fe-Cr-Ni alloys are discussed and related to phenomenological treatments and low temperature microstructures of both Fe-Cr-Ni research alloys and commercial stainless steels.

TABLE OF CONTENTS

FINAL SCIENTIFIC REPORT

on

Projects Relating

to

METAL PHYSICS AND TITANIUM-ALUMINUM ALLOYS

by

E. W. Collings

1. INTRODUCTION

This is the Final Report on AFOSR Grant 75-2786 covering the period January 1, 1975 to December 31, 1977. Support from the AFOSR commenced in May 1971, and Table 1 lists the titles of the research programs completed since that date. Research carried out during the period May 1, 1971 to December 31, 1974, was a natural precursor to that discussed in this report, which deals with various aspects of the interrelationship between physical property studies and problems of metallogical interest, viz:

- studies of the physical properties of Ti-Al alloys in the vicinity of the intermetallic compound TiAl with a view towards understanding the brittleness of that compound,
- use of physical property measurements in an investigation of the equilibrium phase diagram of Ti-Al over the composition range 30-57 at.% Al,
- an extension of the physical/mechanical property concept into a new technically useful alloy system, stainless steel, in order to study the interrelationship between bcc/fcc stability and magnetic properties at low temperatures.

TABLE 1. LIST OF AFOSR-SUPPORTED RESEARCH TOPICS
MAY 1971 to DECEMBER 1977

Period	Topic
May 1971 - May 1972	Electronic Effects due to Microinhomogeneities in Metastable Solid Solution Alloys
May 1972 - May 1973	Electronic Effects due to Microinhomogeneities in Metastable Solid Solution Alloys
May - December 1973	A Fundamental Approach to Solid-Solution Strengthening in Dilute hcp Titanium Alloys
January - December 1974	The Fundamentals of Solid Solution Strengthening
January - December 1975	The Fundamental Design of Titanium-Aluminide-Base Intermetallic Compounds
January - December 1976	The Fundamental Design of Titanium-Aluminide-Base Intermetallic Compounds
January - December 1977	Physical Metallurgy and Fundamental Design of Titanium Alloys and Titanium-Aluminide-Base Intermetallic Compounds

In the next section the essential results of the research carried out during the period of this report, 1975-1977, are outlined. And in a subsequent section we list publications, manuscripts, and talks which appeared, were prepared, and were presented, respectively, during 1975-1977. As for the content of these communications, there is naturally some overlap between the earlier and the later phases of the OSR-sponsored programs.

2. DISCUSSION OF THE RESEARCH PROGRAMS

2.1 The Fundamental Design of Titanium-Aluminide-Base Intermetallic Compounds, Phase I (1975) -- Magnetic Investigations of Electronic Bonding and γ through γ Phase Equilibria in the Titanium-Aluminum System

In this program, the conclusions of which were reported at the meetings of the Aluminide Development Committee, and at the Third International Conference on the Science and Technology of Titanium,

the results of physical property measurements and calculations were applied to the Ti-Al system in order, to acquire understanding of the room-temperature brittleness of the intermetallic compound TiAl. Magnetic susceptibility measurements were carried out on a series of Ti-Al alloys which had been quenched from various temperatures between 900 and 1265°C. The susceptibility-composition dependence over the entire composition range, coupled with the composition dependence of the electronic specific heat coefficient, yielded an electronic density of states picture for Ti-Al alloys and the three intermetallic compounds Ti_3Al, TiAl and $TiAl_3$. An heuristic model for the electronic structures of Ti-Al alloys and compounds was proposed; and interatomic bonding in the three compounds, as it relates to some of their mechanical characteristics, was considered.

2.2 The Fundamental Design of Titanium-Aluminide-Base Intermetallic Compounds, Phase II (1976) -- Magnetic Studies of Phase Equilibria in Ti-Al(30-57 at.%) Alloys

During 1975, it became clear that uncertainties existed in the equilibrium phase diagram, particularly in connection with the boundaries of the single-phase γ regime which contains the intermetallic compound TiAl. Ti-Al is a system which has been the subject of numerous reports since 1951. The early period (1951-1960), in which some twelve publications appeared, saw rather complete compositional coverage; while much of the recent work dealt with partial phase diagrams, focussing on the Ti-rich end, the α_2-phase field, and the compound Ti_3Al. Techniques used were optical and electron microscopy, x-ray diffraction, thermal analysis, hardness, electrical resistivity, magnetic susceptibility, and dilatometry.

Our 1976 investigation was stimulated by a dispute over the location of the $(\alpha_2+\gamma)/\gamma$ - phase boundary, which had previously been defined using qualitative metallography and electron microscopy. Equilibration is not a trivial problem, and with reactive alloys such as Ti-Al it is particularly troublesome. If a true (as distinct from practical) equilibrium diagram is sought, it is necessary to be able to follow an approach to equilibrium, and to use quantitative methods that are able to distinguish between a true two-phase situation and that representing

incomplete equilibrium in a single-phase field. For this and other reasons magnetic susceptibility, a bulk quantitative procedure, was adopted as a diagnostic tool.

The magnetic phase diagram studies were augmented by the results of comprehensive optical metallographical survey, and by hardness measurements on a matrix of quenched alloys. The equilibrium transition obtained as a result of this work enabled us to identify several points of agreement and disagreement with, respectively, several of the important published diagrams. A full description of the phase equilibrium investigation, which has not yet been published, is given in Appendix 1.

2.3 Physical Metallurgy and Fundamental Design of Titanium Alloys and Titanium-Aluminide-Base Intermetallic Compounds (1977)

During the initial portion of the year the emphasis lay on the Ti-Al system and the resolution of some difficulties remaining at the end of 1976. However, the spirit of the 1977 program consisted of dealing in a more general way with the manner in which physics could be applied to the solution of metallurgical problems. As stated in the proposal it was intended to discuss such problems as strengthening, deformation, order-disorder transformations, phase stability, etc. After searching for further alloy systems of current interest and technical importance we identified Fe-Ni-Cr-base alloys (i.e., stainless steels) as systems in which there was a close interplay between electronic and magnetic properties and structural stability. Moreover they were systems which warranted further investigation because of their importance as components in emerging energy-related technologies such as plasma-fusion and new applications of cryogenics.

Traditionally the design of stainless steel alloys has been motivated primarily by chemical, mechanical, and thermal stability considerations, in response to the traditionally important properties of (a) corrosion resistance, (b) modulus, strength, and properties associated with mechanical failure, (c) weldability and the properties of the heat-affected zone. However, for many present-day applications the behavior of stainless steel in unusual environments, such as high neutron fluences, very low

temperatures, and high magnetic fields, is becoming increasingly important. Accordingly it is necessary to learn what "secondary" properties accrue from the chemically- and mechanically-motivated compositional modifications of the Fe-Ni-Cr basic alloy. What advantages or disadvantages do they possess from other standpoints? What relationships exist between structural and magnetic states? The 1977 investigation focused attention on the magnetic properties of stainless steel alloys within the context of transition-metal-alloy magnetism. A review of the magnetic properties of binary transition metal alloys, with particular emphasis on spin glasses, followed by a discussion of some physical property measurements on specific Fe-Cr-Ni alloys, was prepared. The review, a copy of which is attached as Appendix 2, also contains a phenomenological treatment of magnetic transformations in a comprehensive matrix of Fe-Cr-Ni research alloys and commercial stainless steels concludes with suggestions for future research aimed at determining their essential magnetic structures.

3. COMMUNICATION OF THE RESULTS

3.1 Seminars, Colloquia, and Presentations

Listed below are the various seminars, colloquia, and research reports presented during the Grant period 1975 through 1977. They were based on research carried out during the entire period of AFOSR support.

1. PHYSICS OF STRENGTHENING IN TITANIUM-ALUMINIDE-TYPE ALLOYS, Aerospace Research Laboratories, WPAFB, OH, June 1975.

2. SOLUTE-INDUCED LATTICE STABILITY AS IT RELATES TO SUPER-CONDUCTIVITY IN TI-MO-BASED ALLOYS, March Meeting, APS (Poster Session), Atlanta, GA, March, 1976.

3. MAGNETIC SUSCEPTIBILITY, METALLOGRAPHY, AND MICROHARDNESS OF QUENCHED Ti-Al ALLOYS, AND A NEW DETERMINATION OF A PORTION OF THE EQUILIBRIUM PHASE DIAGRAM, Wright-Patterson Air Force Base, OH, April 1977.

4. MAGNETIC INVESTIGATION OF THE Ti-Al EQUILIBRIUM PHASE DIAGRAM, Wright-Patterson Air Force Base, OH, August 1976.

5. TRANSITION TEMPERATURE AND MICROSTRUCTURE IN TITANIUM ALLOY SUPERCONDUCTORS, Seminar, Metal Science Section, Battelle, September, 1976.

6. TRANSITION TEMPERATURE AND MICROSTRUCTURE IN TITANIUM ALLOY SUPERCONDUCTORS, TMS-AIME Symposium on Superconductivity, Niagara Falls, NY, September, 1976.

7. TRANSITION TEMPERATURE AND MICROSTRUCTURE IN TITANIUM ALLOY SUPERCONDUCTORS, Seminar, Battelle-Geneva Research Center, Geneva, Switzerland, November, 1976.

8. TRANSITION TEMPERATURE AND MICROSTRUCTURE IN TITANIUM ALLOY SUPERCONDUCTORS, Seminar, Lehrstuhl Werkstoffwissenschaft (Metalle), Erlangen, Germany, December, 1976.

9. DEFORMATION- AND SOLUTE-INDUCED MICROSTRUCTURAL EFFECTS IN THE SUPERCONDUCTIVITY OF TITANIUM ALLOYS, International Conference on the Physics of Transition Metals, Toronto, Canada, August, 1977.

10. ANOMALOUS ELECTRICAL RESISTIVITY AND MAGNETIC SUSCEPTIBILITY TEMPERATURE DEPENDENCES IN Ti-V ALLOYS EXHIBITING REVERSIBLE SOFT-PHONON-INDUCED STRUCTURAL INHOMOGENEITIES, Conference on Electrical Transport and Optical Properties of Columbus, OH, September, 1977.

11. INFLUENCE OF METALLURGICAL MICROSTRUCTURE ON THE SUPER-CONDUCTING TRANSITION TEMPERATURE IN TITANIUM ALLOY SUPERCONDUCTORS, Symposium on Superconductivity and Metallurgy, TMS/AIME Fall Meeting, Chicago, IL, October, 1977.

12. MAGNETIC PROPERTIES OF STAINLESS STEELS, NBS-ERDA Workshop on Materials at Low Temperatures, Vail, CO., October, 1977.

3.2 Publications and Manuscripts

Listed below are the publications and manuscripts based on AFOSR-sponsored research which appeared, or were submitted for publication, during the Grant period 1975 through 1977.

1. MAGNETIC STUDIES OF OMEGA-PHASE PRECIPITATION AND AGING IN TITANIUM VANADIUM ALLOYS", J. Less-Common Metals, 39, 63 (1975).

2. SUPERCONDUCTING TRANSITION TEMPERATURE IN MARTENSITIC TITANIUM-BASE TRANSITION METAL BINARY ALLOYS, with J. C. Ho; J. Less-Common Metals, 41, 157 (1975).

3. PHYSICAL PRINCIPALS OF SOLID-SOLUTION STRENGTHENING IN ALLOYS, With H. L. Gegel, in "Physics of Solid Solution Strengthening", Plenum Press, N.Y. (1975), p. 147.

4. LOW-TEMPERATURE CALORIMETRIC STUDIES OF SUPERCONDUCTIVITY AND MICROSTRUCTURE IN TITANIUM-VANADIUM ALLOYS, with J. C. Ho and P. E. Upton; J. Less-Common Metals, 42, 285 (1975).

5. CALORIMETRIC STUDIES OF SUPERCONDUCTIVITY PROXIMITY EFFECT IN TITANIUM-VANADIUM ALLOYS, with J. C. Ho; Proc. 14th International Conference on Low Temperature Physics (LT-14), 1975.

6. MAGNETIC SUSCEPTIBILITY OF Ti-Nb ALLOYS with R. D. Smith; J. Less-Common Metals, 48, 187 (1976).

7. SOLUTE-INDUCED LATTICE STABILITY AS IT RELATES TO SUPERCONDUCTIVITY IN TITANIUM-MOLYBDENUM ALLOYS with J. C. Ho; Solid State Comm., 18, 1493 (1976).

8. MAGNETCOCRYSTALLINE ANISOTROPY IN MONOCRYSTALLINE AND TEXTURED POLYCRYSTALLINE Ti-Al ALLOYS, Third International Conference on Titanium -- to be published.

9. MAGNETIC INVESTIGATION OF ELECTRONIC BONDING AND PHASE EQUILIBRIA IN THE Ti-Al SYSTEM, Third International Conference on Titanium -- to be published.

10. RESPONSE OF SUPERCONDUCTING TRANSITION TEMPERATURE AND OTHER PHYSICAL PROPERTIES TO PHASE TRANSFORMATION, PRECIPITATION AND AGING IN TITANIUM-BASE TRANSITION-METAL-BINARY ALLOYS, Third International Conference on Titanium -- to be published.

11. ANALYSIS OF CALORIMETRICALLY-OBSERVED SUPERCONDUCTING TRANSITION TEMPERATURE ENHANCEMENT IN Ti-Mo (5 at.%)-BASED ALLOYS, in Magnetism and Magnetic Materials--1976, AIP. 1976, p. 75.

12. DEFORMATION-AND SOULUTE-INDUCED MICROSTRUCTURAL EFFECTS IN THE SUPERCONDUCTIVITY OF TRANSITION-METAL ALLOYS, with J. J. White, International Conf. Physics of Transition Metals -- to be published.

13. ANOMALOUS ELECTRICAL RESISTIVITY AND MAGNETIC SUSCEPTIBILITY TEMPERATURE DEPENDECES IN Ti-V ALLOYS EXHIBITING REVERSIBLE SOFT-PHONON-INDUCED STRUCTURAL INHOMOGENEITIES, Conference on Electrical Transport and Optical Properties of Inhomogeneous Media" -- to be published.

14. AUSTENITIC STAINLESS STEELS AS MAGNETIC TRANSITION METAL ALLOYS, with H. W. King, Symposium on the Metal Physics of Stainless Steels Proceedings -- to be published.

3.3 Symposia and Books

Research conducted under AFOSR support stimulated the organization of two symposia held and to be held, respectively, in conjunction with TMS(AIME) meetings.

The first of these, entitled "The Physics of Solid Solution Strengthening", was held as an ASM-TMS(AIME) Symposium in Chicago, IL on October 2, 1973. The proceedings, edited by E. W. Collings and H. L. Gegel, published by Plenum Press in 1975.

The second symposium, entitled "The Metal Physics of Stainless Steels" will be held in conjunction with the AIME Annual Meeting in Denver, CO on March 2, 1978. The proceedings, to be edited by E. W. Collings and H. L. King, is scheduled to appear in 1978 as a book published by the Metallurgical Society.

4. APPENDIXES

4.1 Appendix 1 -- "Magnetic Studies of Phase Equilibria in Ti-Al(3057 at.%) Alloys" -- attached.

4.2 Appendix 2 -- "Austenitic Stainless Steels as Magnetic Transition Metal Alloys" -- attached.

APPENDIX 1

MAGNETIC STUDIES OF PHASE EQUILIBRIA IN Ti-Al (30-57) at.% ALLOYS

E. W. Collings
Battelle Memorial Institute
Columbus, OH 43201

ABSTRACT

Room temperature magnetic susceptibility studies have been made on a series of Ti-Al alloys in the composition range 30-57 at.% Al, quenched from anneals at 900, 1065, 1165, 1215, 1265, 1315, and 1365°C. As a result of this work an equilibrium partial phase diagram has been constructed, compared with literature data, and discussed with reference to the results of a comprehensive metallographic and microhardness study.

1. INTRODUCTION

This certainly is not the first study of phases in Ti-Al, a system which has been the subject of numerous reports since 1961. As indicated in Table I (References [1]-[12]) the early period (1951-1960) saw rather complete compositional coverage, while much of the recent work, for example that of Crossley [10] and Blackburn [11,12] focused on the Ti-rich end, i.e., the α_2 (i.e., Ti_3Al-base) phase field, and the compound Ti_3Al. Techniques used in the previous work were optical and electron microscopy, X-ray diffraction, thermal analysis, hardness, electrical resistivity, magnetic susceptibility, and dilatometry.

The present study was stimulated by a recent dispute over the $(\alpha_2 + \gamma)/\gamma$ phase boundary, whose position had been located using qualitative metallography and electron microscopy. Equilibration is not a trivial problem, and with reactive alloys such as Ti-Al it is particularly troublesome. If a true (as distinct from a "practical") equilibrium diagram is sought, it is necessary to be able to trace an approach to equilibrium, and to use quantitative methods that are able to distinguish between a true two-phase situation and that representing incomplete equilibrium in a single-phase field. For this and other reasons magnetic susceptibility, a bulk quantitative procedure, was adopted as a diagnostic tool.

2. MATERIALS

2.1 Alloy Preparation and Composition

Sixteen Ti-Al alloys in the composition range 30 to 57 at.%Al (henceforth HP-30 to HP-57) were prepared as 40g buttons from high-purity ingredients (Appendix A) by multiple arc melting on a water-cooled copper hearth. Since in determining phase boundaries accurate compositional information is required the samples were sent to several laboratories for independent evaluation. On most alloys four composition determinations were made and the results of this work, shown in Table II, which also lists average accepted compositions and corresponding molar weights, indicates that the average uncertainty in Al concentration (average std. error) is $\pm$ 0.46 at.% Al.

2.2 Heat Treatment

Since Ti-base alloys are very susceptible to oxidation at elevated temperatures, extended high-temperature solution heat treatment is not feasible, and only the shortest reasonable annealing times are permissible. By examining alloy properties after successively longer exposures to a given temperature, approaches to equilibrium could be followed and minimal equilibration times established.

During this investigation extreme precautions were taken to avoid sample contamination by oxygen and nitrogen. In preparation for annealing, samples of Ti-Al were wrapped in Ta foil and placed, together with Ta-wrapped getter-packages of Ti chips, in small quartz tubes. After sealing off under argon (the filling pressure of which was adjusted so as to yield a final pressure of about 1 atmosphere at temperature) the getter packages were activated either by the torch or inductively in order to scavenge any remaining traces of air. Excess Ti was able to provide continuous gettering during the subsequent heat treatments which were abruptly terminated in each case by quenching into iced brine. Annealing schedules were guided initially by the work of Crossley [10] and the experiences of other investigators; furnace temperatures were checked against a calibrated thermocouple. The heat treatment-composition matrix for material intended for magnetic susceptibility measurement, optical metallography, and hardness determination, is presented in Table III.

3. MAGNETIC SUSCEPTIBILITY MEASUREMENT

3.1 Technique

Magnetic susceptibility (χ) was determined by the so-called Curie method by measuring the force $f = m\chi H(\partial M/\partial Z)$ on a small sample

(mass, m) suspended in a magnetic field (H) of gradient $\partial H/\partial Z$. The field, of controlled vertical gradient, was generated by an electromagnet fitted with 7-inch diameter "constant-force" pole caps. The system was calibrated with the aid of a small piece of high-purity Pt, a material whose susceptibility and susceptibility temperature dependence are well known. The presence of ferromagnetic contamination, to which metallic samples are particularly prone, may lead to serious errors in susceptibility determination. However, these can easily be detected, and corrected for, by the "Honda-Owen method" in which the susceptibility of the matrix is obtained as the intercept, χ_∞, in a reciprocal-field plot based on the equation $\chi = \chi_\infty + M/H$ where M is the magnetization of the ferromagnetic component. M, of course, must be constant for all values of H -- thus, as is generally the case, the ferromagnetic component must be saturable in fields lower than those (3.75 to 10.02 kOe) used in the susceptibility measurement.

3.2 Paramagnetic Anisotropy

The magnetic susceptibility of a crystal is a second-rank tensor whose average value may be expressed as either

$$3\langle\chi\rangle = \chi_1 + \chi_2 + \chi_3 \qquad 1(a)$$

or

$$3\langle\chi\rangle = \chi_{11} + \chi_{\perp_1} + \chi_{\perp_2} \qquad 1(b)$$

depending on whether the crystal is orientated in an arbitrary direction (Equation 1(a)), or with its principal axis parallel to the magnetic field (Equation 1(b)).

For a polycrystalline sample Equation (1(a)) is appropriate; and for "ideal" polycrystalline material (large number of randomly oriented grains) $\langle\chi\rangle = \chi_1 = \chi_2 = \chi_3$, and a single susceptibility measurement suffices.

In order to test for magnetic isotropy in the present Ti-Al samples susceptibilities were initially measured in each of three coplanar directions, by simply rotating the axis of the electromagnet into the three directions indicated in Figure 1(a). If no appreciable differences were detected, an average susceptibility was calculated and a "measure of anisotropy", given by the average of $|\chi_B - \chi_A|$ and $|\chi_B - \chi_C|$, was assigned. This procedure was found to be satisfactory when applied to HP-30 through HP-49. It was soon noted, however, that the susceptibilities of alloys beyond HP-49 were markedly anisotropic. Magnetic anisotropy in a polycrystalline material occurs when an inherent magnetocrystalline anisotropy is combined with some form of texturization. The latter is usually the result of an insufficient number of grains in the sample under investigation (i.e., large grain size compared to specimen dimensions) rather than a true polycrystalline texture such as that obtained through mechanical deformation. In order to obtain a valid average susceptibility under such conditions, it is necessary to average the results of measurements made in each of three mutually orthogonal directions--Figure 1(b). This is a laborious process requiring great care in detaching the sample, rotating it exactly 90 degrees about a reference direction (say, χ_2, as in Figure 1(b)), and recementing it to its suspension fiber. Such a full "rotation measurement", as it is called [13], is only carried out when significant specimen anisotropy is present, as it was in HP-50, 51, 52, 55 and 57. For these, the assigned "measure of anisotropy" is the average of $|\chi_2 - \chi_1|$ and $|\chi_2 - \chi_3|$.

Figure 2, a composite plot of "anisotropy" *versus* composition, shows that whereas anisotropy is undetectable in HP-30 through HP-49 it increases rapidly beyond 50 at.% Al, an effect which is clearly related to the properties of the single-phase γ-Ti-Al. In view of the rather large anisotropy associated with the γ phase, the absence of a linear (tie-line-like) anisotropy across the $\alpha_2+\gamma$ field is at first glance rather surprising. However, the sudden onset of anisotropy is explicable in terms of the change of microstructure seen on crossing from the two-phase to the single-phase field. In the former, a fine lamellar structure ensures randomization of γ crystallite orientation, a situation which (as we shall see) does not exist in γ-Ti-Al.

3.3 Susceptibility-Composition Dependence as it Relates to the Development of Equilibrium Phase Diagrams

Susceptibility-composition characteristics of single-phase alloys are generally curvilinear, e.g., $\chi_\alpha(c)$ and $\chi_\beta(c)$ in Figure 3. However, any line crossing a two-phase field must be uncompromisingly straight, e.g., $\chi_{(\alpha+\beta)}(c)$ in Figure 3. That this is so can be demonstrated by the following manipulation of a pair of continuity equations appropriate to average solute concentration, c, and average magnetic susceptibility, χ, respectively:

$$\left.\begin{aligned} c &= f_A c_A + (1-f_A)c_B \qquad \text{(the 'lever' rule)} \quad , \\ \text{and} \qquad \chi &= f_A\chi_A + (1-f_A)\chi_B \quad , \end{aligned}\right\} \qquad (2)$$

where f_A represents the mole-fraction of phase A, c_A represents the concentration of solute in the A-phase, and c_B that of solute in B-phase.

It follows that

$$\chi = \frac{c_B\chi_A - c_A\chi_B}{c_B - c_A} + \frac{\chi_B - \chi_A}{c_B - c_A} \cdot c \quad , \qquad (3)$$

hence a plot of χ versus c for a series of equilibrated two-phase alloys is linear with intercept $(c_B\chi_A - c_A\chi_B)/(c_B - c_A)$ and slope $(\chi_B - \chi_A)/(c_B - c_A)$. This is referred to as a "tie-line", proper identification of whose end-points can result in the accurate determination of a pair of phase boundaries. In practice, several series of alloys are prepared, equilibrated at a set of temperatures, and quenched. The quenched structure is assumed to reflect that at equilibrium, due regard being given to the possibility of athermal transformation (such as $\beta \rightarrow \alpha$ or $\alpha \rightarrow \alpha_2$ for Ti-Al alloys) which, however, does not influence the position of the tie-line end-points. From the family of magnetic "isothermals" so generated, loci of end-points can be constructed to form the equilibrium phase boundaries. A corollary to this has to do with the identification of single-phase regimes. With the exception of the situation in which the boundaries enclosing a two-phase field are both "vertical", a non-responsiveness of the magnetic susceptibility of an alloy of given composition to changes of equilibration temperature indicates that all the (χ,c) points lie in a single-phase field.

Generally the transformation kinetics are sufficiently sluggish that the elevated-temperature phase proportionality is retained on quenching. On the other hand, if necessary, the entire magnetic study can be carried out "at temperature".

4. MAGNETIC SUSCEPTIBILITY OF Ti-Al

4.1 Matrix of Magnetic Susceptibility Measurements

Magnetic susceptibility measurements have been made on 16 alloys in the composition range 30-57 at.% Al quenched from anneals at temperatures between 900 and 1365°C. The numerical results of the work are presented in Table IV (average susceptibilities) and Table V (anisotropies).

4.2 The Single-Phase Isotherms--Experimental Precision

An inspection of Table IV reveals that the susceptibilties of many alloys are insensitive to changes of equilibration temperature within certain ranges. Thus, for example, the susceptibilities of HP-51 remain invariant ($\pm$ 0.6% std. error) over the entire pre-quench temperature range of 900-1315°C. This is also true for the alloy groups HP-(30 to 41) and HP-(50 to 57) at both ends of the composition range considered, as indicated in Table VI. These data plotted as in Figure 4 define a pair of "single-phase isotherms" between which tie-lines can be constructed and phase boundaries established.

The data of Table VI, in association with other information may also be used to provide an estimate of the overall precision of the susceptibility determination as influenced by (a) possible sample inhomogeneity, (b) contamination during heat treatment, (c) sample positioning, (d) magnetic field setting, and (e) magnetic force measurement. It is concluded that, commencing with an as-cast button from which small samples are removed for measurement, that the susceptibilities of Ti-Al alloys heat treated at elevated temperatures are reproducible to about $\pm$ 0.4 μ emu/mole (about 0.4%). Previous studies of the susceptibilities of numerous samples of

polycrystalline (6 determinations) and monocrystalline (4 determinations) pure Ti yielded uncertainties of $\pm$ 0.4 to $\pm$ 0.6 μemu/mole [14]. It follows that causes (a) and (b) above are not contributing significantly to the overall uncertainty.

4.3 Compositional Homogeneity

Upper limits to compositional inhomogeneity can be assigned by ascribing all of the susceptibility scatter to that source--unlikely in the light of the results for pure Ti. By combining standard error data from Tables II and VI with the slopes of segments of the isothermals of Figure 4, as in Table VII, we find compositional uncertainties of $\pm$ 0.36 at.% Al (HP-37 through HP-41) and $\pm$ 1.48 at.% Al (HP-50 through HP-52). This was not substantiated by chemical analysis which yielded $\pm$ 0.83 at.% Al and $\pm$ 0.29 at.%, respectively, including analytical uncertainty. Thus considering errors inherent in the susceptibility measurement itself (0.4%) and in chemical analysis, compositional inhomogeneity, although undetected, must be regarded as an insignificant source of uncertainty.

4.4 Construction of the Tie-Lines

The susceptibility composition dependences follow a definite trend as we proceed from pre-quench temperatures of 900°C to 1265°C. Accordingly, it is possible to construct, between the "single-phase isotherms", linear tie-lines whose positions and slopes change in a systematic way. In placing these lines we are guided by the as-cast data, valuable reference points which are used in the following way. As annealing proceeds the susceptibilty datum point moves away from the "as-cast" position. Thus the equilibrium value is either the as-measured one, or

it lies on the side of the measured datum point remote from the as-cast value. Linear susceptibility isotherms in the two-phase field must therefore be drawn either through (or close to) measured points or else past them on the "far side".

An example of this procedure is given in Figure 5. Using the method it has been possible to construct a mutually consistent set of tie-lines as shown in Figure 6 and summarized in Figure 7. The results for 1315°C were too scattered in the two-phase region to yield a single well-defined tie-line. In fact close examination of the data suggests the existence of a pair of lines. This uncertainty is taken as evidence for the occurrence of a horizontal boundary between the $(\alpha+\gamma)$ and $(\beta+\gamma)$ phases at about 1315°C. Small variations in annealing temperature from sample to sample would permit this boundary to be crossed, and lead to apparently inconsistent properties in the quenched alloys.

4.5 Magnetically Derived Contribution to the Equilibrium Phase Diagram

Following the rationale just described, a set of tie-lines are drawn and their points of intersection with the "single-phase isotherms" determined. These data, as listed in Table VIII, augmented by the results of the most recent previous investigation [12], Table IX, contribute to the construction of a portion of the equilibrium phase diagram. The result is given in Figure 8 and discussed below.

Previous investigations of the composition range of interest here are those of Jaffee, et al. [1], Hansen, et al. [2], Kornilov, et al. [3], and Sato and Huang [5]. In the first-named paper regions designated $(\alpha+\gamma)$ and γ are contained between three parallel "vertical" phase

boundaries (750-1100°C) positioned at 38, 47, and 60 at.%Al, respectively. According to Hansen, et al. [2] the corresponding vertical phase boundaries (700-900°C) are located at 36.5, 49.5, and 58.5 at.%Al*; but the $(\alpha+\gamma)/\gamma$ boundary bulges out towards the Ti axis at (1240°C, 48.5 at.%Al). A $(\beta+\gamma)/(\alpha+\gamma)$ transus, not present in Reference [1] is at 1240°C. Kornilov's [3] diagram is quite similar to that of Hansen, et al. A slight variance is the raising of the $(\beta+\gamma)/(\alpha+\gamma)$ transus (and the height of the bulge) to about 1300°C. The diagram of Sato and Huang [5] differs considerably from its predecessors, particularly with regard to the proposed existence of a "δ" solid solution above 1050°C centered at about 40 at.%Al. This phase was claimed to be retainable on quenching, but decomposable into $(\alpha_2+\gamma)$ below the 1050°C transus. In the previous work the δ-phase space was occupied by $(\beta+\gamma)$. The γ region itself was defined by 45.0 to 60.5 at.%Al at 900°C, with a bulge towards the Ti axis centered at (1050°C, 41.5 at.%Al). It is difficult to reconcile the details of Sato's diagram, the configuration of which depends heavily on the interpretation of resistivity-temperature curves, with those of References [1], [2], and [3].

As a result of the present investigation it is possible to identify several points of agreement and disagreement with the pictures of Jaffee, Hansen, and Kornilov

(a) At 900°C the $(\alpha_2+\gamma)/\gamma$ phase boundary is at 47.5 at.%Al in good agreement with, and slightly on the "conservative side" of, the 46.7 at.%Al of Jaffee, et al. [1]; while at 1240°C it is at 48.5 at.%Al, in perfect agreement with the results of Hansen, et al. [2].

*converted from weight percent to the nearest 0.5 at.%Al.

(b) The horizontal $(\beta+\gamma)/(\alpha+\gamma)$ transus is now estimated to be at 1315°C, but significantly higher than the 1240°C claimed by Hansen et al. [2].

(c) The results of the present work, in contrast to [2] and [3], show no "bulge" in the $(\alpha_2+\gamma)/\gamma$ phase boundary.

5. OPTICAL METALLOGRAPHY

Metallography was performed on the sixteen alloys HP-30 through HP-57 in the as-cast condition and after quenching from heat treatments at seven temperatures, 900 through 1365°C according to the schedule of Table III. The resulting set of micrographs (magnification of the original 6cm x 6cm pictures, 200X) is reproduced in Figure 9 through 12.

5.1 Metallography of HP- (30 to 52)

The purpose of the metallography was to clarify, and aid in the interpretation of, the magnetic results. The converse also turned out to be true. For example, when a predominantly γ-phase alloy was noted to contain small amounts of α_2, application of the magnetic technique enabled it to be identified as incompletely equilibrated single-phase rather than equilibrium two-phase -- an important distinction in the determination of phase boundaries.

Specifically, let us compare the micrographs for alloys HP-39 through HP-52 quenched from 1215°C, Figure 13(a) with the susceptibility diagram of Figure 13(b). The alloys are single phase prior to HP-43 which is at the threshold of the $(\alpha_2+\gamma)$ field. The next two alloys (HP-45 and HP-46) exhibit the lamellar structure characteristic of $\alpha_2+\gamma$ after which

HP-47 and HP-48 show large regions of γ-phase interspersed with patches of $\alpha_2+\gamma$ lamellae. According to the magnetic diagram HP-49 and HP-50 are practically fully equilibrated γ; and the micrographs show only very small volume fractions of $\alpha_2+\gamma$ enclaves interspersed within the dominant single-phase matrix. The linear arrangement of the $\alpha_2+\gamma$ patches in HP-48 suggests that these residual regions may derive from traces of as-cast dendritic segregation not yet completely erradicated. The magnetic work shows unambiguously that the equilibrium two-phase field terminates between 48 and 49 at.%Al and not at the slightly higher Al concentration indicated by the photomicrographs coupled with the assumption of complete equilibrium.

As a second example it is useful to compare a series of micrographs of Ti-Al alloys quenched from 1065°C with the corresponding susceptibility diagram (Figures 14(a) and (b)). According to both figures, the $\alpha_2+\gamma$ threshold occurs near 39 at.% Al. In HP-43 to HP-46, which occupy the middle of the two-phase field, the characteristic lamellar structure is seen; and this again gives way to large γ grains with inclusions of lamellae. The only possible interpretation of the magnetic results gives the single-phase-threshold at 47.5% at.% Al and the added information that equilibrium has not been completed in alloys between HP-46 and HP-48 whose susceptibilities fall on a rounded curve lying below the linear tie-line and the single-phase isotherm. Thus the presence of traces of α_2 in alloys beyond HP-48 is again due to incomplete equilibrium.

Qualitative metallography is unable to distinguish between incomplete equilibrium and intrinsic two-phasedness. Quantitatively, if volume fractions of component phases can be computed, tie-lines can be

constructed and the separation made. But it is difficult to put this into practice with the necessary degree of precision, particularly if electron microscopy is required to detect the presence of trace second-phase precipitation. On the other hand, magnetic susceptibility, a bulk measurement, responds readily to changes of component fractions in a two-phase mixture, and as such is a useful adjunct to conventional metallurgical approaches.

The equilibration problem of course goes away if alloys can be annealed for extremely long periods of time prior to qualitative metallography (optical or electron). Unfortunately, in systems such as Ti-Al the influence of oxygen and/or nitrogen contamination always intervenes, even under optimal encapsulation conditions, and perturbs the desired equilibrium. An example of this is given in Appendix B in which the contamination of HP-50 during moderate-time annealing at 1315°C is discussed.

5.2 Metallography of HP-(55 and 57)

The microstructures exhibited by quenched HP-55 and HP-57 were unable to be correlated with those of the lower concentration block of alloys whose structures were characteristic of either $\alpha_2+\gamma$ or single-phase γ. We were concerned, in the case of HP-55 that the structure being seen was the effect of residual coring remaining after possibly inadequate solution heat treatment. This was a rather unlikely state of affairs since HP-52 and 55 had experienced similar heat treatments and (a) the former alloys were all obviously well annealed and (b) so also was HP-55 (1365°C/1h). Nevertheless new samples of HP-55 and HP-57 were cut and all given the successful 1365°C/1h heat treatment followed by

further heat treatments at lower temperatures according to the Table III schedule. Metallography and hardness were again carried out. The results of this work, given in Figure 15, reproduce the original set of microstructures. It seems that HP-55 lies in a new two-phase field the determination of whose constitution and boundaries awaits further investigation.

6. MICROHARDNESS STUDIES

Microhardness investigations have been carried out on most of the mounted metallographic samples (c.f., Table III). A load of 2.5 kg weight was applied to a Vickers diamond pyramid indentor in making a series of about 30 impressions, typically 100 μm square, per sample. In two-phase material or when severe twinning occurred, as for example in all of the HP-41 material, a large spread in hardness number was noted. Otherwise the scatter was remarkably small as evidenced by Table X, a typical set of data.

The results of the hardness study are presented numerically in Table XI. The data when plotted yielded a set of curves all of which were remarkably similar, a typical example being Figure 16. No progression of tie-lines could be constructed as in the susceptibility work. This could be explained if hardening produced by second-phase precipitation is strongly nonlinear and quickly saturates for small volume fractions of precipitate. This would have two related effects on the form of the hardness "isothermals" and is consistent with the following observations:

(a) The two-phase regions are all of similar extent -- since non-equilibrated α_2 was always present in supposedly single-phase alloys towards the Al-rich end of the $\alpha_2+\gamma$ field.

(b) The hardness minimum which would be anticipated at exactly 50 at.%Al was moved to 51 at.%Al, presumably the first γ-phase alloy entirely free of α_2 precipitation.

As a result of spurious hardening effects resulting from the non-attainment of complete equilibrium, the hardness profile (e.g., Figure 16) had no discernible relationship to the phase boundaries depicted in Figure 8.

Finally, regarding the reproducibility of microstructures following heat treatment of the two sets of HP-55 and HP-57 alloys, it is important to note with reference to Table XI that the initial and repeated hardness values agreed quite well, usually within one standard deviation.

7. CONCLUDING DISCUSSION

7.1 Experimental Techniques in Phase Diagram Construction

Physical property measurements have been frequently employed as an adjunct to metallographic and crystallographic studies in the determination of phase equilibria and the establishment of phase equilibrium diagrams. Properties usually selected are: electrical resistivity, thermoelectric power, magnetic susceptibility, dilatometry, elastic modulus, and hardness; and the approach used is to study the compositional dependence of a selected property with respect to a sequence of alloys quenched from a given temperature. In the hands of Kurnakov [15] and Kornilov [16] this technique has been elaborated into the method of "physico-chemical analysis".

In investigating phase equilibria using composition-dependent physical-property diagnostics two features are sought: (a) cusps, which may be either positive- or negative-going, and which may indicate the occurrence of line compounds; (b) straight lines, tie-lines, with which we have been concerned in this paper. Tie-lines delimit a two-phase field, and rely for their existence on a strictly linear relationship between the magnitude of the property being measured, and end-point compositions, and properties according to

$$P = \frac{c_B P_A - c_A P_B}{c_B - c_A} + \frac{P_B - P_A}{c_B - c_A} c \qquad (4)$$

where P represents a molal property, c a concentration in atomic percent, and the subscripts denote end-points. Alternatively, we may work in terms of property-per-unit-mass associated with weight percent. The mixing of mass and atomic units will of course lead to a spurious nonlinearity.

In order to ensure linearity of the relationship between average property and phase composition down to extremely small amounts (precipitates) of A in B, and vice versa, the property measured must be bulk and short-range. For this reason transport properties are not at all satisfactory (electrical resistivity will respond to interface, and other, effects) while electronic density of states properties are ideal. Of the latter, magnetic susceptibility is most suitable in that it is capable of providing bulk values even for precipitate particles less than 100 Å in diameter (such as omega-phase precipitates [17]) and is, moreover, extremely sensitive. As for hardness, there is of course no established relationship of the type presented above in Equation (4) connecting measured average hardness with those of the two constituent phases.

7.2 Problems and Solutions Associated with the Unattainability of Complete Phase Equilibrium

Estimates of equilibration times at given temperatures are usually obtained empirically by trial and error. Samples are annealed for various lengths of time and stable "recrystallized" optical microstructures or the attainment of constant values of some diagnostic parameter, are sought. Equilibrium is, however, an exponential process so that near the edges of a single-phase field extremely long equilibration times may be required to dissolve the last electron-microscopically-observable traces of second-phase precipitation. Thus, a thermodynamically single-phase region may be incorrectly designated as "equilibrium two-phase". This situation is particularly true in the case of reactive alloys, since the increasing danger of contamination defeats the purpose of prolonged annealing. For example, the positions of some phase boundaries of the Ti-Al system have been shown to be strongly influenced by oxygen pick-up [18], an effect which would cause the sought-after boundaries to shift as annealing to the expected equilibrium condition proceeds.

Using the magnetic method, however, it is possible to cope with small departures from equilibrium which would otherwise wash out or round off the two-phase boundaries. Provided enough data points are collected, and that a closely spaced set of isothermals is examined, a family of linear tie-lines can be constructed (to either pass through datum points, or on the "far sides" of sets of points -- see Section 4.4) the ends of which define the equilibrium phase boundaries, even though the actual end-region data may deviate from the line on account of still-undissolved precipitation. Thus, appropriate physical-property diagnostics can lead

to a determination of equilibrium phase boundaries in cases where the results of qualitative metallography, and transmission electron microscopy in particular, are misleading.

In the present work we did, however, encounter problems with the results of the anneal at 1365°C, presumably because of further transformation during quenching. These difficulties are of course shared by other techniques that rely on deductions based on quenched microstructures. With suitable equipment though the magnetic experiment can be carried out at temperature, under which conditions it responds to the existing rather than inferred structure. Used in this way magnetic susceptibility is a particularly powerful diagnostic tool since the results, unlike those of x-ray observations, are not seriously perturbed by the presence of thin layers of surface contamination.

7.3 Results of the Magnetic and Optical Studies

Using the magnetic technique the positions of the $\alpha_2/(\alpha_2+\gamma)$ and $(\alpha_2+\gamma)/\gamma$ phase boundaries were determined, and compared with the estimates of Jaffee, et al. [1] and Hansen, et al. [2]. An estimate was also made of the temperature of the horizontal $(\beta+\gamma)/(\gamma+\alpha)$ transus.

The results of the magnetic anisotropy studies were also interesting in that, even though the γ phase is highly anisotropic, the susceptibility of all the $\alpha_2+\gamma$ alloys showed little anisotropy. The reason for this has to do with the fact, evidenced in the optical micrographs, that the α_2 and γ phases were finely interleaved in a lamellar structure. This ensured that, on the scale of the susceptibility sample, the γ exhibited no preferred orientation. On the other hand in the single-phase γ regime the large

relative grain size, coupled with intrinsic magnetic anisotropy, guaranteed that the polycrystalline samples retained appreciable anisotropy. As discussed in Section 3.2 the occurrence of this anisotropy is good evidence that the sample is predominantly single-phase γ.

The magnetic anisotropy itself is of considerable fundamental interest in that it relates to the electronic structure of the intermetallic compound. Although TiAl is magnetically anisotropic, $TiAl_3$ (judging by magnetic results not reported here) is even more so -- and even more brittle at room temperature. The preparation and measurement of the properties of single crystals of these materials would make a useful study, and help to shed light on the relationships between their mechanical, structural, and electronic properties. Finally, we draw attention to what appears to be an unusually strong affinity of TiAl for interstitial contamination which, as is pointed out in Appendix B, warrants special investigation.

8. ACKNOWLEDGEMENTS

The research described above was financially supported by the U. S. Air Force Office of Scientific Research (AFSC) under Grant No. 71-2084, and monitored by Dr. A. H. Rosenstein. The Ti-Al alloys were arc-melted at Battelle by Mr. F. P. Holcomb and chemically analyzed by Mr. D. L. Chase. They were again chemically analyzed through the courtesy of Dr. H. A. Lipsitt of the Air Force Materials Laboratory, Wright-Patterson Air Force Base. At Battelle, the optical metallography was carried out by Mr. R. L. Pratt, and the magnetic suxceptibility and hardness measurements were made by Mr. R. D. Smith. I am grateful to various members of Dr. Lipsitt's Aluminide Working Group, at a meeting of which this work was first presented, for helpful discussion, critical comment, and encouragement to prepare this paper.

9. REFERENCES

[1] H. R. Ogden, D. J. Maykuth, W. L. Finlay, and R. I. Jaffee, Trans. AIME, 191, 1190 (1951).

[2] E. S. Bumps, H. D. Kessler, and M. Hansen, Trans. AIME, 194, 609 (1952).

[3] I. I. Kornilov, E. N. Pylaeva, and M. A. Volkova, Izv. Akad. Nauk SSSR, Otd. Khim. Nauk, No. 7, 771 (1956).

[4] K. Sagel, E. Schultz and U. Zwicker, Z. Metallk., 46, 529 (1956).

[5] T. Sato and Y. Huang, Trans. Jap. Inst. Metals, 1, 22 (1960).

[6] E. Ence and H. Margolin, Trans. Met. Soc. AIME, 221, 151 (1961).

[7] Y. L. Yao, Trans. ASM, 54, 241 (1961).

[8] D. Clark, K. S. Jepson, and G. I. Lewis, J. Inst. Metals, 91, 197 (1962).

[9] I. I. Kornilov, E. N. Pylaeva, M. A. Volkova, P. I. Kripyakevich, and V. Ya Markiv, Dokl. Akad. Nauk, SSSR, 161, 842 (1965).

[10] F. A. Crossley, Trans. Met. Soc. AIME, 236, 1174 (1966).

[11] M. J. Blackburn, Trans. Met. Soc. AIME, 239, 1200 (1967).

[12] M. J. Blackburn in "The Science Technology and Application of Titanium", Ed. by R. I. Jaffee and N. E. Promisel, Pergamon Press, 1970, p. 633.

[13] E. W. Collings and R. D. Smith, J. Appl. Phys., 39, 4462 (1968).

[14] E. W. Collings and J. C. Ho, Phys. Rev. 4, 349 (1971).

[15] N. S. Kurnakov "Introduction to Physico-Chemical Analysis", USSR Academy of Sciences Publishers, 1940.

[16] I. I. Kornilov, Proceedings of the Third International Conference on Titanium Science and Technology, Moscow, USSR, 1976 -- to be published.

[17] E. W. Collings, J. Less-Common Metals, 39, 63 (1975).

[18] E. K. Molchanova, "Phase Diagrams of Titanium Alloys", Ed. by S. E. Glazunov, Israel Program for Scientific Translations, Jerusalem, 1965, pp. 253-255.

TABLE I. LIST OF INVESTIGATIONS DIRECTED TOWARDS A DETERMINATION OF THE Ti-Al EQUILIBRIUM PHASE DIAGRAM

Year	Authorship	Reference	Temperature Range for Equilibrated Solid Alloys °C	Composition Range (at.%Al)	Principal and Auxiliary Techniques Described
1951	Ogden et al	[1]	750-1100	0-64	optical metallography; with X-ray diffraction and thermal analysis.
1952	Bumps et al	[2]	700-1400	0-75	optical metallography; with X-ray diffraction and Vickers hardness.
1956	Kornilov et al	[3]	700-1200	0-75	optical metallography; with X-ray diffraction, Vickers hardness, thermal analysis and centrifugal bend tests.
1956	Sagel et al	[4]	550-1050	5-49	electrical resistivity, magnetic susceptibility; with optical metallography and X-ray diffraction.
1960	Sato and Huang	[5]	450-1350	0-63	electrical resistivity; with optical metallography and X-ray diffraction.
1961	Ence and Margolin	[6]	800-1450	0-48	optical metallography and X-ray diffraction.
1961	Yao	[7]	400-1100	5-38	magnetic susceptibility
1962	Clark et al	[8]	550-1200	0-38	optical metallography, electrical resistivity and X-ray diffraction.
1965	Kornilov et al	[9]	550-1200	5-43	electrical resistivity and Vickers hardness; with thermal analysis, dilatometry, and X-ray diffraction.
1966	Crossley	[10]	550-1100	7-35	Optical metallography; with electron microscopy, X-ray diffraction, differential thermal analysis, electrical resistivity and dilatometry.
1967	Blackburn	[11]	500-1100	5-25	electron microscopy.
1970	Blackburn	[12]	1025-1225	27-45	electron microscopy.

TABLE II. CHEMICALLY ANALYZED ALUMINUM CONCENTRATIONS (at.%), AND MOLAR WEIGHTS FOR THE Ti-Al ALLOYS STUDIED IN IN THIS PROGRAM

Alloy Name	First Analysis[1]	Second Analysis[2]	Third Analysis[2]	Fourth Analysis --two determinations[1]		Average (accepted) Value (at.%)	Molar Weight (g)
HP-30	30.8	30.20	-	-	-	30.50 ± 0.40	41.5_2
-33	33.8	33.10	-	-	-	33.45 ± 0.49	40.8_9
-37	37.6	36.67				37.14 ± 0.66	40.1_3
HP-39	-	39.41	40.12 40.48	38.29	39.76	39.15 ± 0.77	39.7_1
-41	-	40.12	40.48 41.08 43.87	40.84	42.27	41.16 ± 1.30	39.2_9
HP-43	43.0	42.50	-	44.02	43.79	43.33 ± 0.70	38.8_4
-45	(46.5)[3]	44.83	-	45.06	44.72	44.87 ± 0.17	38.5_1
-46	(48.5)	45.51	-	45.97	46.20	45.89 ± 0.35	38.3_0
HP-47	47.0	47.05	-	46.65	46.76	46.87 ± 0.19	38.1_0
-48	-	-	47.77	48.54	47.77	48.03 ± 0.45	37.8_5
-49	-	-	49.17	50.07	49.75	49.66 ± 0.46	37.5_1
HP-50	49.8	50.50	-	49.96	50.29	50.14 ± 0.32	37.4_1
-51	(53.3)	51.08	-	51.90	52.00	51.66 ± 0.50	37.0_9
-52	-	52.50	-	52.43	52.43	52.45 ± 0.04	36.9_3
HP-55	54.5	55.02	-	54.82	54.82	54.79 ± 0.22	36.4_4
HP-57	(59.3)	56.75	-	57.25	57.45	57.15 ± 0.36	35.9_5
				Average Std. Error		= ± 0.46	

(1) Battelle analysis.

(2) Analyzed, courtesy of Air Force Materials Laboratory, Wright-Patterson Air Force Base.

(3) Bracketed quantities were omitted before computing the mean composition.

TABLE III. INDEX OF HEAT TREATMENTS AND MAGNETIC (m) METALLOGRAPHIC (o) AND HARDNESS (h) STUDIES

Heat Treatment including ice-brine quench (IBQ) (temp, °C/time, h)	Alloy Name															
	HP-30	HP-33	HP-37	HP-39	HP-41	HP-43	HP-45	HP-46	HP-47	HP-48	HP-49	HP-50	HP-51	HP-52	HP-55	HP-57
1365/1 + IBQ														oh	o•h•	o•h•
1065/24 + 1365/1 + IBQ						moh	moh	moh	moh	moh	moh	moh	moh			
1315/1 + IBQ	moh	moh	moh•	moh	moh	m	m	m	m•	m	m	m	m	moh	moh	moh
1315/4 + IBQ							m	m	m	m•	m•	m	m			
1315/24 + IBQ						moh	moh	moh	moh	m•oh	m•oh	m•oh	moh			
1365/1 + 1315/1 + IBQ															oh	oh
1265/1 + IBQ	moh	moh	moh•	m	m	m	m	m	m			m	moh	moh	moh	moh
1265/8 + IBQ				moh	moh	moh	moh	moh	moh	moh	moh	moh				
1365/1 + 1265/1 + IBQ															oh	oh
1215/8 + IBQ				moh	moh	moh	moh	moh	moh	moh	moh	moh				
900/48 + 1215/2 + IBQ	moh	moh	moh•			m	m	m	m			m	moh	moh	moh	moh
1365/1 + 1215/2 + IBQ															oh	oh
1165/24 + IBQ				moh	moh	moh	moh	moh	moh	moh	moh	moh				
900/48 + 1165/4 + IBQ	moh	moh	moh•			m	m	m	m			m	moh	moh	moh	moh
1365/1 + 1165/8 + IBQ															oh	oh
1065/24 + IBQ	moh	moh	moh•			m	m	m	m			m	moh	moh	moh	moh
1065/48 + IBQ				moh	moh	moh	moh	moh	moh	moh	moh	moh				
1365/1 + 1065/24 + IBQ															oh	oh
900/48 + IBQ	m	m	m			m	m	m	m			m	m	m	m	m
1065/24 + 900/500 + IBQ	moh	moh	moh•	moh	moh	moh	moh	moh	moh	moh	moh	m•oh	moh	moh	moh	moh
1365/1 + 900/500 + IBQ															o	o
As-Cast	moh	moh	moh•	moh	moh	moh	moh	moh	moh	moh	moh	moh	moh	moh	moh	moh

•Indicates multiple determinations.

TABLE IV. MAGNETIC SUSCEPTIBILITIES OF ANNEALED-AND-QUENCHED Ti-Al ALLOYS

The rectangles define regions within which averages have been taken.

Heat Treatment including ice-brine quench (IBQ) (temp, °C/time, h)	Alloy Name															
	HP-30	HP-33	HP-37	HP-39	HP-41	HP-43	HP-45	HP-46	HP-47	HP-48	HP-49	HP-50	HP-51	HP-52	HP-55	HP-57
1065/24 + 1365/1 + IBQ						106.2	104.6	108.3	124.7	120.0	116.0	114.7	113.1			
1315/1 + IBQ	113.9	113.9	112.0	110.8	108.4	106.0	105.2	104.8	125.0 117.5	117.9	116.4	114.5	113.1	110.2	95.8	87.0
1315/4 + IBQ							106.1	110.6	115.0	116.3 117.6	114.8 116.3	115.9	114.4			
1315/24 + IBQ						108.7	118.3	121.0	119.8	120.1 111.8	117.8 111.5	103.8 104.0 103.6 103.5	113.6 114.0			
1265/1 + IBQ	113.1	113.7	112.2	111.0	108.2	106.2	116.3	116.0	120.0			119.0	114.0	109.9	95.4	86.7
1265/8 + IBQ				110.3	108.4	105.8	108.1	113.1	116.8	119.2	119.0	118.2				
1215/8 + IBQ				110.8	108.5	109.6	115.6	118.2	122.1	122.7	122.0	119.5				
900/48 + 1215/2 + IBQ	116.0[1]	114.8[1]	112.6			107.2	116.2	118.7	119.7[2]			118.9	114.0	110.3	95.4	87.3
1165/24 + IBQ				110.7	108.4	113.0	121.7	122.8	124.8	125.3	121.7	119.6				
900/48 + 1165/4 + IBQ	113.2	113.3	111.9			113.5	119.6	121.5	122.4			118.8	114.2	110.0[3]	95.9	87.2
1065/24 + IBQ	113.4	113.8	111.8			119.8	125.3	126.0	125.6			119.5	115.4	110.5	96.2	88.0
1065/48 + IBQ				111.3	115.9	119.4	124.8	125.7	126.2	125.3	121.8	119.3				
900/48 + IBQ	113.6	114.2	112.5			122.6	126.2	126.5	125.6			119.3	114.9	110.4	95.9	87.6
1065/24 + 900/500 + IBQ	113.5	113.6	112.8	117.6[4]	120.6[4]	121.8	125.4	125.7	126.1	122.1[5]	122.8[5]	119.0 119.9[6] 119.9 120.0	113.9	110.5	95.6	87.7
As-Cast	113.3	114.1	112.3	110.5	108.6	106.4	123.4	122.8	120.2	119.2	117.2	116.5	114.4	109.9	95.0	87.6

(1) Not included in mean.
(2) 1065/24 + 1215/2 + IBQ.
(3) 1065/24 + 1165/4 + IBQ.
(4) Only 900/500 + IBQ.
(5) Only 900/666 + IBQ.
(6) 1065/24 + 900/527 + IBQ.

TABLE V RELATIVE MAGNETIC ANISOTROPIES IN ANNEALED-AND-QUENCHED Ti-Al ALLOYS

The rectangles define regions within which averages have been taken.

Heat Treatment including *ice-brine quench* (IBQ) (temp, °C/time, h)	Alloy Name															
	HP-30	HP-33	HP-37	HP-39	HP-41	HP-43	HP-45	HP-46	HP-47	HP-48	HP-49	HP-50	HP-51	HP-52	HP-55	HP-57
1065/24 + 1365/1 + IBQ						0.18	0.07	0.14	0.03	0.06	0.19	0.33	0.52			
1315/1 + IBQ	0.07	0.04	0.00	0.04	0.04	0.04	0.00	0.18	0.03 0.06	0.03	0.03	0.72	0.59	0.97	2.44	1.24
1315/4 + IBQ							0.11	0.10	0.07	0.07 0.00	0.03 0.16	0.13	0.39			
1315/24 + IBQ						0.07	0.03	0.09	0.10	0.09 0.10	0.06 0.20	0.11 0.11 0.07	0.65 0.98			
1265/1 + IBQ	0.11	0.18	0.11	0.32	0.15	0.07	0.10	0.40	0.16			0.72	1.76	0.57	1.15	1.08
1265/8 + IBQ				0.04	0.11	0.07	0.14	0.17	0.16	0.10	0.06	0.06				
1215/8 + IBQ				0.07	0.04	0.07	0.17	0.26	0.19	0.09	0.12	0.13				
900/48 + 1215/2 + IBQ	0.11[1]	0.14[1]	0.14			0.11	0.07	0.10	0.38[2]			0.28	0.46	0.37	0.76	2.52
1165/24 + IBQ				0.11	0.07	0.07	0.25	0.25	0.21	0.06	0.12	0.25				
900/48 + 1165/4 + IBQ	0.26	0.07	0.11			0.27	0.06	0.09	0.16			0.16	0.58	0.44[3]	0.38	0.58
1065/24 + IBQ	0.11	0.00	0.04			0.16	0.25	0.12	0.06			0.56	0.87	0.40	0.80	1.15
1065/48 + IBQ				*0.11*	*0.03*	*0.10*	*0.03*	*0.15*	*0.15*	*0.09*	*0.06*	*0.60*				
900/48 + IBQ	0.29	0.18	0.21			0.29	0.18	0.12	0.06			0.13	0.94	0.77	0.65	2.18
1065/24 + 900/500 + IBQ	0.04	0.11	0.00	0.00[4]	0.10[4]	0.19	0.15	0.09	0.15	0.09[5]	0.09[5]	0.47 0.53 0.97 1.06 [6]	0.10	0.84	0.19	1.28
As-Cast				0.14	0.11					0.10	0.06	0.77	0.32	0.17	1.47	3.37

(1) Not included in mean.
(2) 1065/24 + 1215/2 + IBQ.
(3) 1065/24 + 1165/4 + IBQ.
(4) Only 900/500 + IBQ.
(5) Only 900/666 + IBQ.
(6) 1065/24 + 900/527 + IBQ.

TABLE VI. AVERAGE SUSCEPTIBILITIES AND STANDARD ERRORS FOR Ti-Al ALLOYS WITHIN THE COMPOSITION RANGES 30-41 at.%Al and 50-57 at.%Al

Alloy Name	Al Concentration (at.%)	Temperature of Anneal Prior to Quench (°C)	No. of Datum Points	Magnetic Susceptibility (μ emu/mole)
HP-30	30.5	900 - 1315	7	113.5 ± 0.3
-33	33.5	900 - 1315	7	113.8 ± 0.3
-37	37.1	900 - 1315	7	112.3 ± 0.4
HP-39	39.2	1065 - 1315	6	110.8 ± 0.3
-41	41.2	1165 - 1315	5	108.4 ± 0.1
HP-50	50.1	900 - 1265	13	119.3 ± 0.5
-51	51.7	900 - 1315	11	114.2 ± 0.6
-52	52.5	900 - 1315	7	110.3 ± 0.2
HP-55	54.8	900 - 1315	7	95.7 ± 0.3
-57	57.2	900 - 1315	7	87.4 ± 0.4
				Average Std. Error = ± 0.4

TABLE VII. UNCERTAINTIES IN SUSCEPTIBILITIES AND CHEMICAL ANALYSES

Composition Range (at.%Al)	Slope of $\chi(c)$ from Fig. 4 (μ emu/mole - at.%)	Standard error in susceptibility measurement (μ emu/mole)	Corresponding uncertainty in composition at.%Al	Actual scatter in composition at.%Al
37 - 41	0.9	$\pm$ 0.4	$\pm$ 0.36	$\pm$ 0.83
50 - 52	3.7	$\pm$ 0.4	$\pm$ 1.48	$\pm$ 0.29

TABLE VIII. POINTS OF INTERSECTION OF THE TIE-LINES WITH THE SINGLE-PHASE ISOTHERMS

Pre-Quench Temperature (°C)	Aluminum Concentration (at. %)	
	Intersection with α_2 or α	Intersection with γ
1265	44.0	49.2
1215	42.5	48.9
1165	41.2	48.4
1065	39.0	47.5
900	36.5	47.5

TABLE IX. TRANSI OF THE Ti-Al EQUILIBRIUM PHASE DIAGRAM. Pairs of Data read off from a published diagram due to Blackburn [12].

	Temperature (°C)	Aluminum concentration (at.%)
(a) The $\beta/(\beta+\alpha)$ Transus	1250	31.9
	1240	30.6
	1230	29.3
	1220	28.0
	1210	26.3
	1200	25.0
(b) The $(\beta+\alpha)/\alpha$ Transus	1210	35.0
	1200	33.5
	1190	32.1
	1180	31.0
	1170	29.9
	1160	28.1
	1150	26.6
	1140	25.0
(c) The $\alpha/(\alpha+\alpha_2)$ Transus	1130	38
	1130	35
	1125	30
	1100	25
(d) The $(\alpha+\alpha_2)/\alpha_2$ Transus	1120	38
	1118	35
	1105	30
	1100	29

TABLE X. HARDNESS DATA FOR HP-51 (1265°C/1h + IBQ)$_2$ AND COMPUTED HARDNESS NUMBERS (VHN, kg/mm^2, LOAD - 2.5 kg)

Diagonal Lengths, d, of Impression (μm)			
d1	d2	<d>	VHN (kg/mm^2)
162	161	161.5	178
164	163	163.5	173
161	164	162.5	176
165	162	163.5	173
161	161	161.0	179
160	159	159.5	182
159	158	158.5	185
174	178	176.0	150
165	168	166.5	167
152	153	152.5	199
158	158	158.0	186
165	163	164.0	172
159	158	158.5	185
153	156	154.5	194
157	155	156.0	190
154	157	155.5	192
155	155	155.0	193
161	161	161.0	179
Average			182± 9

TABLE XI. VICKERS DIAMOND PYRAMID HARDNESS NUMBERS (VHN, KG/MM^2) FOR ANNEALED-AND-QUENCHED Ti-Al ALLOYS

Heat Treatment including ice-brine quench (IBQ) (temp, °C/time, h)	Alloy Name															
	HP-30	HP-33	HP-37	HP-39	HP-41	HP-43	HP-45	HP-46	HP-47	HP-48	HP-49	HP-50	HP-51	HP-52	HP-55	HP-57
1365/1 + IBQ														233±22	326±18 303±14	258±4 261±15
1065/24 + 1365/1 + IBQ						426±34	425±29	451±34	405±21	348±29	287±11	265±15	184±16			
1315/1 + IBQ	463±18	402±21	383±28 370±31	421±53	463±39(1)									186±12	289±9	249±12
1315/4 + IBQ										293±12	264±9	251±12	174±22			
1315/24 + IBQ						458±54	454±23	384±30	303±15	259±9	240±7	354±34(2)	197±20			
1365/1 + 1315/1 + IBQ															293±12	253±12
1265/1 + IBQ	476±10	393±21	386±23 367±36										182±9	197±8	263±9	239±11
1265/8 + IBQ				442±28	446±51(1)	402±25	414±17	354±12	312±21	267±13	240±17	230±16				
1365/1 + 1265/1 + IBQ															270±8	262±15
1215/8 + IBQ				408±55	461±33(1)	418±21	333±14	319±31	294±16	251±9	237±14	224±14				
900/48 + 1215/2 + IBQ	436±11	436±13	383±35 368±45										189±11	196±15	272±12	252±26
1365/1 + 1215/2 + IBQ															264±8	258±10
1165/24 + IBQ				392±67	442±52(1)	401±31	319±21	287±13	270±10	245±14	233±15	207±17				
900/48 + 1165/4 + IBQ	427±13	409±29	380±35 351±31										180±10	185±6(3)	268±14	234±13
1365/1 + 1165/8 + IBQ															269±11	265±13
1065/24 + IBQ	368±10	362±60	291±43 295±36										180±9	184±10	261±10	278±30
1065/48 + IBQ				314±24	388±29(1)	347±20	312±21	288±12	285±9	247±10	236±12	217±16				
1365/1 + 1065/24 + IBQ															269±12	258±10
1065/24 + 900/500 + IBQ	380±14(4)	365±43	332±26 313±22 323±28	375±26(5)	438±35(5,6)	343±13	337±31	310±40	262±11	259±5(7)	278±6(7)	198±10	170±8	178±14	251±7	250±14
As-Cast	289±29(4)	370±13	358±60 348±64 341±57	407±41	447±51(1)	390±22	453±16	436±32	359±11	294±9	269±27	255±13	229±17	219±15	293±17	250±19 251±10

(1) All twinned.
(2) See Appendix B for further data.
(3) 1065/24 + 1165/4 + IBQ.
(4) All cracked.
(5) Only 900/500 + IBQ.
(6) Mostly twinned.
(7) Only 900/666 + IBQ.

FIGURE CAPTIONS

FIGURE 1. METHODS OF SAMPLE SUSPENSION IN MAGNETIC SUSCEPTIBILITY MEASUREMENTS: (a) triple measurement (coplanar) for isotropic (<0.2% relative anisotropy) samples. (b) (b) "Double Rotation" method for anisotropic samples ($\chi_2 \equiv \chi_2'$ is the "reference" direction)

FIGURE 2. COMPOSITION DEPENDENCE OF PARAMAGNETIC ANISOTROPY IN POLYCRYSTALLINE Ti-Al ALLOYS. In the composition ranges 30 to 41 at.% and 50 to 57 at.% (mostly single phase) average values are plotted; whilst in the range 43 to 49 at.% (for two-phase alloys) in which averages are meaningless, individual data are plotted (c.f. Table V)

FIGURE 3. TIE LINE CONCEPT IN DETERMINING EQUILIBRIUM PHASE BOUNDARIES. The method requires well-defined "single-phase curves" (insensitive to annealing temperature), in the construction of which some extrapolation may be necessary near the phase boundaries. $\chi(c)$ in the two-phase region is linear and is constructed either through datum points or on their "far sides" (with respect to some reference condition -- say as-cast)

FIGURE 4. THE ANNEALING-TEMPERATURE-INVARIANT (900-1315°C) SINGLE-PHASE $\chi(c)$ CURVES, FROM THE DATA OF TABLE VI

FIGURE 5. EXAMPLE OF TIE LINE CONSTRUCTION. $\chi(c)$ in Ti-Al for a pre-quench temperature of 1215°C. In this figure, the tie-line passes through or touches nearly all the datum points. The heavy lines are the invariant single-phase $\chi(c)$ curves. In the two-phase region relatively extensive migration of the points (circles) from the as-cast positions (diamonds) are noted.

FIGURE 6. SET OF $\chi(c)$ CURVES FOR THE TEMPERATURE RANGE 900 - 1315°C. Points to be noted are (a) at 1315°C no tie-lines can be constructed, suggesting that a horizontal transus exists at or near that temperature, above and below which the two-phase field is of markedly differing width (Figure 8). (b) From 1265°C through 900°C a systematic upward migration of tie-line data (circles) is noted, resulting in a steady shifting and changing of slope of the tie-line. (c) The systematics assisted tie-line construction; in addition the point of intersection of the tie-line with the γ-phase (right-hand) branch was forced as far to the right (high Al concentration) as the data and data-trend would permit, since recent TEM work had suggested that equilibrium single-phase γ would not exist below 50 at.% Al.

FIGURE CAPTIONS (Continued)

FIGURE 7. SET OF TIE-LINES FOR THE TEMPERATURE RANGE 900-1265°C, obtained by superimposing five curves from Figure 6. End-points lie on boundaries of the two-phase field

FIGURE 8. PORTION OF THE EQUILIBRIUM PHASE DIAGRAM FOR Ti-Al BASED ON MAGNETIC DATA (circles). The boundaries of the ($\beta + \alpha$) and ($\alpha_2 + \alpha$) fields were established previously by Blackburn [12] -- see Table IX. The magnetic work does not distinguish between $\alpha+\gamma$ and $\alpha_2+\gamma$

FIGURE 9. OPTICAL MICROGRAPHS OF HP-30 THROUGH HP-39 QUENCHED INTO ICED BRINE FROM THE TEMPERATURES INDICATED (°C). See Table III for heat treatment details. Magnification of the initial 6cm x 6cm micrographs, 200X.

FIGURE 10. OPTICAL MICROGRAPHS OF HP-41 THROUGH HP-46 QUENCHED INTO ICED BRINE FROM THE TEMPERATURES INDICATED (°C). See Table III for heat treatment details. Magnification of the initial 6cm x 6 cm micrographs, 200X.

FIGURE 11. OPTICAL MICROGRAPHS OF HP-47 THROUGH HP-50 QUENCHED INTO ICED BRINE FROM THE TEMPERATURES INDICATED (°C). See Table III for heat treatment details. Magnification of the initial 6cm x 6cm micrographs, 200X.

FIGURE 12. OPTICAL MICROGRAPHS OF HP-51 THROUGH HP-57 QUENCHED INTO ICED BRINE FROM THE TEMPERATURES INDICATED (°C). See Table III for heat treatment details. Magnification of the initial 6cm x 6cm micrographs, 200X.

FIGURE 13. COMPARISON OF THE RESULTS OF MAGNETIC SUSCEPTIBILITY WITH METALLOGRAPHY (Magnification of the initial 11cm x 8.5cm micrographs, 200X). The alloys HP-43 through HP-49 are two-phase and lie on the magnetic tie-line.

FIGURE 14. COMPARISON OF THE RESULTS OF MAGNETIC SUSCEPTIBILITY MEASUREMENTS WITH METALLOGRAPHY (Magnification of the initial 11cm x 8.5cm micrographs, 200X). Alloys HP-39 through HP-48 are equilibrium two-phase. The magnetic tie-line is uniquely drawn, as are the "single-phase curves". The deviation of the data points from the tie-line at the Al-rich end is an indication of incomplete equilibrium.

FIGURE CAPTIONS (Continued)

FIGURE 15. COMPARISON OF THE MICROSTRUCTURES OF HP-55 AND HP-57 PREPARED UNDER TWO HEAT TREATMENT CONDITIONS. In an attempt to achieve homogeneity (with minimal contamination) the second set of samples (right) was given an initial anneal of 1 hour at 1365°C. There is generally good agreement between the two sets of microstructures, suggesting that the precipitate, apparent in HP-55, is an equilibrium property of the alloy system.

FIGURE 16. TYPICAL SET OF HARDNESS DATA. No heat-treatment dependence was noted -- all the Hardness/Composition curves coinciding when superposed.

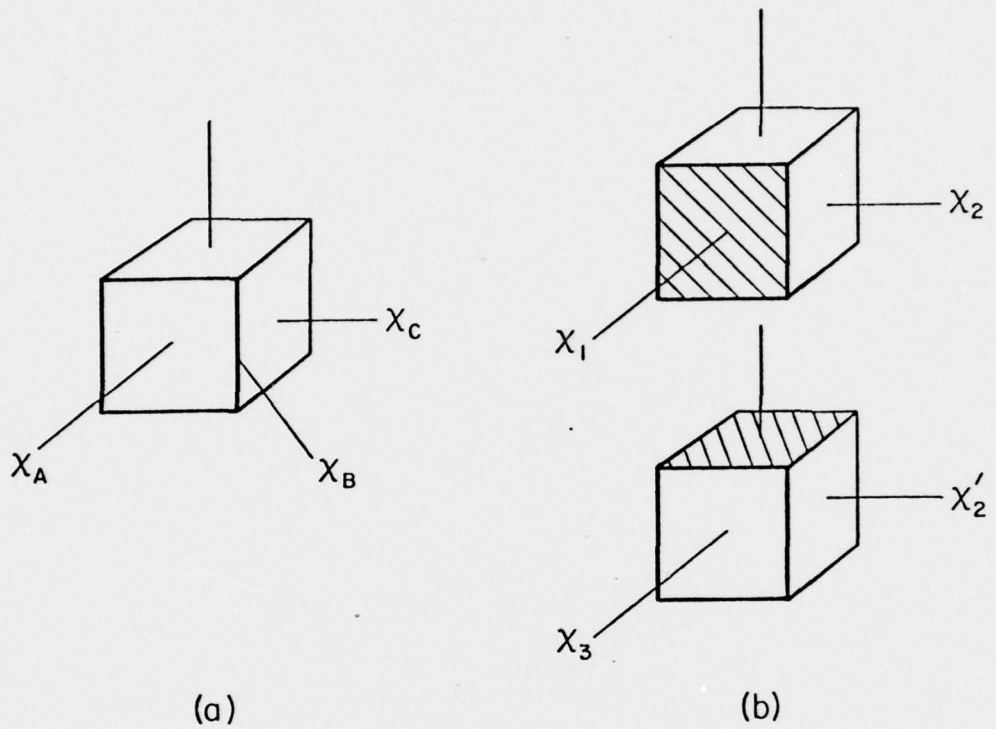

FIGURE 1. METHODS OF SAMPLE SUSPENSION IN MAGNETIC SUSCEPTIBILITY MEASUREMENTS: (a) triple measurement (coplanar) for isotropic (<0.2% relative anisotropy) samples. (b) (b) "Double Rotation" method for anisotropic samples ($\chi_2 \equiv \chi_2'$ is the "reference" direction)

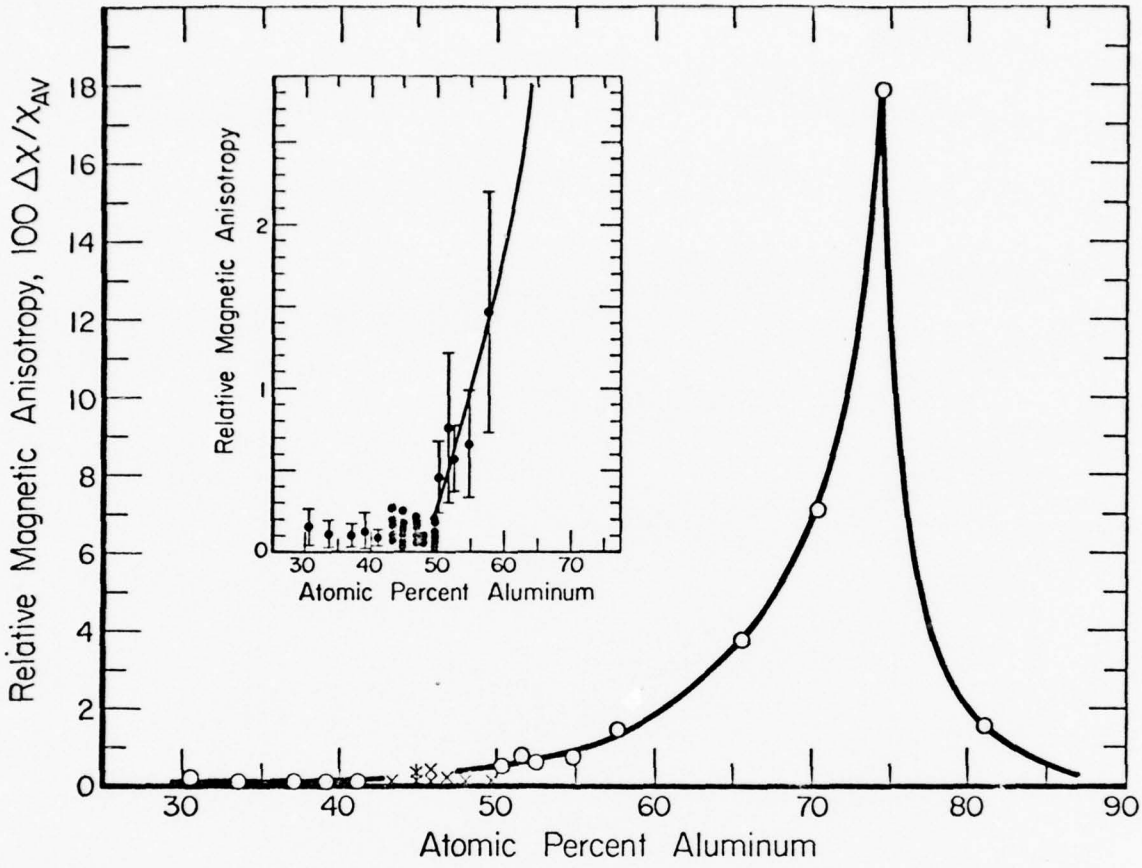

FIGURE 2. COMPOSITION DEPENDENCE OF PARAMAGNETIC ANISOTROPY IN POLYCRYSTALLINE Ti-Al ALLOYS. In the composition ranges 30 to 41 at.% and 50 to 57 at.% (mostly single phase) average values are plotted; whilst in the range 43 to 49 at.% (for two-phase alloys) in which averages are meaningless, individual data are plotted (c.f. Table V)

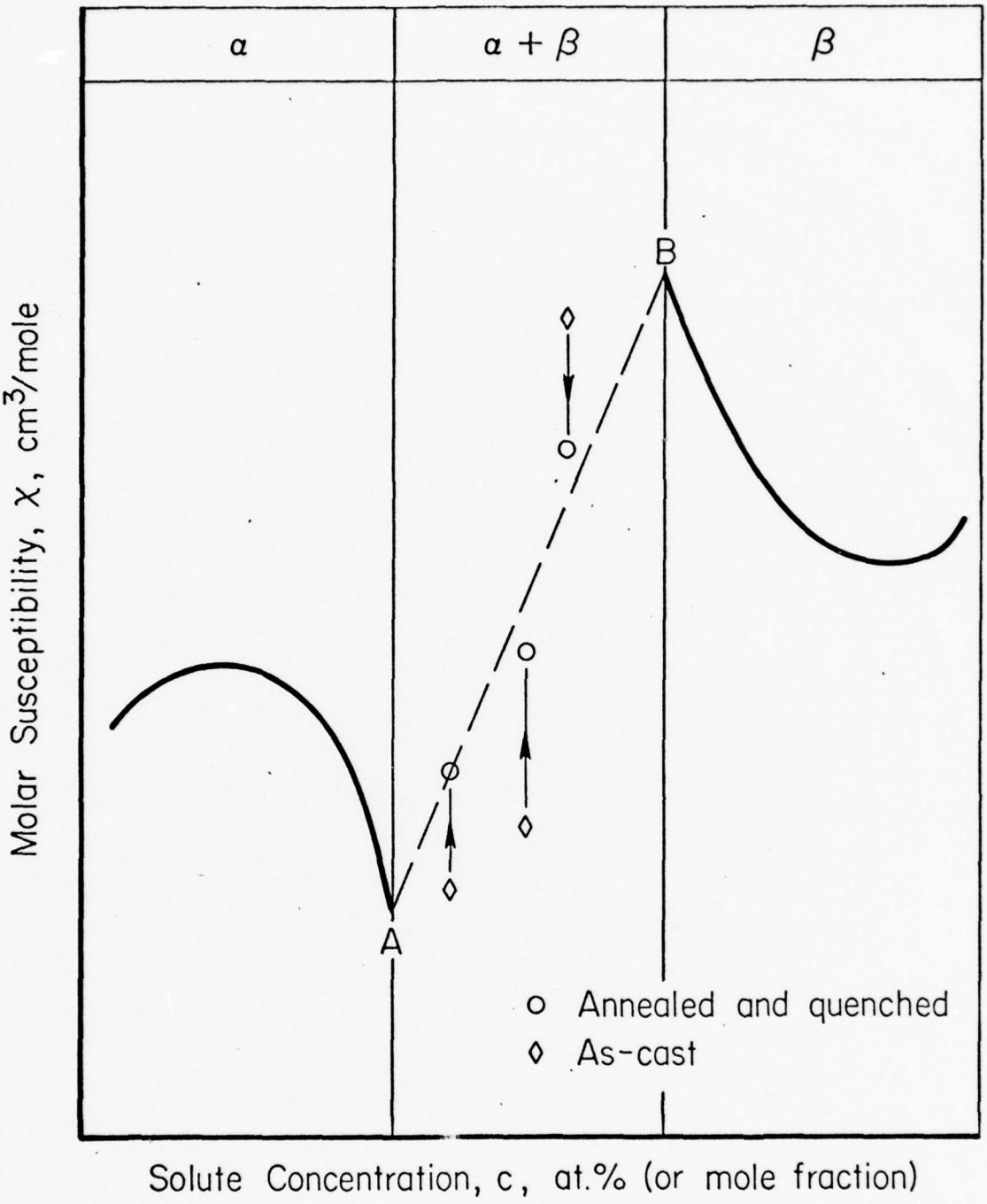

FIGURE 3. TIE LINE CONCEPT IN DETERMINING EQUILIBRIUM PHASE BOUNDARIES. The method requires well-defined "single-phase curves" (insensitive to annealing temperature), in the construction of which some extrapolation may be necessary near the phase boundaries. $\chi(c)$ in the two-phase region is linear and is constructed either through datum points or on their "far sides" (with respect to some reference condition -- say as-cast)

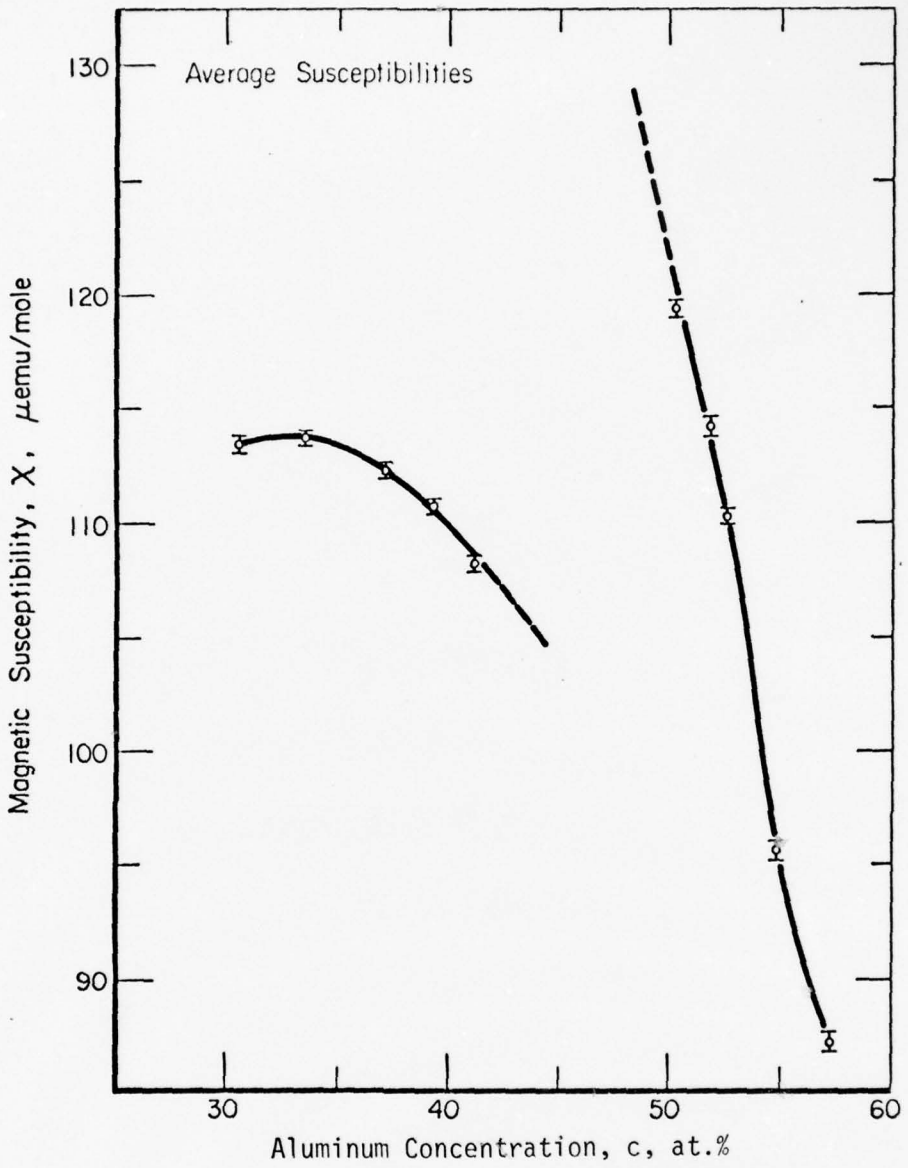

FIGURE 4. THE ANNEALING-TEMPERATURE-INVARIANT (900-1315°C) SINGLE-PHASE $\chi(c)$ CURVES, FROM THE DATA OF TABLE VI

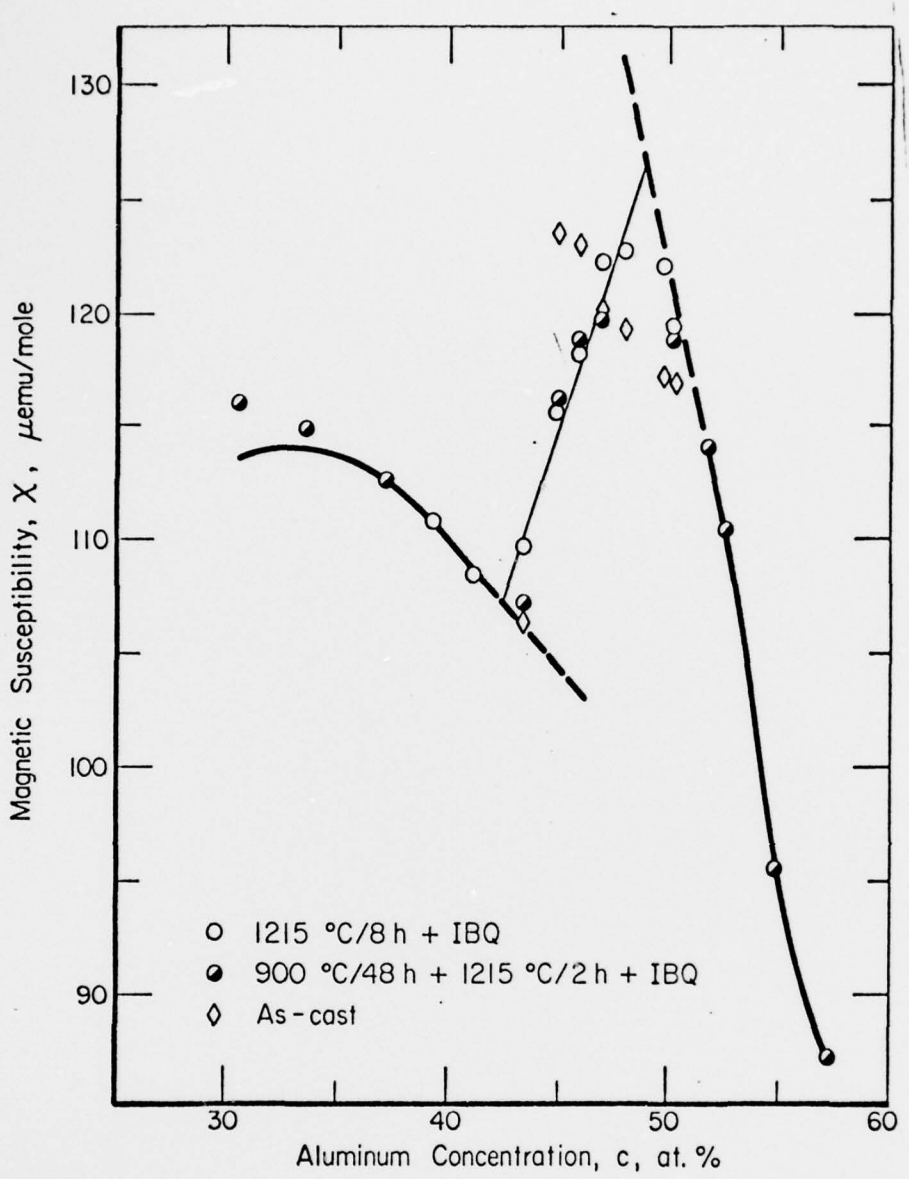

FIGURE 5. EXAMPLE OF TIE LINE CONSTRUCTION. $\chi(c)$ in Ti-Al for a pre-quench temperature of 1215°C. In this figure, the tie line passes through or touches nearly all the datum points. The heavy lines are the invariant single-phase $\chi(c)$ curves. In the two-phase region relatively extensive migration of the points (circles) from the as-cast positions (diamonds) are noted.

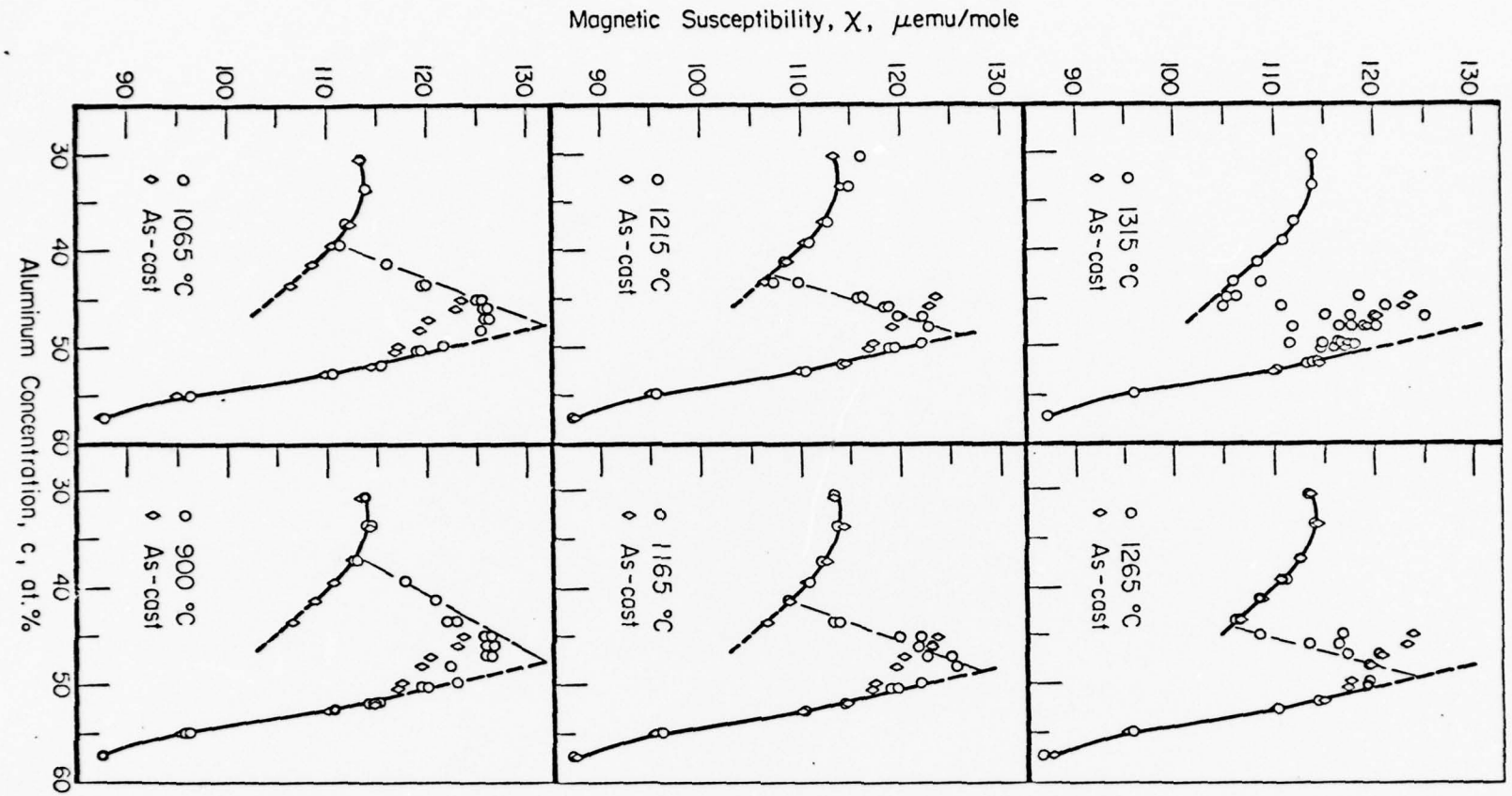

FIGURE 6. SET OF χ(c) CURVES FOR THE TEMPERATURE RANGE 900 - 1315°C. Points to be noted are (a) at 1315°C no tie-lines can be constructed, suggesting that a horizontal transus exists at or near that temperature, above and below which the two-phase field is of markedly differing width (Figure 8). (b) From 1265°C through 900°C a systematic upward migration of tie-line data (circles) is noted, resulting in a steady shifting and changing of slope of the tie-line. (c) The systematics assisted tie-line construction; in addition the point of intersection of the tie-line with the γ-phase (right-hand) branch was forced as far to the right (high Al concentration) as the data and data-trend would permit, since recent TEM work had suggested that equilibrium single-phase γ would not exist below 50 at.% Al.

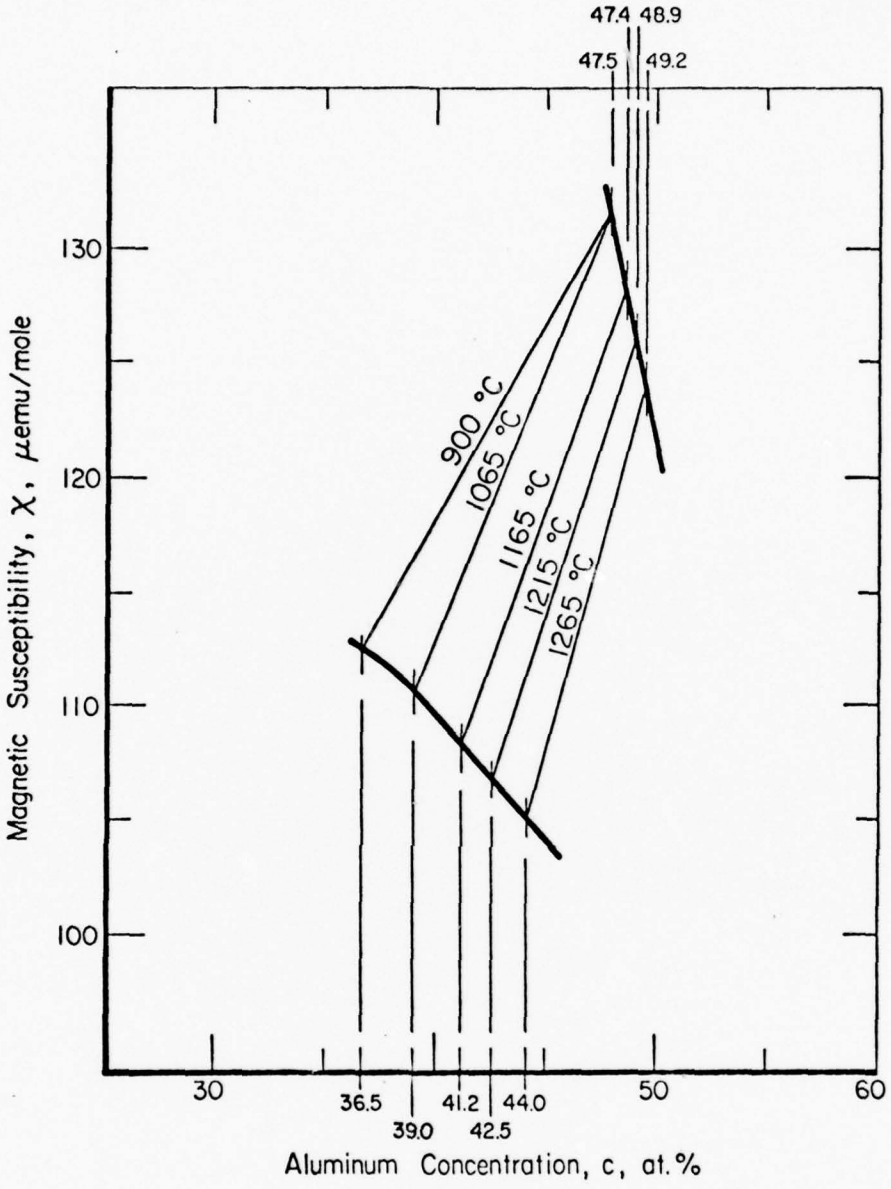

FIGURE 7. SET OF TIE-LINES FOR THE TEMPERATURE RANGE 900-1265°C, obtained by superimposing five curves from Figure 6. End-points lie on boundaries of the two-phase field

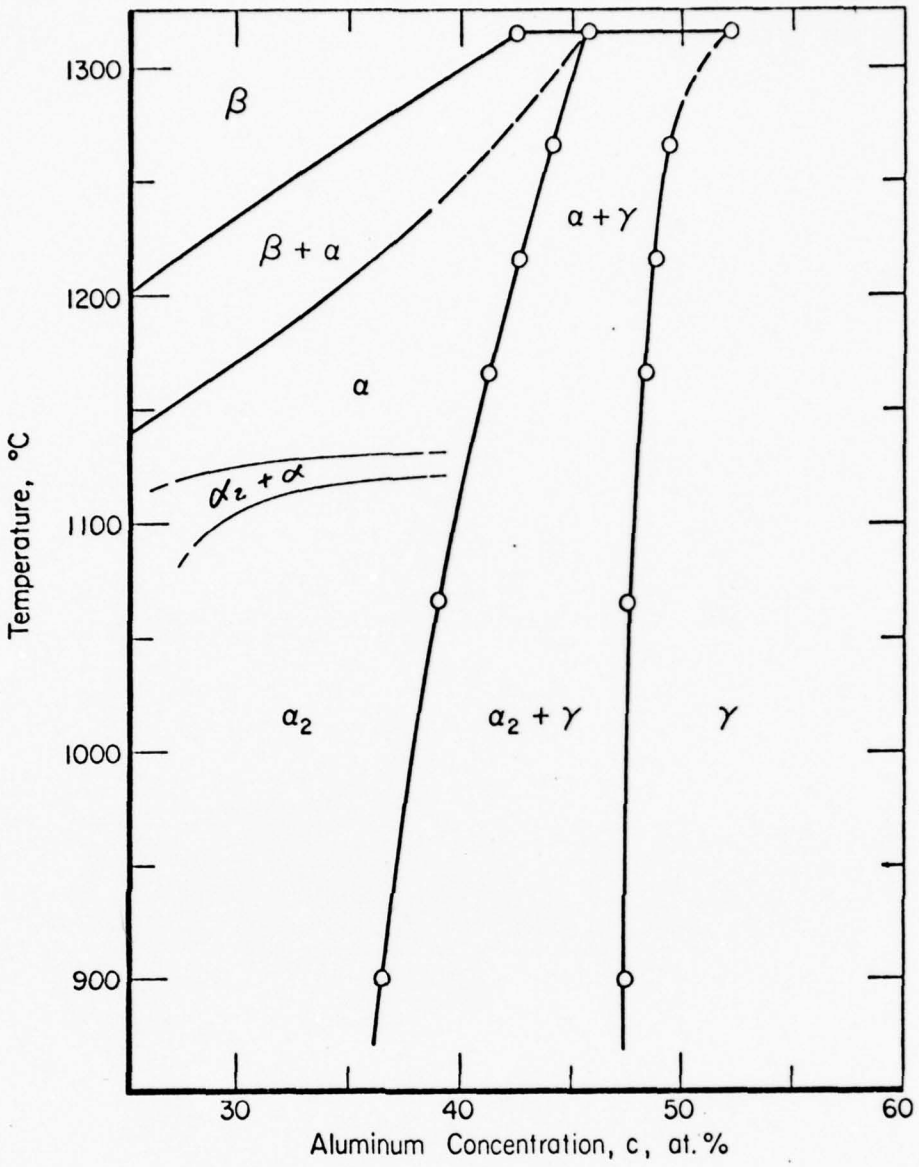

FIGURE 8. PORTION OF THE EQUILIBRIUM PHASE DIAGRAM FOR Ti-Al BASED ON MAGNETIC DATA (circles). The boundaries of the (β + α) and (α_2 + α) fields were established previously by Blackburn [12] --- see Table IX. The magnetic work does not distinguish between $\alpha+\gamma$ and $\alpha_2+\gamma$

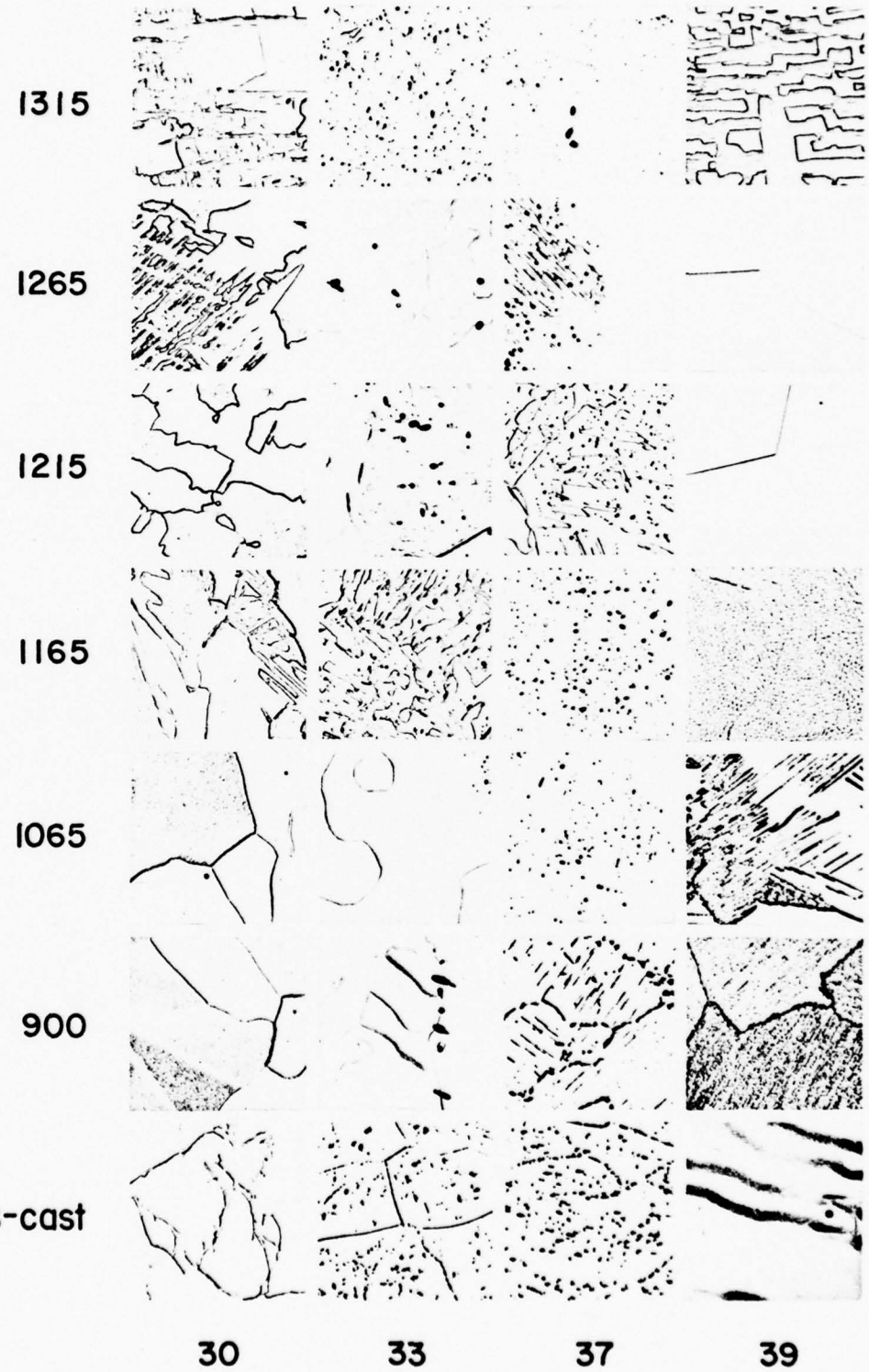

FIGURE 9. OPTICAL MICROGRAPHS OF HP-30 THROUGH HP-39 QUENCHED INTO ICED BRINE FROM THE TEMPERATURES INDICATED (°C). See Table III for heat treatment details. Magnification of the initial 6cm x 6cm micrographs, 200X.

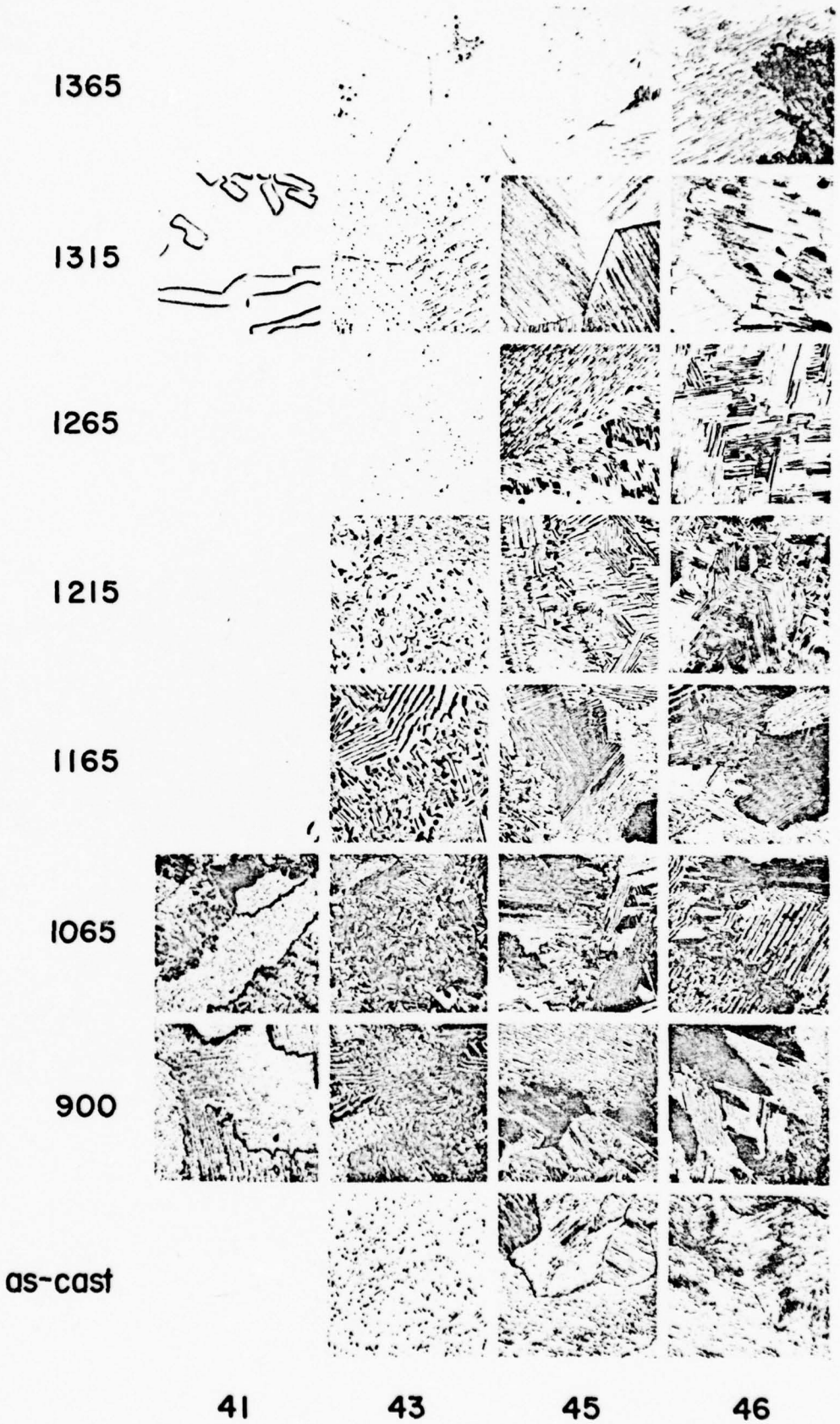

FIGURE 10. OPTICAL MICROGRAPHS OF HP-41 THROUGH HP-46 QUENCHED INTO ICED BRINE FROM THE TEMPERATURES INDICATED (°C). See Table III for heat treatment details. Magnification of the initial

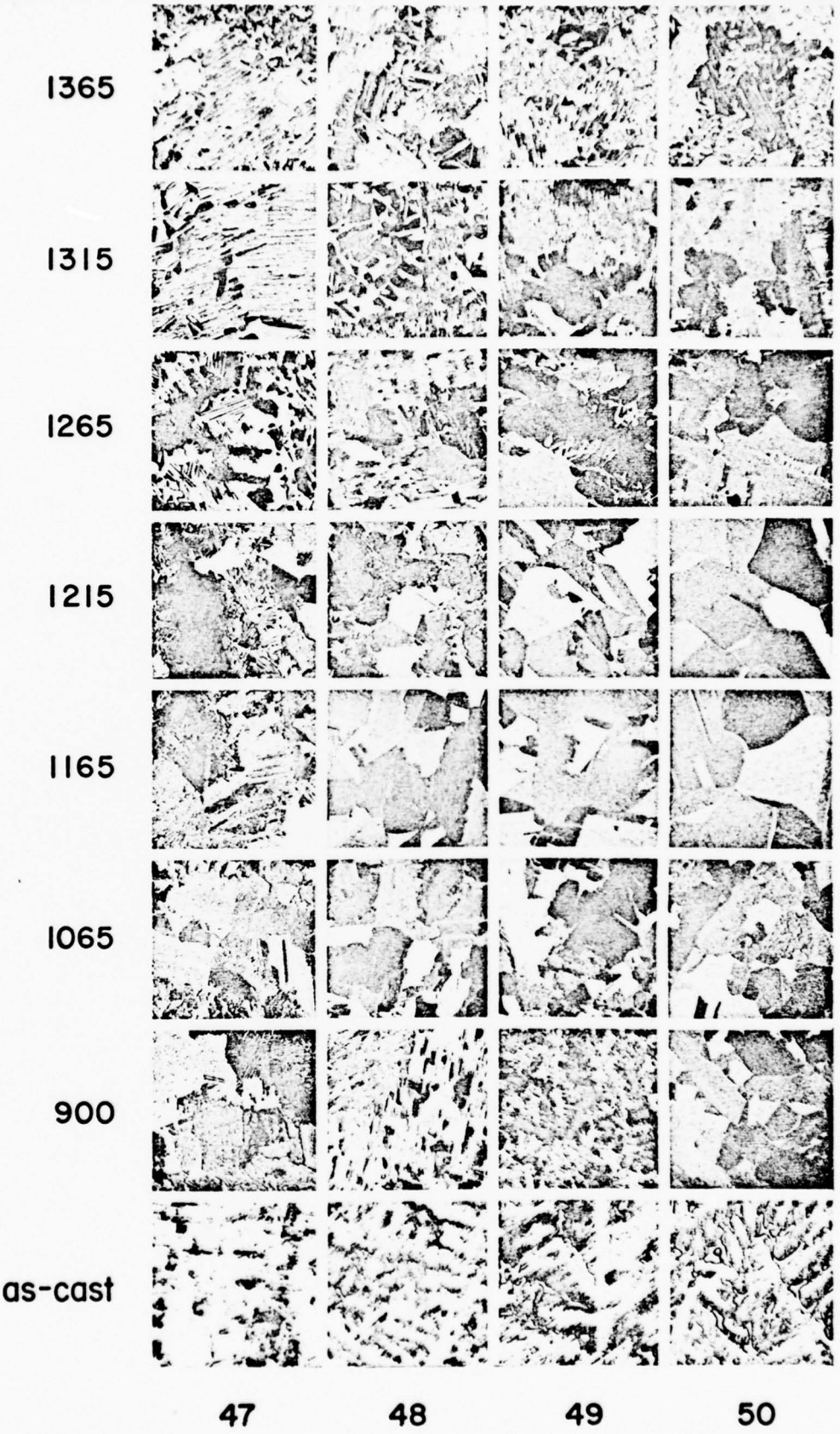

FIGURE 11. OPTICAL MICROGRAPHS OF HP-47 THROUGH HP-50 QUENCHED INTO ICED BRINE FROM THE TEMPERATURES INDICATED (°C). See Table III for heat treatment details. Magnification of the initial 6cm x 6cm micrographs, 200X.

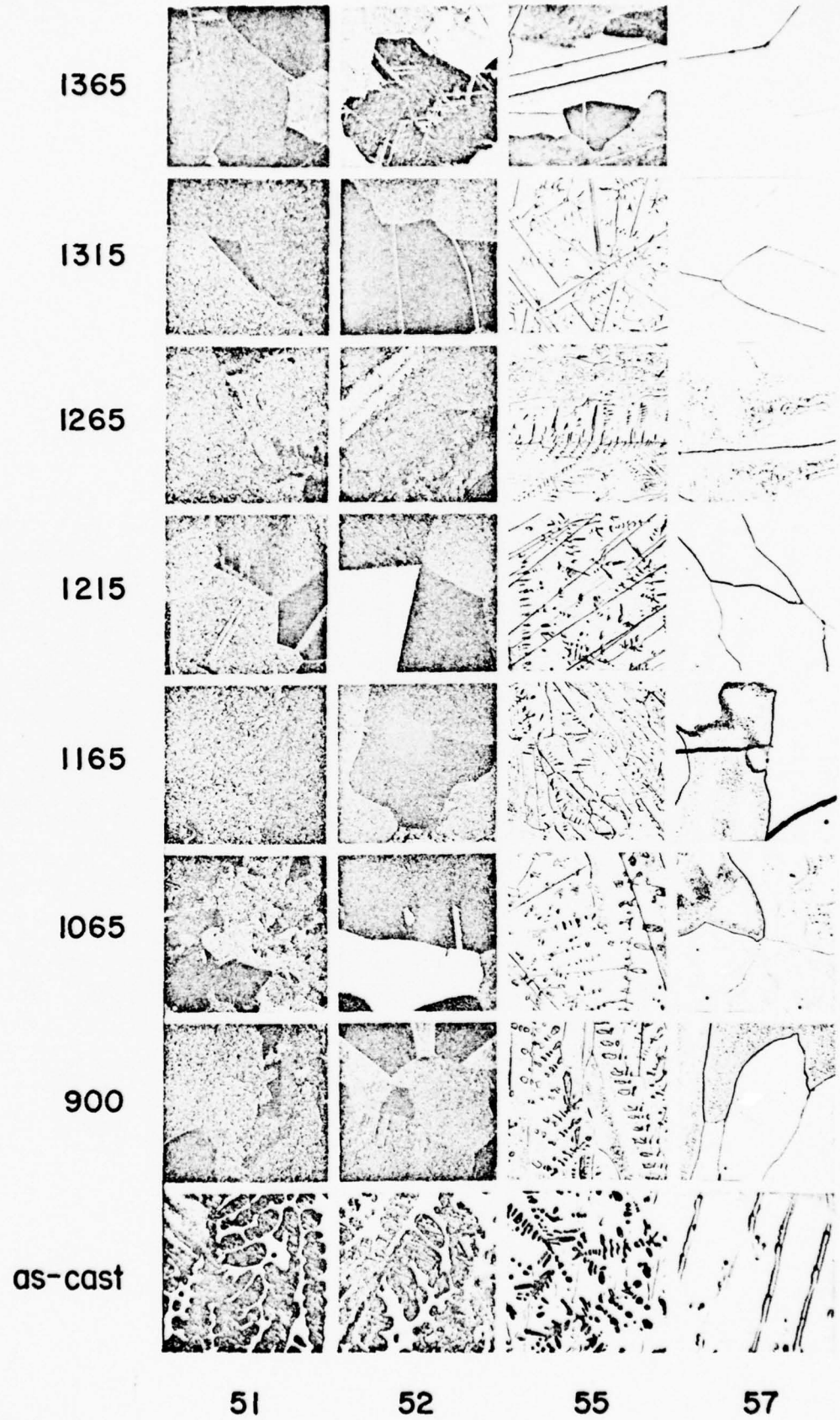

FIGURE 12. OPTICAL MICROGRAPHS OF HP-51 THROUGH HP-57 QUENCHED INTO ICED BRINE FROM THE TEMPERATURES INDICATED (°C). See Table III for heat treatment details. Magnification of the initial 6cm x 6cm micrographs, 200X.

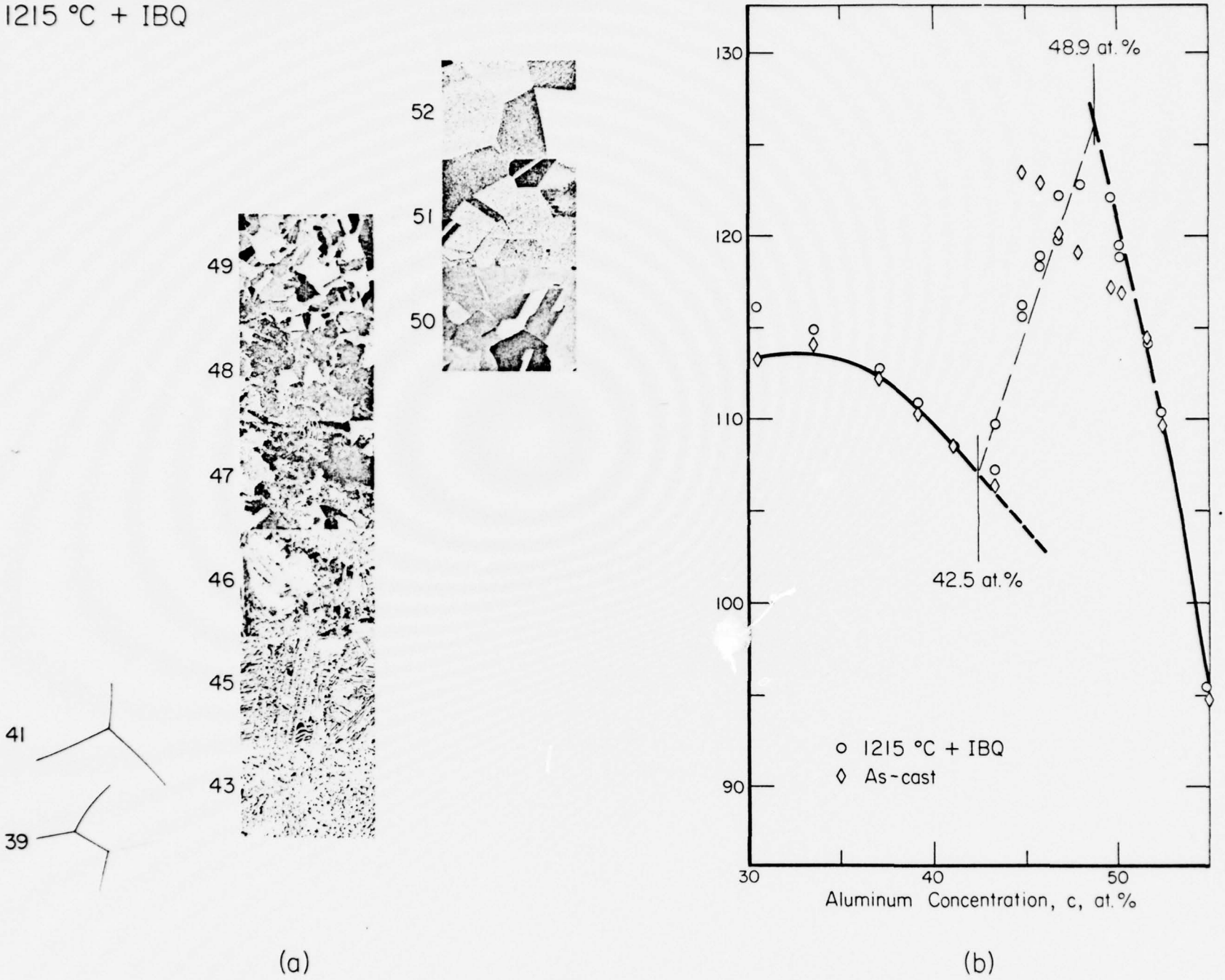

FIGURE 13. COMPARISON OF THE RESULTS OF MAGNETIC SUSCEPTIBILITY WITH METALLOGRAPHY (Magnification of the initial 11cm x 8.5cm micrographs, 200X). The alloys HP-43 through HP-49 are two-phase and lie on the magnetic tie-line.

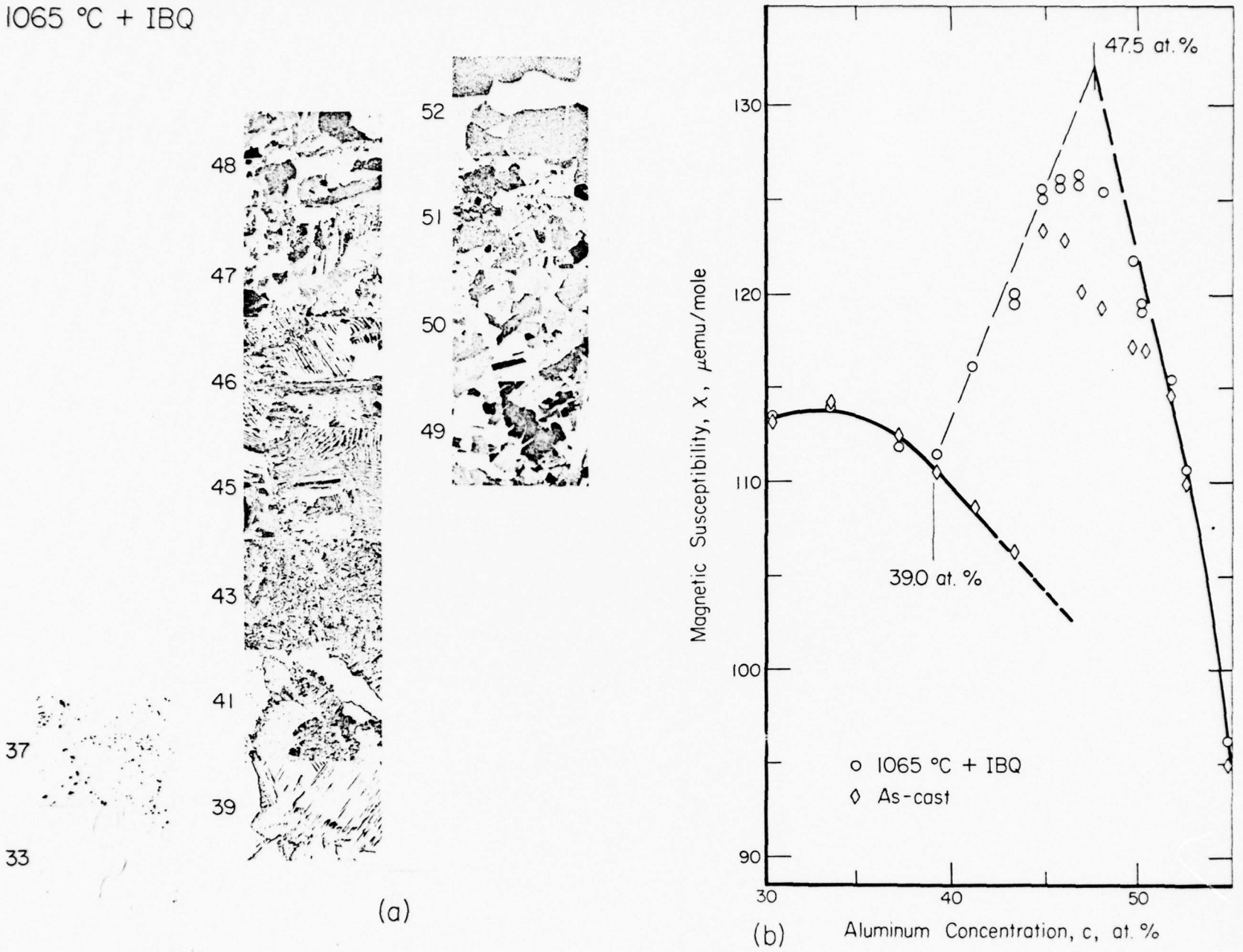

FIGURE 14. COMPARISON OF THE RESULTS OF MAGNETIC SUSCEPTIBILITY MEASUREMENTS WITH METALLOGRAPHY (Magnification of the initial 11cm x 8.5 cm micrographs, 200X). Alloys HP-39 through HP-48 are equilibrium two-phase. The magnetic tie-line is uniquely drawn, as are the "single-phase curves". The deviation of the data points from the tie-line at the Al-rich end is an indication of incomplete equilibrium

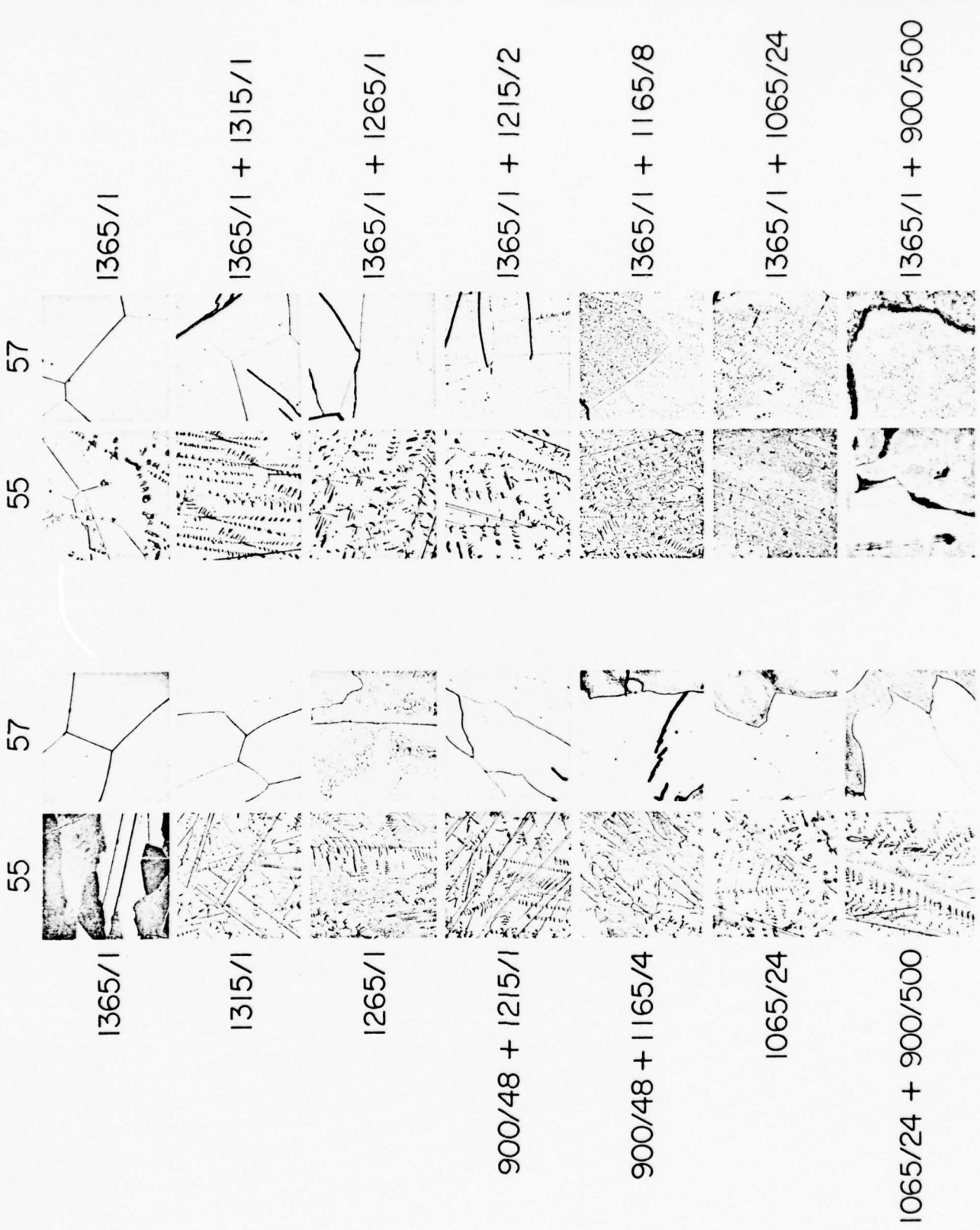

FIGURE 15. COMPARISON OF THE MICROSTRUCTURES OF HP-55 AND HP-57 PREPARED UNDER TWO HEAT TREATMENT CONDITIONS. In an attempt to achieve homogeneity (with minimal contamination) the second set of samples (right) was given an initial anneal of 1 hour at 1365°C. There is generally good agreement between the two sets of microstructures, suggesting that the precipitate, apparent in HP-55, is an equilibrium property of the alloy system.

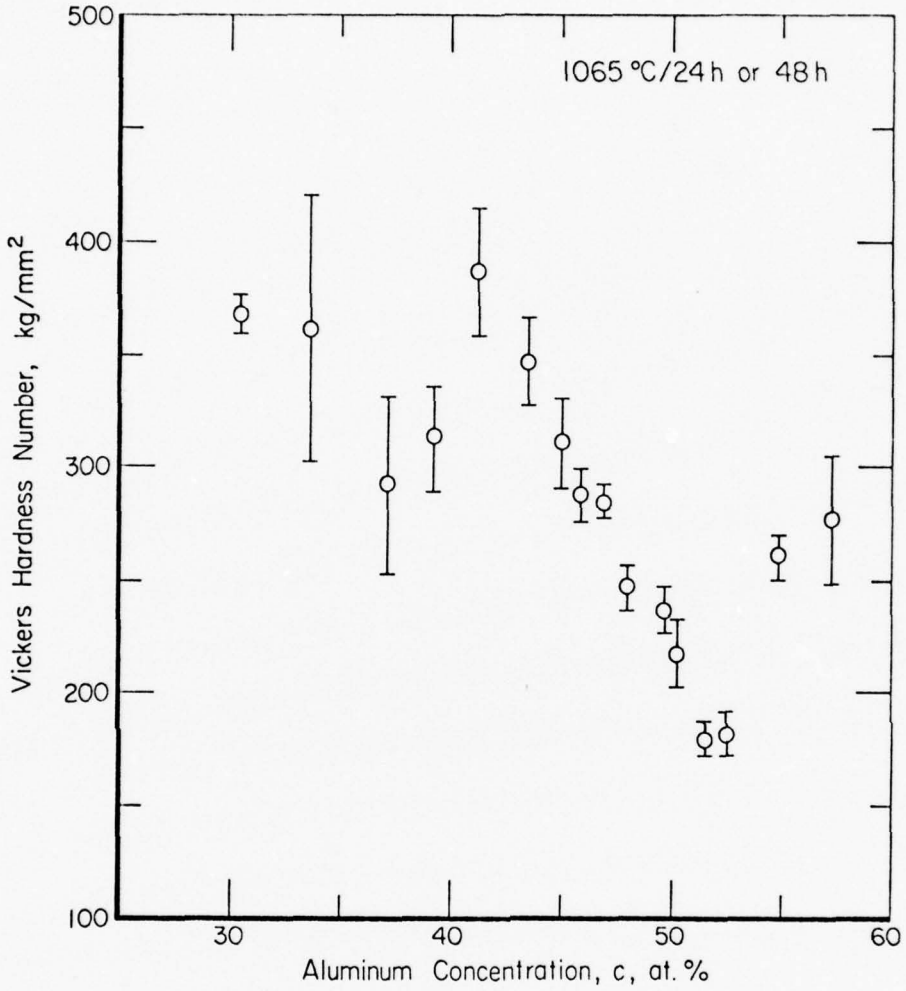

FIGURE 16. TYPICAL SET OF HARDNESS DATA. No heat-treatment dependence was noted -- all the Hardness/Composition curves coinciding when superposed.

APPENDIX A

CHEMICAL ANALYSES OF STARTING MATERIALS

Typical impurity contents, according to information provided by the vendors, of the titanium and aluminum starting material are:

Ti (Titanium Metals Corporation (wgt PPM):

N,30; C,100; Cl,590; H,30; O,410; H_2O,80; Si,20; Na,220; Fe,< 10; Cr,60; Mo, < 10; Al, <10; Sn, < 200; Mn, < 10; Ni,50; Cu, < 10; Mg, < 10; Zr, < 10; B, < 10.

Al (A. D. Mackay, Inc.) (wgt. pct):

Ag, 0.2;	Ca, 0.2;	Cu, 2.0;	Fe, 1.0;
Mg, 0.2;	Si, 2.0.		

APPENDIX B

HEAT TREATMENT CONTAMINATION
Ti-Al (50 at.%)

As mentioned in Section 2.2 great care was taken to prevent sample contamination during heat treatment, the duration of which was kept as short as possible consistent with a reasonable approach to equilibrium. The importance of using minimal heat treatment times, especially at elevated temperatures, is illustrated by the following experience with HP-50 and neighboring alloys.

Table B-I compares the susceptibilities of alloys HP-48 through HP-51 as quenched from 1315°C after annealing times of 24, 4, and 1 h, in a study of equilibration kinetics. A surprising result of the 24 h anneal was the occurrence of a sharp dip in the susceptibility at HP-50 (Figure B-1). The minimum seemed at first to be an intrinsic property of 1315°C-equilibrated HP-50 since it was reproduced in a second completely independent set of experiments (Column 2, Table B-1). On the other hand, as shown in Table B-II, the 1265°C and 1365°C properties could not be recovered by subsequent appropriate annealing. Such irreversible, although reproducible, behavior could only result from sample contamination. That this was so was confirmed by repeating the heat treatments on fresh groups of alloys, using shorter annealing times such as 4 h or 1 h (Columns 3, 4, and 5, Table B-I).

Other properties of the 24 h-annealed HP-50 were a pronounced resistance to attack by the usual etchants, as evidence by the micrographs of Figure B-2, and an anomalously high hardness value (Table B-III).

Whether the contaminant was oxygen or nitrogen has not been determined. The remarkable features of these observations are: (a) that serious contamination should occur at all in view of the elaborate precautions taken to avoid it (good vacuum, continuous gettering, and Ta sample wrapping); and (b) that it should be so selective with respect to HP-50. We are convinced that the observation is more than just artifactual, and that what seems to be an anomalously high solubility of interstitials in stoichiometric TiAl, warrants special investigation.

TABLE B-I. INFLUENCE OF ANNEALING TIME ON THE SUSCEPTIBILITIES OF ALLOYS NEAR HP-50 -- RESULTS OF FIVE INDEPENDENT ENCAPSULATIONS

Sample Name	Average Chemical Composition (at.%Al)	Susceptibilities (μ emu/mole) after annealing at 1315°C for the times				
		24 h		4 h		1 h
		1	2	3	4	5
HP-48	37.8_5	120.1	111.8	116.3	117.6	117.9
HP-49	37.5_1	117.8	111.5	114.8	116.3	116.4
HP-50	37.4_1	103.7	103.5		115.8	114.5
HP-51	37.0_9	113.6	114.0		114.4	113.1

TABLE B-II. SUSCEPTIBILITY OF HP-50 AFTER ANNEALING AT 1315°C FOR 24 h FOLLOWED BY TREATMENTS SPECIFIED

Heat Treatment (Temp. °C/Time, h)	Magnetic Susceptibility (μ emu/mole)	
	Measured Value	Expected Value after Tables IV and VI
1315/24	103.4	
1315/24 +1265/1	103.3	119.3
1315/24 +1265/1 +1265/24	103.1	119.3
1315/24 +1265/1 +1265/24 +1365/1	104.2	114.7

TABLE B-III. MICROHARDNESS OF ALLOYS NEAR HP-50 AFTER HEAT TREATMENT FOR VARIOUS TIMES AT 1315°C

Sample Name	Microhardness (kg/mm^2) after annealing at 1315°C for the times specified	
	24 h	4 h
HP-48	259 ± 9	293 ± 12
HP-49	240 ± 7	264 ± 9
HP-50	354 ± 34	251 ± 12
HP-51	197 ± 20	174 ± 22

FIGURE CAPTIONS

FIGURE B-1. SUSCEPTIBILITY COMPOSITION DEPENDENCE OF SAMPLES QUENCHED FROM 1315°C. The considerable scatter in the data suggests the existence of a horizontal transus at 1315°C and that equilibration has taken place on either side of it. In fact a pair of tie-lines can be discerned. The point to be emphasized here is the anomalous, and reproducible, minimum that occurs in HP-50 under the 1315°C/24 h heat treatment, but which does not occur for a shorter heat treatment time. The corresponding microstructures are given in Figure B-2.

FIGURE B-2. OPTICAL MICROSTRUCTURES OF Ti-Al (50 at.%) AFTER ANNEALING AT 1315°C for 24h and 4h, respectively. The anomalous magnetic susceptibility and hardness are associated with the 24h anneal, and are presumably due to an especially high propensity towards interstitial contamination for that particular alloy.

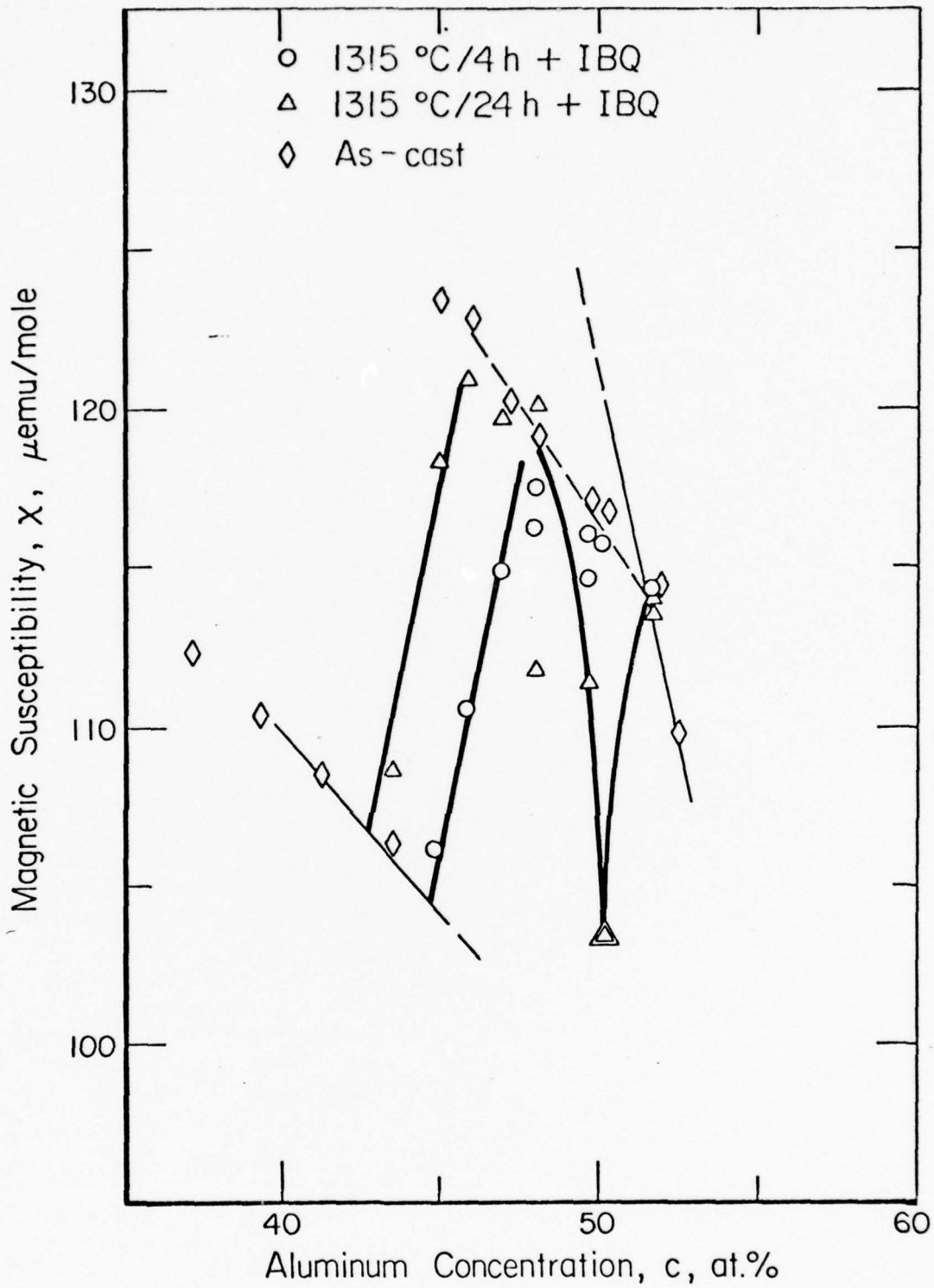

FIGURE B-1. *SUSCEPTIBILITY COMPOSITION DEPENDENCE OF SAMPLES QUENCHED* FROM 1315°C. The considerable scatter in the data suggests the existence of a horizontal transus at 1315°C and that equilibration has taken place on either side of it. In fact a pair of tie-lines can be discerned. The point to be emphasized here is the anomalous, and reproducible, minimum that occurs in HP-50 under the 1315°C/24 h heat treatment, but which does not occur for a shorter heat treatment time. The corresponding microstructures are given in Figure B-2.

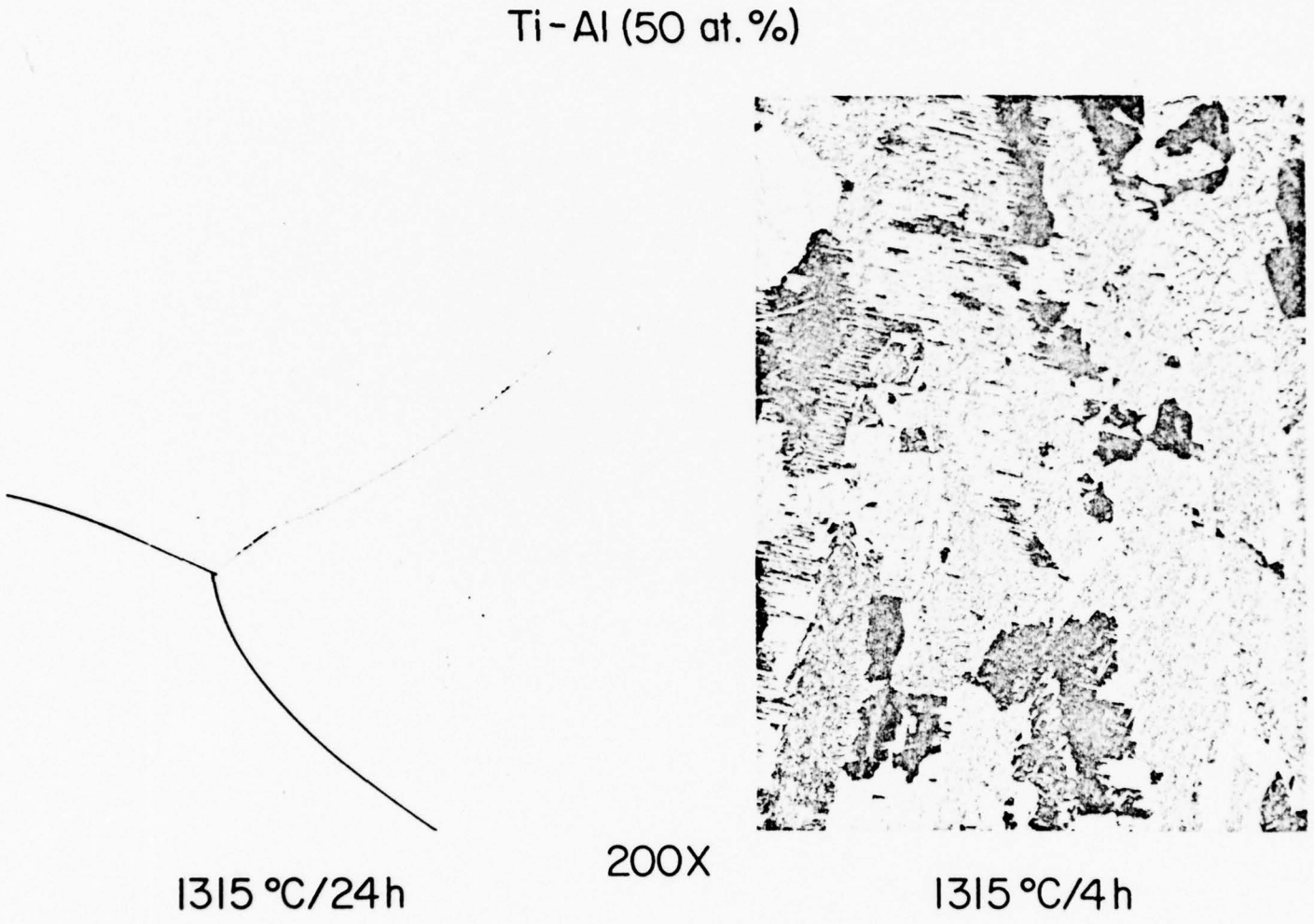

FIGURE B-2. OPTICAL MICROSTRUCTURES OF Ti-Al (50 at.%) AFTER ANNEALING AT 1315°C for 24h and 4h, respectively. The anomalous magnetic susceptibility and hardness are associated with the 24h anneal, and are presumably due to an especially high propensity towards interstitial contamination for that particular alloy.

APPENDIX 2

AUSTENITIC STAINLESS STEELS AS MAGNETIC TRANSITION METAL ALLOYS

E. W. Collings
Battelle Memorial Institute
Columbus, OH 43201

and

H. W. King
Dalhousie University
Halifax, N.S. B3H 3J5, Canada

ABSTRACT

The magnetic properties of stainless steels are considered within the context of transition metal alloy magnetism. A review of the magnetic properties of binary transition metal alloys, with particular emphasis on spin glasses, superparamagnetism, and mictomagnetism, is followed by a discussion of some magnetic property measurements on Fe-Cr-Ni and Fe-Cr-Ni-Mn. The paper continues with a phenological treatment of magnetism, microstructure, and lattice stability in Fe-Cr-Ni research alloys and commercial stainless steels, and concludes with some suggestions for future research.

1 INTRODUCTION

The behaviors of stainless steels and related alloys in unusual environments, such as high neutron fluences, very low temperatures and high magnetic fields, are becoming increasinly important for many present-day applications of these versatile materials. Accordingly, it is necessary to learn about the magnetic properties that accrue from compositional specifications which were originally formulated to give properties such as corrosion resistance, mechanical strength, toughness and weldability.

An extensive literature deals with the magnetic and calorimetric properties of binary systems based on iron and nickel, particularly within the composition range containing the transition to ferromagnetism. An even more extensive literature deals with the properties of dilute binary alloys with magnetic solutes, the interactions among which are the fundamental underpinnings of the theory of more concentrated systems. This literature is reviewed with particular emphasis on the relationship between spin glass and the magnetic states of superparamagnetism and mictomagnetism.

The magnetic properties of Fe-Cr-Ni alloys are more complicated than those of the binary systems and must be considered in terms of several simultaneous operative effects, one of these being the microstructure of the alloy. In considering these effects, attention is focused on the magnetic properties of stainless steels within the context of transition metal magnetism. Phenomenological treatments of magnetic transitions are also considered for a comprehensive matrix of Fe-Cr-Ni research alloys, in addition to commercial stainless steels.

2 MAGNETIC PROPERTIES OF BINARY TRANSITION METAL ALLOYS

In studying magnetic alloy systems one must be concerned with the EXISTENCE of magnetic moment, and with INTERACTIONS between moment carriers.

Dilute Alloys -- Local Moments

Important contributions to the theory of localized moment existence in dilute systems were made in the 1950's and 60's by Friedel [1], Anderson [2], Kondo [3], and many others. In describing magnetic effects

temperature is an important parameter. At sufficiently high temperatures local moment systems tend to obey a Curie law, while at low temperatures several alternative effects, one of which is the well-known Kondo effect [3], may take place. The entire picture of moment formation was beautifully summarized by Coles in a contribution to the Michigan 1972 Summer School on Alloys [4], and by others [5]; and key papers are frequently referred to in the introductions to research articles.

Magnetic spins generally interact; except when they are sufficiently separated, or at high temperatures when thermal effects dominate. Interactions lead to ordering of one kind or another. The commonest forms of long-range order are ferromagnetic (↑↑↑↑↑↑) and antiferromagnetic (↑↓↑↓↑↓↑↓). However, in recent years the idea of magnetic condensation (so-called "freezing") to a state of <u>long-range disorder</u> has been attracting considerable attention. The concept of spin-glass alloys has been discussed by Edwards and Anderson [6], Fischer [7], Mydosh [8], and many others. The random freezing of spins manifests itself as a sudden Mossbauer hyperfine splitting [9] and by a sharp cusp in the zero-field magnetic susceptibility temperature dependence [10]. Edwards [11] has explained how a spin-glass condensation can, in principle, arise when spins on randomly distributed sites are coupled by interactions whose sign (i.e., ferromagnetic or antiferromagnetic) depends on spacial separation. In an over-simplified spin-disorder model, although spins have random orientations both above some critical temperature, T_g (i.e., in the paramagnetic region) and below it (spin glass state); the two states differ in that below T_g the spins are locked into their random directions by $J\tilde{s}_i.\tilde{s}_j$ interactions, whilst above it no preferences exist

and they are free to respond paramagnetically to an applied field. In the vicinity of T_g, a strong applied magnetic field tends to perturb the $J\tilde{s}_i.\tilde{s}_j$ interaction and results in a severe broadening of the transition (*i.e., of the cusp in* $\chi(T)$). A local maximum in $\chi(T)$ at low temperatures for dilute and "almost dilute" alloys has long been noted. Very early work (for example that of Kittel and co-workers [12]) offered a heuristic interpretation in terms of conventional two-sublattice antiferromagnetism. It was not until Cannella and Mydosh (e.g., [13]) conducted susceptibility measurements in vanishingly small magnetic fields that the sharpness of the transition, and its importance in terms of a "spin glass" condensation was fully recognized. Interested readers are referred to Reference [13] for a comprehensive survey of previous work.

On the theoretical side, the spin-glass state has been discussed in terms of mean-field theory [6,7,14], and cluster theory [15,16, 17] which is based on a postulated existence of rigid clusters of spins, and the "cluster-percolation" approach [18,19]. These theories as they stand have found difficulty in justifying the observed existence of a sharp magnetic susceptibility anomaly, with a rounded specific heat anomaly at a somewhat higher temperature. However, a recent paper [20] which describes a simple model for spin glasses, and incorporates both mean-field-theoretical and cluster approaches, is in accord with the magnetic and calorimetric observations.

There was a time when it was believed that spin glass behavior was confined to interactions between localized moments in dilute alloys, and that superparamagnetism in concentrated alloys resulted

in "mictomagnetism" (a cluster equivalent of a spin glass by the above definition) at sufficiently low temperatures. Currently, there is thought to be not such a clear-cut distinction between the magnetic interactions which occur in experimentally-viable "dilute alloys" and those in the more concentrated ones for which nearest-neighbor-type clustering is expected from both statistical and thermodynamic grounds.

Concentrated Binary Alloys -- Clustering, Superparamagnetism and Mictomagnetism

Included in this category are alloys of pairs of transition elements such as Fe-Ni, Fe-Mn, etc.; or those of a transition element with a non-transition element, for example Fe-Rh, Ni-Cu, etc.

In the latter category Ni-Cu stands out as a system of perennial interest both with regard to the compositional transition to the ferromagnetic state through a regime of magnetic clustering, to the magnetic and calorimetric properties of the paramagnetic state. The compositional dependence of ferromagnetism in Cu-Ni was for many years a bulwark of the rigid-band model [21]. However, as a result photo-emission studies [22], theoretical work based on the CPA method [23] and more recent work on angular-resolved photo-emission in association with CPA theory [24] it turns out that a better qualitative description is in terms, more-or-less, of two individual bands almost as if the alloy were a mechanical mixture of Cu and Ni atoms. It is uncertain to what

extent band theory can come to grips with clustering in Cu-Ni, an effect which is essential to descriptions of its paramagnetic behavior.

(a) Clustering and Superparamagnetism

In extremely dilute alloys one is, in principle, interested in the properties of the isolated solute atom in response to an environment supplied by an infinite matrix. In concentrated alloys this situation no longer holds and clustering effects, among others, must be considered. Clustering in an alloy (say A-B) is of course the tendency for A-A and B-B associations which can occur either statistically, through energetically-motivated nearest-neighbor associations, or through appropriate long-range interactions. It can result in the formation of giant moments--groups of several tens of atoms with parallel spins. Magnetic interactions within the context of an ideal random solid solution may also lead to giant moments; but in either case the stage is set for the phenomenon of superparamagnetism, which relies on "large" values of the quotient $\mu H/kT$ (wherein H is magnetic field; T, temperature; k, Boltzmann's constant; and μ is the magnetic moment of the atom or cluster of atoms). There are numerous examples of superparamagnetic alloys -- many solid solutions of Mn, Fe, Co, Ni in noble metals [25]; and related alloys such as $Ni_{0.63}Rh_{0.37}$ [26]*. Typical magnetization (σ) versus field (H) relationships are indicated in Figure 1 which shows that σ seems to consist of a linear term (constant χ) plus a possible Langevin-like component**

---

*For the sake of accuracy it should, however, be stated that although Ni-Cu (Ni + noble metal) and Ni-Rh appear to be analogous, their detailed magnetic properties are quantitatively very different .

**Since $\lim_{x\to 0} L(x) = \lim_{x\to 0}(\coth x - 1/x) = 1/3$, the small $\mu H/kT$ limit of the Langevin relationship is the Curie law.

Indeed a relationship of the form

$$\sigma = \chi \cdot H + \mu \cdot n \cdot L(\mu H/k[T-\theta]) \quad , \qquad (1)$$

is frequently found to be an adequate simple description of the higher-temperature magnetic behavior [27]. At low temperatures, when clusters begin to interact, the magnetic behavior of "simple" concentrated alloy systems can be very complicated. Both ferromagnetic and antiferromagnetic clustering interactions may occur simultaneously, an effect which gave rise to the name "mictomagnetism" [18,27].

(b) Mictomagnetism

A mictomagnet is a concentrated spin glass; although for both dilute and concentrated alloys the temperature, T, at which the transition from the paramagnetic (or superparamagnetic) to the "frozen-disordered-spin" state takes place, seems always to be referred to as the (spin) glass (transition) temperature. The 1975 paper by Smith [18] together with a more recent one [19] present important discussions on the characteristics of spin glasses and mictomagnets and an interpretation of the magnetic interactions which take place within them. Another useful recent theoretical paper is by Levin et al [20]. A key experimental review paper which categorizes the magnetic characteristics of the mictomagnetic state and lists the numerous binary alloy systems which exhibit them is of course the classical work by Beck [27], to whom the term 'mictomagnetism' itself is due.

As has been indicated, mictomagnetic alloys are supposed to be superparamagnetic above some critical temperature, T_g; and on cooling through T_g freeze into a system of randomly-orientated large moments. The

clusters are constructed from both local and long-range (RKKY) interactions, and themselves interact with the remainder of the alloy, referred to as the matrix. Cooling in a magnetic field, etc., results in special hysteretic effects. The cusp (or rounded peak) in $\chi(T)$ has frequently in the past been misinterpreted as being evidence for conventional antiferromagnetism. Antiferromagnets do not exhibit field cooling effects or remanence. But, as evidenced by neutron diffraction results, they do, of course possess long-range magnetic order, a property which is not shared by mictomagnets.

Mictomagnetism is wide-spread among concentrated binary alloys formed between suitable pairs of metallic elements. Elements which crop up frequently in this context are: the first-row transition elements, Rh, Pd, associated either with each other (e.g., V-Fe, Ni-Rh) or with non-transition elements such as the noble metals or Al (e.g., Cu-Mn, Ni-Al).

Because the magnetic interactions are already themselves complicated, all fundamental studies have been carried out on binary alloys. However, it is necessary for both fundamental and practical reasons to be able to understand the magnetic and structural properties of stainless steels, all of which are multicomponent alloys, and many of which can be modeled by the ternary system Fe-Cr-Ni.

3 MAGNETIC PROPERTIES OF SOME SPECIFIC Fe-Cr-Ni STAINLESS STEELS

As the following brief review of the literature will indicate magnetic properties of stainless steels have generally been treated from a phenomenological standpoint. Much of the early work involved macroscopic observations on individual alloys; and not until quite recently has an attempt been made to formulate heuristic equations descriptive of the various regimes of magnetic phase stability comparable to those which defined some compositional requirements for structural stability. Awaiting future research is a microscopic specification of the roles of the various alloying additions in controlling magnetic and structural properties.

Some Early Experiments

In 1960, Kondorsky and Sedov [28] reported the results of magnetic susceptibility temperature dependence experiments carried out on the alloy Fe-18Cr-9Ni. A cusp in $\chi(T)$ was noted at 40 K, and after extrapolating a plot of χ^{-1} *versus* T, a paramagentic Curie temperature of -28 ± 3 K was obtained. It is interesting to note that no temperature-independent component of susceptibility (i.e., a χ_o) was required to linearize the inverse-susceptibility plot. The cusp was attributed to an antiferromagnetic transition, which, since $\chi_o=0$, would have to involve *all* the moment carriers.

Following this work, Meiklejohn [29] carried out magnetization studies on a similar alloy after heavy cold work. It was postulated that small amounts of bcc material (ferromagnetic) so induced would yield "shifted" hysteresis loops below 40K due to interaction with the antiferromagnetic matrix. That this did indeed occur was taken as further evidence for the existence of a conventional antiferromagnet below 40K; although neutron diffraction studies were suggested as a means of clearing up any remaining doubt. Such measurements carried out on the alloy $Fe_{0.71}Cr_{0.18}Ni_{0.11}$ by Nathans and Pickart [30] and reported in 1964, yielded no evidence for long-range antiferromagnetic order (upper limit for ordered moment, about 0.25, μ_B). In response to this and other conclusions, Ishikawa et al [31] also sought long-range antiferromagnetic order in monocrystalline $Fe_{0.70}Cr_{0.15}Ni_{0.15}$ using neutron diffraction. In this case the results indicated an ordered atomic moment of 0.4 μ_B and a Néel temperature of 21K. The results were, however, anomalous and a suitable model to represent them could not be unambiguously constructed. The results fitted equally well (a) "band ferromagnetism in which the Stoner condition for the appearance of ferromagnetism is just broken", and (b) "a model in which localized moments (ferromagnetically interacting) are loosely coupled with an antiferromagnetic lattice"; and which, physically, is consistent with an alloy whose composition fluctuates spacially between Fe-rich and Ni-rich regions.

Finally, it is interesting to note the results of the early experiments of Mardion et al [32] who studied the magnetic properties of an alloy corresponding approximately to Fe-25Cr-19Ni-1.4Mn.

This turned out to be superparamagnetic (cluster moment, ~145 μ_B) at moderate fields and temperatures, but magnetically ordered at low temperatures. Neutron diffraction yielded an upper limit of 0.5 μ_B for the ordered moment, although at the time of the report (1964) the diffraction work was still in progress.

Anomalous results of low-temperature specific heat experiments, interpretable in terms of magnetic clustering, have also contributed to an understanding of the magnetic and microstructural properties of stainless steels. Some relevant pioneering work on magnetically-clustering binary systems was performed by Beck and his students (e.g., [33]); while measurements on several commercial stainless steel alloys were carried out by Dillinger et al [34] and others [35]. Dillinger studied the Fe-Cr-Ni alloys 304, 304L, 310, 321, and the (Mn + N)-doped stainless steel, Tenelon. The specific heat results could be fitted to a polynomial in T containing a temperature-independent term A, which according to an interpretation initially advanced by Schroeder [35], can be thought of as arising from ferromagnetic (i.e., superparamagnetic) clusters. Recent calorimetric work at Battelle has demonstrated the existence of such a term in stainless steel and related alloys.

Recent Individual Studies

Interesting recent Soviet work has dealt with the temperature dependence of superparamagnetism, with particular reference to a practical Soviet stainless steel alloy [36]; magnetization studies of the "anomalous superparamagnetic alloy" 52Kh2N22 (i.e., Fe-1.6Cr-22Ni-0.5Mn-0.5C) [37]; and the

low-temperature transport properties of $Fe_{0.65}(Cr_xNi_{1-x})_{0.35}$ $(0 \leq x \leq 0.6)$ -- i.e., a series of alloys spanning the composition range between $Fe_{0.65}Cr_{0.0}Ni_{0.35}$ and $Fe_{0.65}Cr_{0.21}Ni_{0.14}$ [38].

Anomalous electrical transport property results do not lend themselves to unique interpretation. By now numerous models can be constructed to explain anomalous effects -- the choice of model generally depending on the context of the measurement. In Deryabin's [38] case, the anomalous resistivity was assumed to derive from the postulated existence of ferromagnetic and antiferromagnetic regions (c.f. Ishikawa [31]) and consequently "ferro-antiferromagnetic interfaces" from which electron scattering could occur. The lack of specificity inherent in the interpretation of resistivity data makes this kind of work of value only in identifying the existences of "anomalies" rather than in defining their origins.

The anomalous superparamagnetism discussed by Voronchikhin et al [37] refers to the temperature dependence of cluster magnetic moment. This, they suggest, is due to an increase in ferromagnetic cluster volume with decreasing temperature. The mechanism postulated is one in which more and more of the boundary atoms of a diffuse cluster with a ferromagnetic core, are "brought into line" with decreasing temperature. An important concept embodied in this paper has to do with magnetically-induced structural transformation. Voronchikhin et al suggest that the superparamagnetic clusters are very likely the seat of martensitic nucleation in a strong magnetic field, and claim to possess evidence for such field-induced transformation in 52Kh2N22 at 77K in fields of 100K Oe. It is certainly reasonable that a high density of superparamagnetic clusters

should exist in the vicinity of a structural phase boundary, and the concept of a magnetic driving force which might, in effect, shift the position of the phase boundary warrants further investigation in view of some of the proposed high-magnetic-field applications for some stainless steels.

Finally, we report on some results by Stutius and Dillinger [39] who studied thermal conductivity and magnetic susceptibility in the same series of commercial alloys, viz. 304, 304L, 321, 310 and Tenelon, whose low-temperature specific heat has been considered earlier.

TABLE I. PRINCIPAL INGREDIENTS OF SEVERAL COMMERCIAL STAINLESS STEELS

	Composition, At. %				
Alloy	Fe	Cr	Ni	Mn	N
321	70.1	18.4	10.1	1.4	
304	71.6	19.5	7.6	1.3	
304L	70.0	19.7	8.9	1.4	
310	53.8	26.0	18.8	1.4	
Tenelon	58.7	18.7	5.2	15.9	1.5

Comparing the compositions of 304L, 304, and 321, all of which contain about 1.4% Mn, with that of the alloy studied in 1960 by Kondorsky and Sedov [28] (viz. Fe-18Cr-9Ni) one would expect to find Néel temperatures in the vicinity of 40K (or a little higher, because of the presence of Mn). Accordingly, the values of >295K, >295K, and 18K, respectively, which were obtained for the above three alloys, respectively, are somewhat surprising. Clearly experimental difficulties have intervened--

it has been suggested that sample imperfections, in the form of either δ-ferrite or machining-induced surface martensite may have been the source of the problem. Certainly Stutius and Dillinger [39] were unable to draw any conclusions from their work regarding the systematics of the magnetic properties of stainless steels. The situation is now much better understood, however, thanks to the detailed studies of King, Larbalestier and Warnes [40-43], to be reviewed in Section 5.

4 MAGNETIC PROPERTIES OF STAINLESS STEELS IN THE CONTEXT OF BINARY TRANSITION METAL ALLOY MAGNETISM

Magnetization

As pointed out in Section 2 superparamagnetism arises through the existence of submicroscopic precipitates of moment μ (several tens of Bohr magnetons) such that $\mu H/kT$ is sufficiently large that Langevin-type paramagnetism is achievable under "normal" laboratory field/temperature conditions. The ferromagnetic moment-carriers may be either crystalline (e.g., precipitated particles) or "diffuse", as a result of clustering in a multicomponent transition-metal alloy such as, for example, $Ni_{0.63}Rh_{0.37}$ and certain classes of stainless steel alloys. Three examples of magnetic moment field dependences characteristic of superparamagnetism in alloys are presented in Figure 1. The curves shown are describable by Equation (1) (Section 2) in which a nonlinear superparamagnetic component of magnetization is superposed on a field-proportional "normal" component, χ, (which may comprise Pauli, orbital, and additional Curie-law terms). Figure 1(a), from Reference [27] illustrates crystalline-precipitate superparamagnetism, while 1(b), from the work of Cottet et al [26], is a classical example of

clustering paramagnetism in a binary transition-metal alloy. Against this background, Figure 1(c) (after Collings et al [44]) shows that 310S stainless steel is also superparamagnetic. This solid solution alloy is, of course, a member of the clustering class of superparamagnets. As a result of the work of Warnes and King [42] the magnetic field dependences (at 10 K) of a series of Fe-20Cr-(16 28)Ni research alloys have also been shown to lie on curves similar to those of Figure 1. It seems that these alloys also possess superparamagnetic components of magnetization even at temperatures below the peaks in their susceptibility temperature dependences (e.g., Figure 7, later).

Low Temperature Specific Heat

Low temperature specific heat measurements make valuable adjuncts to magnetization measurements in the study of magnetic and other electronic effects in alloys. As discussed by several authors, notable Phillips [45] and Wohlfarth et al [26] the specific heat at moderately low temperatures (e.g., 2-20 K) can be adequately described by an expression of the form

$$C = A + \gamma T + \beta T^3 \quad , \qquad (2)$$

where γ, the electronic specific heat coefficient contains information about the Fermi density of states, and thus relates to the Pauli paramagnetism; β, the lattice specific heat, coefficient is related to the Debye temperature through $\theta_D = (1.944 \times 10^6/M\beta)^{1/3}$ in which, if M is the molar weight the units of β must be J/kg K^4; while A, the magnetic cluster contribution to the specific heat is constant within the temperature range specified above. The

magnetic cluster density can be approximated by N (clusters per unit) $\sim$ A/k, where k is Boltzmann's constant and A is the cluster specific heat per unit (mole, g etc.). When the results of the low-temperature specific heat experiments are expressed in the usual format C/T versus T^2, the magnetic contribution manifests itself as a 1/T dependence as shown in Figures 2(a) and (b) which compare specific heat data for the alloy $Ni_{0.63}Rh_{0.37}$ with that for 310S stainless steel. The characteristic superparamagnetic signature is clearly present in both sets of data. In the case of 310S-quenched, A = 18.4 mJ/mole K [44] leading to a cluster density of about 1.3×10^{21} per mole or 1.9×10^{26} per m^3. The value of A which fits the $Ni_{0.63}Rh_{0.37}$ data is 4.5 mJ/mole K. Numerous other alloy systems near the critical composition for the onset of ferromagnetism exhibit superparamagnetism as a result of magnetic clustering, the effects of which are reflected in the low-temperature specific heat. Figure 3(a), from Reference [45] and traceable to the experiments of Cheng et al [33] is another excellent example of this. We introduce this system since it is one of the few for which very low temperature data are available. The constancy of A represents a "high-temperature limiting condition" for the magnetic cluster specific heat, which must eventually go to zero at 0 K. That it does so, in an Einstein-like manner at temperatures below about 1 or 2 K, is shown in Figure 3(b). The calorimetric properties of ferromagnetic clusters have been reviewed by Phillips [45].

Magnetic Transformations

It is well known that dilute local-moment alloys exhibit some kind of maximum in $\chi(T)$ at sufficiently low temperatures. The similarity

of this peak to that occurring at the Néel point of a conventional antiferromagnet gave rise to several antiferromagnet models for the low-temperature ordering of dilute paramagnetic alloys. By now the peak is recognized as indicating a spin-glass transition in which the localized spins order antiferromagnetically but in random directions. As a result of the randomness the magnetic transition is sharp, or cusp-like, only in zero field; while it broadens with the application of stronger and stronger fields. This explains why the magnetic transitions studies in the pioneering work (e.g., Reference [12]) were never sharp. The first definitive work in this field was performed by Cannella and Mydosh [13] some of whose results are reproduced in Figure 4(a). These are juxtaposed against a series of curves representing the susceptibility temperature dependences of Fe-20Cr-16Ni from the work of Warnes and King [42], Figure 4(b). Here again the sharpness of the peak is strongly dependent on the strength of the applied magnetic field. The implication is that the "antiferromagnetic" ordering noted in stainless steels of appropriate constitutions is also due to interaction between randomly orientated moment carriers (in this case the ferromagnetic clusters) rather than conventional long-range-ordered antiferromagnetic spin alignments. The postulated existence of such a superparamagnetic spin-glass state would also justify the lack of specificity in the results of neutron diffraction experiments [31]; but much more research, particularly with the neutron diffractometer, is needed to clarify the situation.

5 SYSTEMATICS OF MICROSTRUCTURE AND MAGNETIC PROPERTIES OF Fe-Cr-Ni STAINLESS STEELS

Microstructure

All stainless steels enter the fcc austenitic γ phase when heated to temperatures in excess of about 1000°C. Even so, not all such steels will be completely homogeneous under these conditions, because residual δ-ferrite formed during the initial solidification from the melt is not easily removed by subsequent thermal and mechanical treatments. On cooling from about 1000°C to room temperature, and from there to about 4 K, some of the stainless steels retain the austenitic structure, while others undergo a solid state transformation either to bcc α-ferrite (or α'-martensite) or to an hcp ϵ-martensite. Since the magnetic properties of austenite are indistinguishable fromthose of the ϵ-martensite, the latter will not be considered further in this paper.

Breedis and Kaufmann [47] have shown that the temperature dependence of the change in Gibb's free energy for the $\alpha \rightarrow \gamma$ phase change in alloys of iron with other transition metals is a quadratic function of the concentrations of the various alloying elements. Using this analysis and the thermodynamic data for pure iron reported by Kaufmann, Clougherty and Weiss [47], Warnes and King [43] have calculated equilibrium temperatures (T_o) for the α and γ phases for several series of Fe-Cr-Ni alloys. A plot of the compositional dependence of T_o at 0 K, based on these analyses is given in Figure 5, which covers the Fe-Cr-Ni system from pure Fe up to 50 wt.% Cr and Ni. All austenitic alloys with compositions to the right-hand side of the T_o = 0 K isothermal can be regarded as completely structurally stable at all temperatures in the solid state. Alloys with

compositions which lie just to the left-hand side of this line may appear to be stable on simply cooling to 4.2 K, but will probably transform to α'-martensite as a result of plastic deformation at low temperatures [43]. Alloys with even lower concentrations of Cr and Ni will become unstable and transform by cooling alone [41].

The region of the phase diagram enclosed by the dashed lines in Figure 5 refers to the limiting Cr and Ni concentrations specified for the AISI 300 series of stainless steels. The plot of $T_o = 0$ lies well to the high alloy concentration end of these specifications, so that (in the absence of C and N) only alloys containing more than 22 wt.%Cr and 19 wt.%Ni (i.e., 310 and 314) can be considered to be completely structurally stable at all temperatures.

Isothermal plots for T_o equal to 300, 400, 500 and 600K, extending over the composition regions of interest, are also included in Figure 5. Since these plots refer to equilibria under diffusion controlled conditions, it is not unexpected to find that there is relatively little displacement (<1wt.%Ni) between the 0 and 300K plots, while the displacements become progressively greater at higher temperatures. In practice, however, it is found that most of the commercial stainless steels with Cr and Ni concentrations which lie in the region between the isothermals for $T_o = 600K$ and 0 K do not in fact transform from the γ to the α phase at low temperatures. This is due to two separate, but related, factors. The first of these is the very low diffusion coefficient for both Fe and Ni in Fe-Ni alloys, which effectively prevents any nucleation and growth by this mechanism below about 600K [48]. The growth process can be much facilitated if the transformation occurs by a martensitic shear, but it still

requires a considerable degree of undercooling (usually several hundreds of degrees below T_o) to stimulate a nucleus to grow martensitically [43,48]. Once formed, however, the martensitic α'-phase grows rapidly in a series of bursts as the temperature is lowered. This type of martensitic transformation is called athermal and the temperature at which the martensite first occurs is referred to as M_s. The second factor, referred to above, is that the degree of undercooling required to trigger the formation of athermal martensite at the M_s temperature is very sensitive to the presence of interstitial solutes such as C and N.

Empirical relationships relating M_s to the concentration of alloying elements in solution in the austenite phase have been developed by Eichelman and Hull [49] and by Monkman, Cuff and Grant [50]. To obtain a wide range of finite M_s values, these authors found it necessary to examine alloys with Cr and Ni contents lower than those of the AISI 300 series of stainless steels and the region of composition over which their relationships are valid is indicated in Figure 5 by the area enclosed by the dotted lines. To relate these equations to the thermodynamic data plotted in Figure 5, it is convenient to convert them from Fahrenheit to Kelvin units and also to include a parameter for Mo based on the work of Hammond [51], as suggested by Larbalestier and King [41]. The respective equations of Eichelman and Hull, and Monkman, Cuff and Grant, then become

$$M_s[K] = 1578-41.7Cr-61.1Ni-33.3Mn-27.8Si-36.1Mo-1667(C+N) \qquad (3)$$

and

$$M_s[K] = 1455-36.7Cr-56.7Ni-1455(C+N) \qquad (4)$$

AD-A059 720 BATTELLE COLUMBUS LABS OHIO F/G 11/6
METAL PHYSICS AND TITANIUM-ALUMINUM ALLOYS.(U)
FEB 78 E W COLLINGS AFOSR-75-2786

UNCLASSIFIED AFOSR-TR-78-1240 NL

2 OF 2
AD A059720

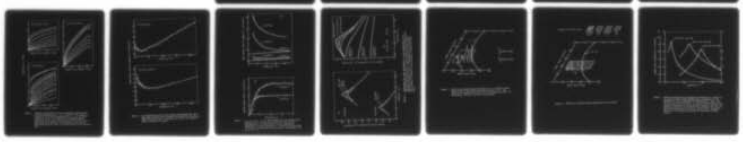

END
DATE FILMED
12-78
DDC

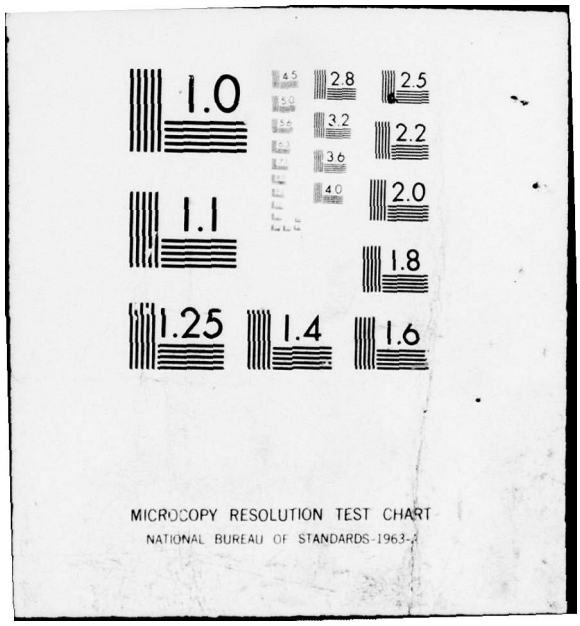
1.0
1.1
1.25
1.4
1.6
1.8
2.0
2.2
2.5
2.8
3.2
3.6
4.0
4.5
5.0
5.6
MICROCOPY RESOLUTION TEST CHART
NATIONAL BUREAU OF STANDARDS-1963-A

where the numbers represent, as usual, the wt.% of the alloying elements in solution in the austenite phase.

Using these equations, isotherms of M_s have been calculated for 300K and 0K, assuming typical concentrations (in wt.%) of 1.0 Mn, 0.7 Si, 0.4 Mo, 0.05C and 0.03N for commercial stainless steels. As may be seen from the plots drawn in Figure 5, apart from a few alloys containing the maximum permitted concentrations of Cr and Ni, most of the alloys studied by these authors transformed to some degree from $\gamma \rightarrow \alpha'$ on cooling to 4.2 K. As the composition ranges overlap, the stable high Cr and Ni concentration alloys are also found to lie within the lower alloy concentration region of the AISI 300 series. An extrapolation of the M_s isotherm at 0 K into the latter composition region would thus indicate that most of the 300 series alloys should be structurally stable on cooling to 4.2K.

Eichelman and Hull [50] have cautioned, however, that their equation should not be extended beyond the range of compositions of the alloys actually studied by them. This caution has been reinforced by Warnes and King [43], who point out that, since the T_o isotherms for Fe-Cr-Ni alloys are quadratic functions of the Cr and Ni concentrations, the empirical relationships for M_s should only be regarded as linear approximations over relatively narrow ranges of composition. Further, as may be seen from the figure, the latter authors have also pointed out that the linear isotherms for M_s lie approximately parallel to the respective T_o isotherms at the midpoint of the range of Cr composition. On this basis, they argue that a linear M_s equation applicable to the higher ranges of Cr content in alloys of the AISI 300 series should require a different ratio of Cr:Ni coefficients. If the M_s plot were to lie parallel to the tangent to the T_o = 0 K plot for this region of

composition, it would mean that the AISI 300 steels should be even less stable than would be indicated by predictions based on simple extrapolations of the relationships of Eichelman and Hull, or Monkman, Cuff and Grant.

A further complication is encountered when considering the weldable grades of the AISI 300 series such as 304L, 321 and 347, whose soluble carbon concentrations lie below 0.03 wt.%. This lack of interstitial solute not only raises the M_s temperature for the athermal transformation, but also increases the tendency for the martensite transformation to be isothermal in nature, so that a distinct M_s temperature can no longer be defined [40]. The isothermal transformations usually occur in the temperature region 130-200K and are thus likely to be suppressed by quenching a steel to 77 or 4.2K. Empirical equations, such as that of Hull [52], which are based on the room temperature examination of previously quenched steels, may result in misleading predictions for the low temperature structure of the weldable grades of stainless steels and are thus not considered in this paper. Hence, at the present time, there appears to be no simple and reliable parameter which can be applied uniformly to all the stainless steels in order to predict their low temperature structural stability.

4.2 Low Temperature Magnetic Properties

To establish a systematic relationship between low temperature magnetic properties and microstructure, Warnes and King [43] have made a detailed comparison between calculated T_o temperatures and the known low temperature magnetic properties of a series of thirty-five Fe-Cr-Ni alloys.

All alloys with T_o<0K, i.e., those which remain austenitic at all temperatures, even when subjected to plastic deformation, were found to exhibit Curie temperatures and thus ferromagnetism at 4.2K, as indicated by the region with horizontal shading in Figure 6. This low temperature magnetic behavior is in effect an extrapolation of the ferromagnetic properties of pure (fcc) Ni, the Curie temperature of which decreases progressively as Fe is substituted for Ni and falls to zero in the region of composition where the T_o = 0K plot intersects the Fe-Ni binary system [48]. Metastable alloys with compositions to the left-hand side of the T_o = 0 K plot, were found to have magnetic properties associated with the presence of superparamagnetic clusters and/or relatively long range antiferromagnetic ordering. To differentiate between the magnetic behavior of the metastable alloys, Warnes and King [43] examined the compositional dependence of the peak observed in magnetic susceptibility at the Néel temperature, T_N, using the magnetic balance results of Kohlhass, Raible and Weiss [53], fluxmeter results of Kondorskii and Sedov [28] and Mikesell and Reed [54], Mössbauer results of Gonser, Meechan, Muir and Wiedersich [55] and Flansberg and Hershkowitz [56], neutron diffraction and vibrating sample magnetometer results of Ishikawa, Endoh and Takimoto [31] and their own moving specimen magnetometer results [42,43]. As the results of Stutius and Dillinger [39] were found to give volume susceptibilities an order of magnitude greater than those obtained by other workers using the same nominal alloys, their alloys were presumed to contain small amounts of ferromagnetic phases, formed either during casting (δ-ferrite) or machining (α'-martensite), and were thus not considered further. Using the T_N values for the remaining alloys, Warnes and King [43] developed

the following empirical equation for the compositional dependence of the Néel temperature, T^*_N

$$T^*_N = 90 - 1.25Cr - 2.75Ni - 5.5Mo - 14Si + 7.75Mn \quad (5)$$

where the elemental symbols again refer to the weight percentages of the respective alloying elements. This equation enabled the known values of T_N to be predicted with an RMS deviation of 3.5K, which represents an accuracy an order of magnitude greater than that of the M_s predictions based on Equations (3) or (4). This increased accuracy is attributed to the smaller values for the numerical constants in Equation (5), so that errors in compositional analysis lead to smaller deviations in T^*_N, a consequence which is particularly significant in the case of C and N as these have the greatest effect on M_s, but cause no measurable change in T_N.

The composition ranges of the various alloys used to derive Equation (5) are (in wt.%) 16-26Cr, 6-32Ni, 0-16Mn, 0-2.4Si, 0-3Mo, 0-0.14C and 0-0.38N, the balance being Fe. These limits are indicated by the region enclosed within the chain-dotted lines in Figure 6. This region encloses the whole Ni range and the upper concentration of the Cr range applicable to Equations (3) and (4) and the entire range of the AISI 300 stainless steels, which is again indicated by dashed lines in Figure 6.

As may be seen in Figure 6, the isotherms for T^*_N = 0, 15, 30 and 45K for typical steels containing 1.0 Mn, 0.7 Si and 0.4 Mo are all approximately parallel to the tangent to the T_o = 0K curve at 21 wt.%Cr, which represents the midpoint of the Cr range under consideration. The maximum displacement between the T^*_N = 0K and T_o = 0K curves, which occurs at this point, amounts to 1.25 wt.%Ni, which is equivalent to a change in T^*_N equal to the RMS deviation of 3.5K. Further, since all

the alloys whose T^*_N values are either negative, or within the RMS deviation of 0 K, show ferromagnetism at low temperatures, it is concluded that values of $T^*_N \leq 0K$ can be taken as predictors of low temperature ferromagnetism and complete structural stability for the γ phase.

Alloys with T^*_N values between 0 and 15K do not exhibit distinct Curie temperatures, nor can values of T_c be derived from graphical analyses such as that proposed by Arrott [57]. Peaks in magnetic susceptibility are observed in these alloys at low temperatures and studies of the temperature dependence of susceptibility in differing fields shows that the maximum susceptibility becomes shifted towards lower temperatures [58], while the peak itself becomes broadened, and often completely flattened, as the magnetic field is increased [42]. This behavior is associated with the small ferromagnetic clusters within the austenite matrix, and the properties of superparamagnetism, discussed in previous Sections. These alloys are also found to be completely structurally stable at low temperatures and it is thus concluded that a T^*_N value of 15 K is related to an M_d value equal to 0 K, where M_d represents the maximum temperature at which α'-martensite can form by deformation, as opposed to simple cooling. Alloys exhibiting these combinations of properties are indicated by the inclined shading in Figure 6.

Alloys with T^*_N values between 15 and 30 K exhibit peaks in low temperature susceptibility which are clearly related to long-range antiferromagnetic ordering [31, 53, 54] of the type discussed previously. While these alloys are found to remain stable on simple cooling to 4.2 K, they will transform martensitically by deformation, confirming that $T^*_N = 15$ K is related to $M_d = 0$ K, as mentioned above. When the respective plots for

M_s and T^*_N in Figures 5 and 6 are compared within the narrow composition region where the specifications for the two sets of equations overlap, it is found that the plot of T^*_N = 30 K lies between the M_s = 0 K plot of Eichelman and Hull and that of Monkman, Cuff and Grant. It can thus be concluded, that for the typical commercial alloy compositions defined for the M_s and T^*_N plots in Figures 5 and 6 (0.05 C, 0.03 N, 1.0 Mn, 0.7 Si, 0.4 Mo) a T^*_N = 30 K can be associated with an M_s = 0 K.

Alloys with T^*_N values greater than 30 K are structurally unstable at low temperatures, again confirming that M_s = 0 K is related to T^*_N = 30 K, and hence their low temperature magnetic properties comprise a mixture of antiferromagnetism from the retained austenite and ferromagnetism from the α'-martensite. These alloys are indicated by the crossed shading in Figure 6. Again, when M_s and T^*_N plots are compared in the overlapping region of composition, it is found that the plot of T^*_N = 45 K lies between the two plots for M_s = 300K, so that under the appropriate compositional conditions (defined in the previous paragraph) a T^*_N = 45K can be associated with an M_s = 300K.

Predictions of structural stability from values of T^*_N should be treated with some care, however, as anomalous results are to be expected for steels with high concentrations of C and/or N, since these interstitials drastically lower M_s, but make no contribution to T^*_N. High concentrations of Mn will also lead to anomalous results, because, while this element lowers M_s, it is the only constituent element in Equation (5) which causes T^*_N to be increased. In this context, a systematic study should be undertaken of the many high Mn alloys which are now available commercially under designations such as Kromarc (Westinghouse), Tenelon

(U.S. Steel) and Nitronic (Armco). While a number of individual measurements have been reported on particular alloys, there has been no systematic study of both the field and temperature dependence of susceptibility. As indicated below maxima observed in low temperature susceptibility should be given particular attention and a detailed examination should be made of different types of magnetism which can occur at low temperatures.

6 CONCLUSIONS

The magnetic and structural properties of Fe-Cr-Ni alloys are probably describable using an extension to three components of conventional alloy theory. In other words it should be possible from an electronic standpoint to relate alloy composition on one hand to the relative stabilities of the α (bcc) and γ (fcc, austenitic) alloy phases, and on the other to the compositional range for ferromagnetism. It is postulated that the superparamagnetism in 310S (which if represented by Fe-25.5Cr-21Ni would yield, according to Equation (5), $T_N \sim 0$ K) and the antiferromagnetism of alloys such as Fe-20Cr-16Ni (T_N = 21 K) are the results of clustering in the critical composition range close to the ferromagnetic phase boundary. Accompanying an alloy-theory investigation, it would be useful to carry out further neutron diffraction studies on a selected series of research-purity Fe-Cr-Ni alloys, preferably in single-crystal form.

In a separate class, also deserving of further study are the Mn-bearing stainless steels, which we believe can be regarded approximately as pseudobinary (Fe-Cr-Ni)-Mn systems. Recent work at Battelle has shown that alloys such as Fe-22Cr-13Ni-5Mn, Fe-21Cr-6Ni-9Mn and Fe-18Cr-3Ni-13Mn, although <u>not</u> superparamagnetic, do yield sharp magnetic transitions in

fields of up to 10 kOe, Figure 7. In order to define the nature of this transition, which increases in temperature as Mn replaces Ni in the system Fe-(18-22)Cr-(16-18)(Ni plus Mn) and which is probably confined to the Mn component in the alloy, further magnetic and magnetic-structural investigations are needed.

ACKNOWLEDGMENTS

This work was supported by the United States Air Force Office of Scientific Research under Grant No. 75-2786 (E.W.C.) and by a Grant from the National Research Council of Canada (H.L.K.).

REFERENCES

[1] J. Friedel, Can. J. Phys. 34, 1190 (1956).

[2] P. W. Anderson, Phys. Rev. 124, 41 (1961).

[3] J. Kondo, Progr. Theo. Phys. Kyoto 36, 429 (1966).

[4] B. R. Coles, Michigan State University Summer School on Alloys, August 21 - Sept. 1, 1972.

[5] J. Kondo in "Solid State Physics", ed. by D. Turnbull and H. Ehrenreich, Academic Press, N.Y., 1969, p. 183; also A. J. Heeger, ibid, p. 283; and M. D. Daybell and W. A. Steyert, Rev. Mod. Phys. 40, 380 (1968).

[6] S. F. Edwards and P. W. Anderson, J. Phys F: Metal Phys. 5, 1975 (1975).

[7] K. H. Fischer, Phys. Rev. Lett. 34, 1438 (1975).

[8] J. A. Mydosh, AIP Conf. Proc. 18, 651 (1975).

[9] B. Window, J. Mag. and Magnetic Materials 1, 167 (1975).

[10] V. Cannella in "Amorphous Magnetism", ed. by H. O. Hooper and A. M. deGraaf, Plenum, 1973, pp. 195-206.

[11] S. F. Edwards, J. Polymer Sci. 17, 933 (1976).

[12] See J. Owen, M. E. Browne, V. Arp, and A. F. Kip, J. Phys. Chem. Solids 2, 85 (1957); J. Owen, M. E. Browne, W. D. Knight, and C. Kittel, Phys. Rev. 102, 1501 (1956).

[13] V. Cannella and J. A. Mydosh, Phys. Rev. B6, 4220 (1972).

[14] D. Sherrington and B. W. Southern, J. Phys. F., Metal Phys. 5, L49 (1975).

[15] J. L. Tholence and R. Tournier, J. Phys. (Paris) Colloq. 35, C4-229 (1974).

[16] K. Binder, Z. Phys. B. 26, 339 (1977).

[17] K. Binder and K. Schroeder, Phys. Rev. B. 14, 2142 (1976).

[18] D. A. Smith, J. Phys. F: Metal Phys. 4, L226 (1974) and 5, 2148 (1975).

[19] F. A. deRozario and D. A. Smith, J. Phys. F: Metal Phys. 7, 439 (1977).

[20] C. M. Soukoulis and K. Levin, Phys. Rev. Lett. 39, 581 (1977).

[21] N. F. Mott and H. Jones, "The Theory of the Properties of Metals and Alloys", Dover Publications Reprint, 1958, p. 196.

[22] D. H. Seib and W. E. Spicer, Phys. Rev. Letters, 20, 1441 (1960); Phys. Rev. B2, 1676, 1694 (1970).

[23] G. M. Stocks, R. W. Williams, and J. S. Faulkner, Phys. Rev. B4, 4390 (1971).

[24] B. Gyorffy, in "Physics of Transition Metals" ed. by E. Fawcett, to be published.

[25] N. E. Phillips in "Critical Reviews in Solid State Sciences", Vol. 2, Issue 4, 1971/72, p. 467.

[26] H. Cottet, P. Donze, J. Ortelli, E. Walket and M. Peter, Helv. Phys. Acta. 41 755 (1968)--Magnetization of Ni-Rh; see also A. Hahn and E. D. Wohlfarth, Helv. Phys. Acta. 41 857 (1968)--calorimetry.

[27] P. A. Beck, in "Magnetism in Alloys" ed. by P. A. Beck and J. T. Waber, TMS-AIME, New York, 1972, p.211 .

[28] E. I. Kondorsky and V. L. Sedov, J. Appl. Phys. 31, 331 Sup. (1960).

[29] W. H. Meiklejohn, J. Appl. Phys. 32, 274 Sup. (1961).

[30] R. Nathans and S. J. Pickart, J. Phys. Chem. Solids 25, 183 (1964).

[31] Y. Ishikawa, Y. Endoh and T. Takimoto, J. Phys. Chem. Solids 31, 1225 (1970).

[32] G. B. Mardion, et al, C. R. Acad. Sci. Paris 259, 4552 (1964).

[33] C. H. Cheng, C. T. Wei, and P. A. Beck, Phys. Rev. 120, 426 (1960).

[34] P. Zoller, P. R. Decker, and J. R. Dillinger, J. Appl. Phys. 40, 1964 (1969).

[35] K. Schroeder, J. Appl. Phys. 32, 880 (1961).

[36] Yu. S. Avraamov, et al, Sov. Phys. Solid State 16, 2071 (1975).

[37] L. D. Voronchikhin, et al, Sov. Phys. Solid State 16, 1708 (1975).

[38] A. V. Deryabin and V. E. Rode, Sov. J. Low Temp. Phys. 2, 710 (1976).

[39] W. Stutius and J. R. Dillinger, J. Appl. Phys. 44, 2887 (1973).

[40] D. C. Larbalestier and H. W. King, Cryogenics 13, 160 (1973).

[41] D. C. Larbalestier and H. W. King, Proc. ICEC 4 (IPC Science & Technology Press, 1975) 338.

[42] L.A.A. Warnes and H. W. King, Cryogenics 16, 473 (1976).

[43] L.A.A. Warnes and H. W. King, Cryogenics 16, 659 (1976).

[44] E. W. Collings, F. J. Jelinek, J. C. Ho, and M. P. Mathur, Adv. Cryo. Eng., 22, 159 (1977).

[45] N. E. Phillips, Critical Reviews in Solid State Sciences, 2, 467 (1972).

[46] J. F. Breedis and L. Kaufmann, Met. Trans. AIME 2, 2359 (1971).

[47] L. Kaufmann, E. V. Clougherty and R. J. Weiss, Acta Met. 11, 323 (1963).

[48] M. Hansen "Constitution of Binary Alloys", McGraw-Hill, 1958, p. 677.

[49] G. H. Eichelman and F. C. Hull, Trans. A.S.M. 45, 77 (1953).

[50] F. C. Monkman, F. G. Cuff and N. Grant, Metal Progress 71, 94 (1957).

[51] C. M. Hammond, Cobalt 25, 195 (1964).

[52] F. C. Hull, Welding Journal 52, 193S (1973).

[53] R. Kohlhass, A. A. Raible and W. D. Weiss, Arch. Eisenhütten. 41, 769 (1970).

[54] R. P. Mikesell and R. P. Reed, J. Res. N.B.S. 70C, 207 (1966).

[55] M. Gonser, C. J. Meechan, A. H. Muir and H. Wiedersich, J. Appl. Phys. 34, 2373 (1963).

[56] L. D. Flansberg and N. Hershkowitz, J. Appl. Phys. 41, 4082 (1970).

[57] A. Arrott, Phys. Rev., 108, 1394 (1957).

[58] R. Kohlhaas, A. A. Raible, and W. Rocker, Z. Angew. Phys., 30, 254 (1970).

FIGURE CAPTIONS

FIGURE 1. EXAMPLES OF MAGNETIZATION FIELD DEPENDENCES CHARACTERISTIC OF SUPERPARAMAGNETISM $\sigma_{sp} = \mu.n.L\ (\mu H/k\ [T- \theta])$, against a background of "normal" paramagnetism, $\sigma_{np} = \chi H$, for three classes of alloy: (a) Au-Mn with a fine ferromagnetic crystalline precipitate--after Reference [27], (b) Ni-Rh, a clustering solid solution--after Reference [26], and (c) 310S stainless steel, also a clustering alloy--after Reference [44].

FIGURE 2. LOW TEMPERATURE SPECIFIC HEAT RESULTS FOR QUENCHED 310S STAINLESS STEEL (BATTELLE DATA) COMPARED WITH THOSE FOR $Ni_{0.63}Rh_{0.37}$ (after Reference [26]). Reasonable accord with the relationship $C + A+\gamma T+\beta T^3$ is evident.

FIGURE 3. LOW-TEMPERATURE SPECIFIC HEAT RESULTS FOR V-Fe ALLOYS--after Reference [45]. In (a) the C/T versus T^2 data fit the relationship $C = A+\gamma T+\beta T^3$ where A is the "temperature independent" cluster contribution. In (b) the A-term is seen to conform to an Einstein-like temperature relationship below about 1 or 2 K.

FIGURE 4. TEMPERATURE AND FIELD DEPENDENCES OF VOLUME SUSCEPTIBILITY OF THE SPIN-GLASS ALLOYS Au-Fe (1 and 2 at.%)--after Reference [13], compared with those for the research stainless steel Fe-20Cr-16Ni--after Reference [42]. A broadening of the transition with increase in magnetic field strength is evident in both cases.

FIGURE 5. PLOTS OF THE COMPOSITIONAL DEPENDENCES OF T_0 AT SEVERAL TEMPERATURES BASED ON THE ANALYSES OF WARNES AND KING [43]. Also shown are the regimes of validity of the Eichelman and Hull [49] and Monkman, Cuff and Grant [50] relationships.

FIGURE 6. PORTION OF A MAGNETIC PHASE DIAGRAM FOR Fe-Cr-Ni ALLOYS.

FIGURE 7. MAGNETIC SUSCEPTIBILITY TEMPERATURE DEPENDENCES OF A SERIES OF Fe-Cr-Ni-Mn ALLOYS (KNOWN COMMERCIALLY (a) NITRONIC 50, (b) NITRONIC 40, AND (c) NITRONIC 33, RESPECTIVELY). Apart from the fact that the temperature of a sharp antiferromagnetic-like transition increases as the Mn content increases, and that the magnetic properties are evidently quite different from those of the Mn-free stainless steels (e.g., Figure 4(b)), nothing is known about the magnetic properties or structures of these alloys.

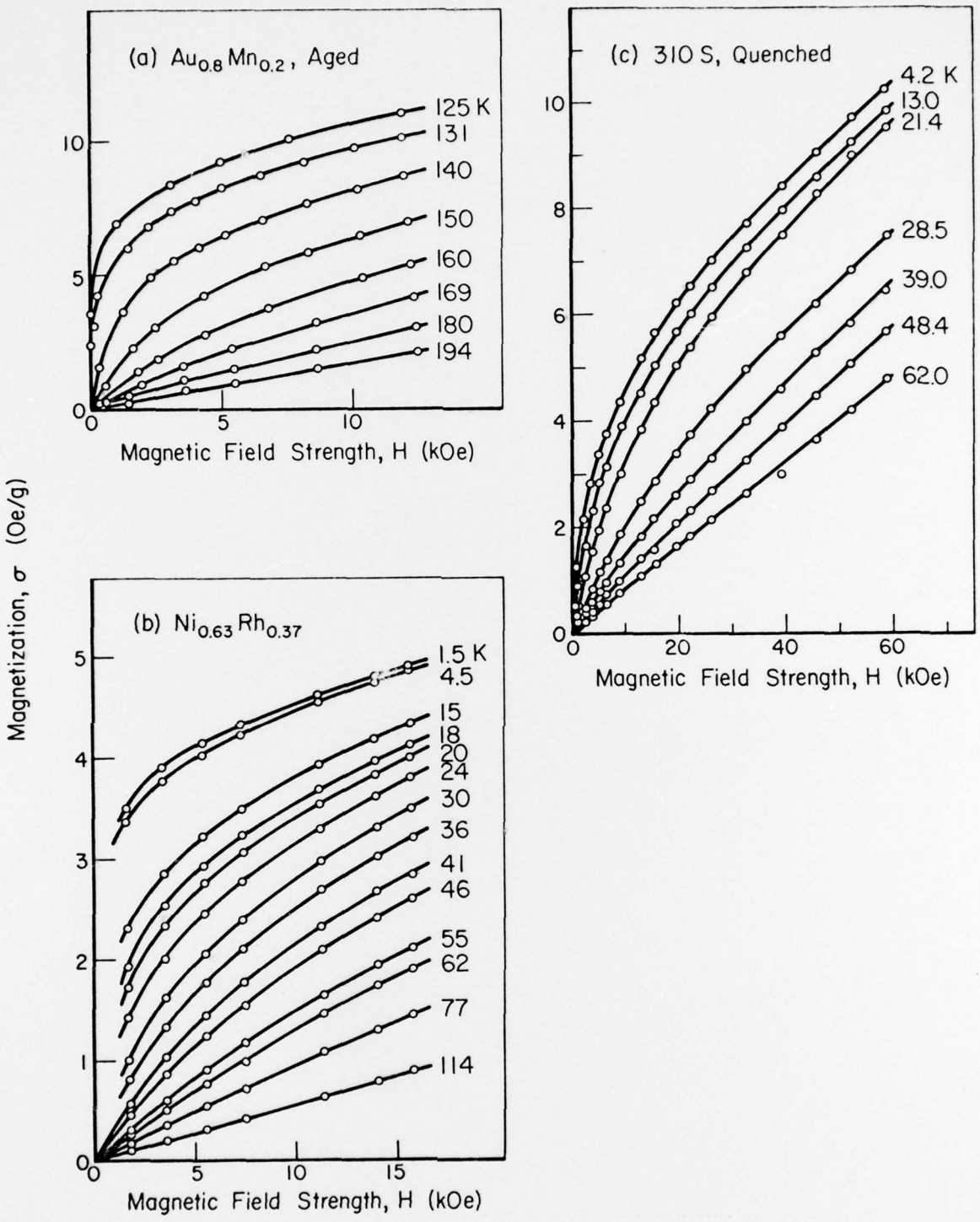

FIGURE 1. EXAMPLES OF MAGNETIZATION FIELD DEPENDENCES CHARACTERISTIC OF SUPERPARAMAGNETISM $\sigma_{sp} = \mu.n.L\ (\mu H/k\ [T-\theta])$, against a background of "normal" paramagnetism, $\sigma_{np} = \chi H$, for three classes of alloy: (a) Au-Mn with a fine ferromagnetic crystalline precipitate--after Reference [27], (b) Ni-Rh, a clustering solid solution--after Reference [26], and (c) 310S stainless steel, also a clustering alloy--after Reference [44].

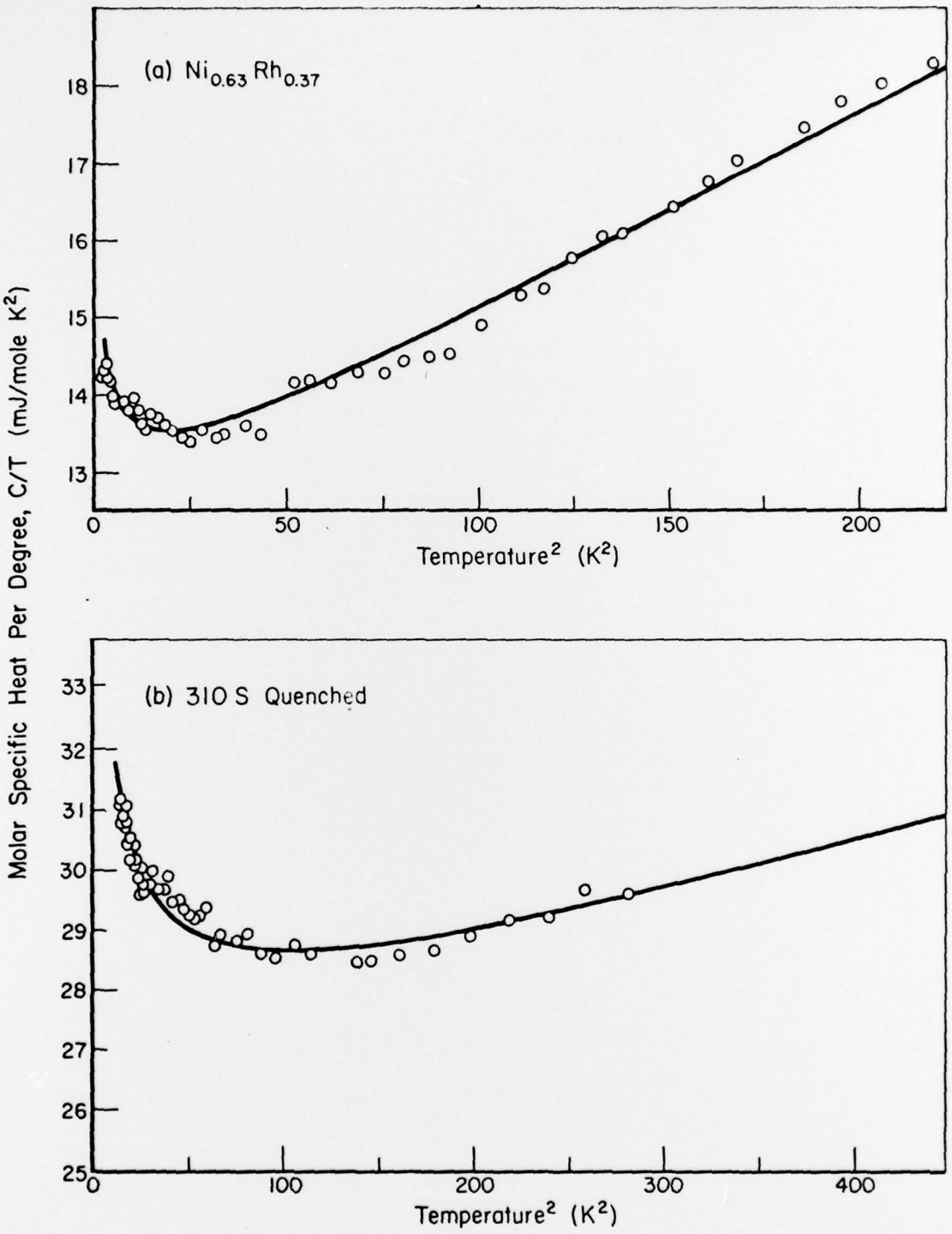

FIGURE 2. LOW TEMPERATURE SPECIFIC HEAT RESULTS FOR QUENCHED 310S STAINLESS STEEL (BATTELLE DATA) COMPARED WITH THOSE FOR $Ni_{0.63}Rh_{0.37}$ (after Reference [26]). Reasonable accord with the relationship $C + A+\gamma T+\beta T^3$ is evident.

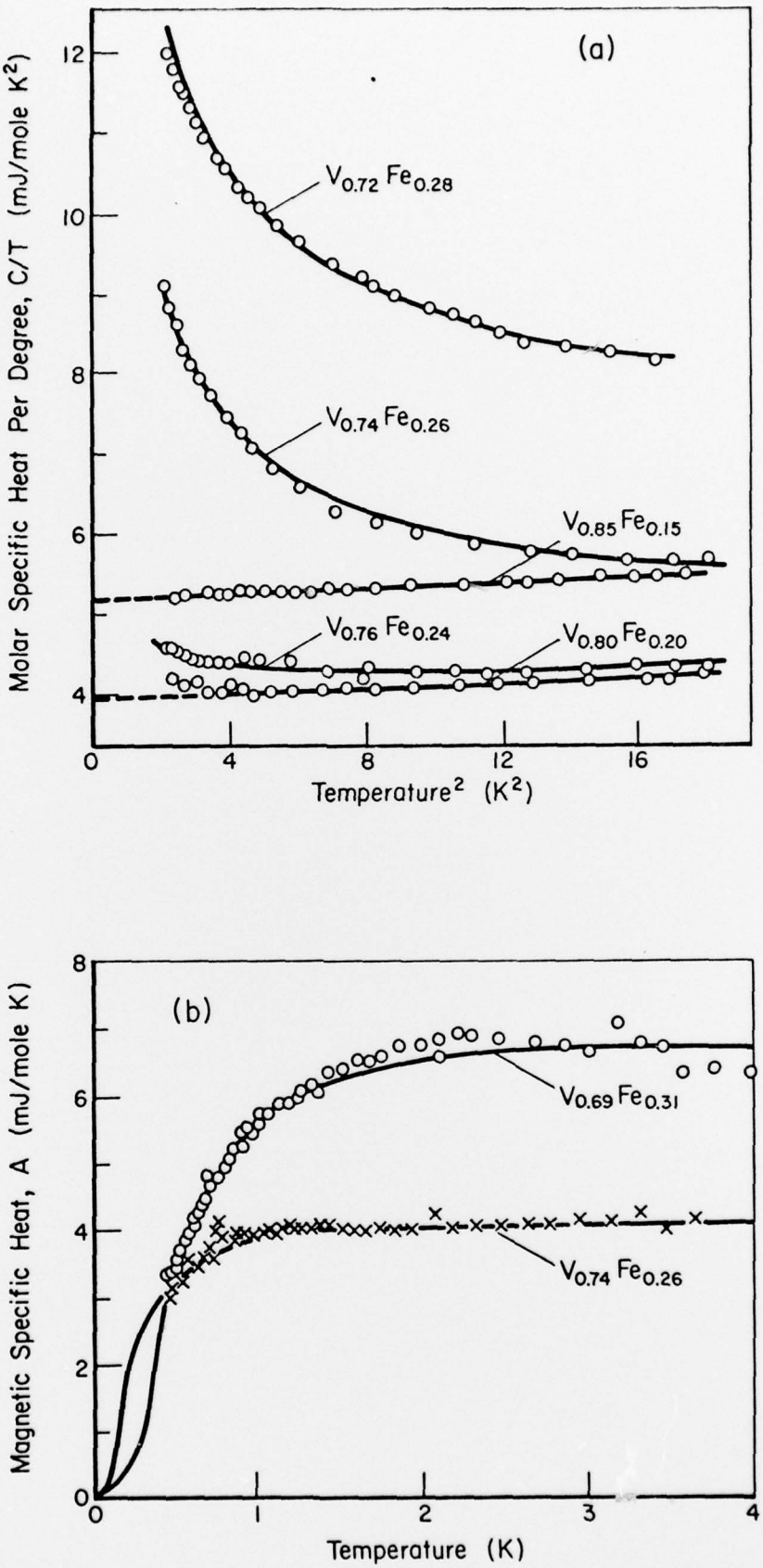

FIGURE 5. LOW TEMPERATURE SPECIFIC HEAT RESULTS FOR V-Fe ALLOYS--after Reference [45]. In (a) the C/T versus T^2 data fit the relationship $C = A+\gamma T+\beta T^3$ where A is the "temperature independent" cluster contribution. In (b) the A-term is seen to conform to an Einstein-like temperature relationship below about 1 or 2 K.

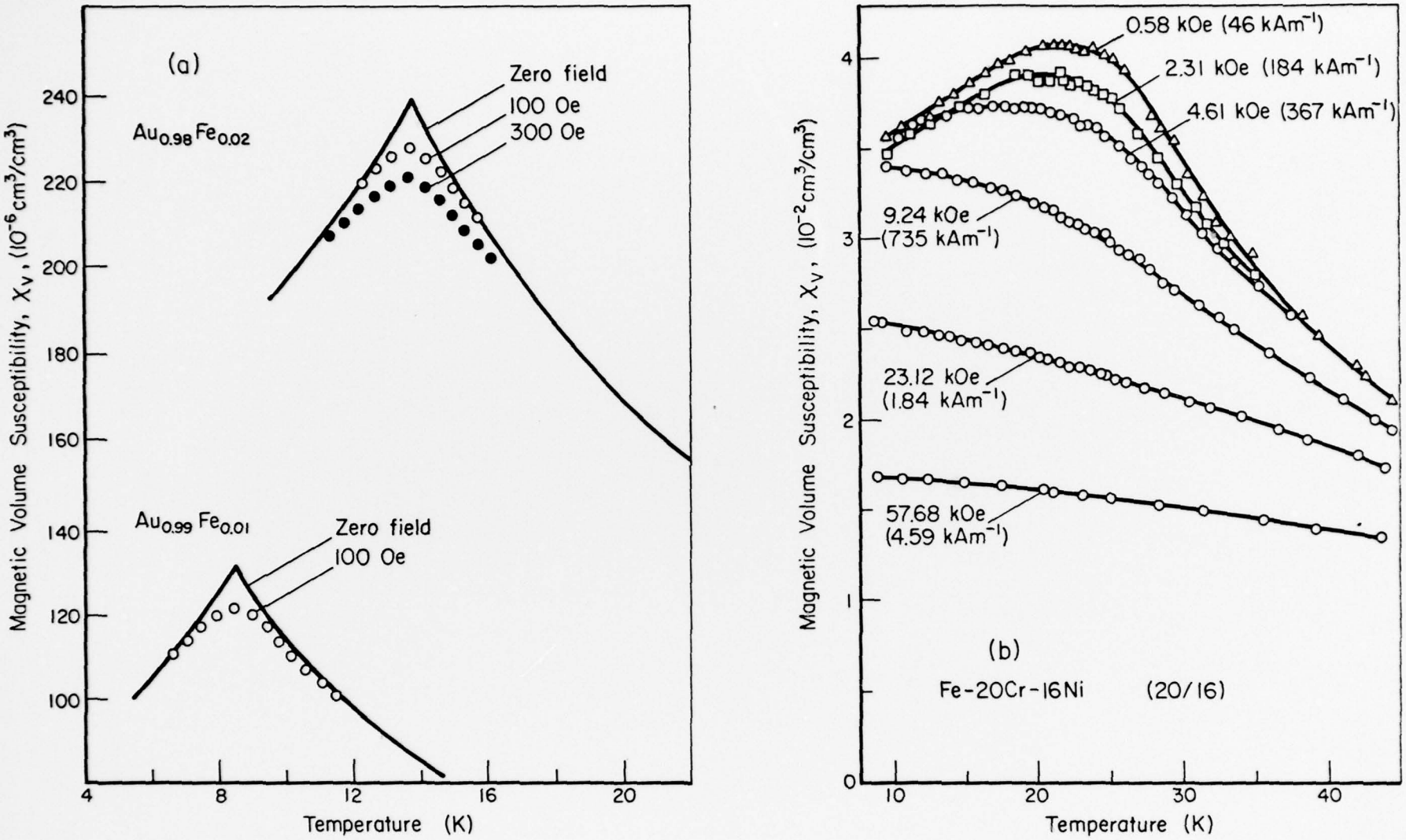

FIGURE 4. TEMPERATURE AND FIELD DEPENDENCES OF VOLUME SUSCEPTIBILITY OF THE SPIN-GLASS ALLOYS Au-Fe (1 and 2 at.%)--after Reference [13], compared with those for the research stainless steel Fe-20Cr-16Ni--after Reference [42]. A broadening of the transition with increase in magnetic field strength is evident in both cases.

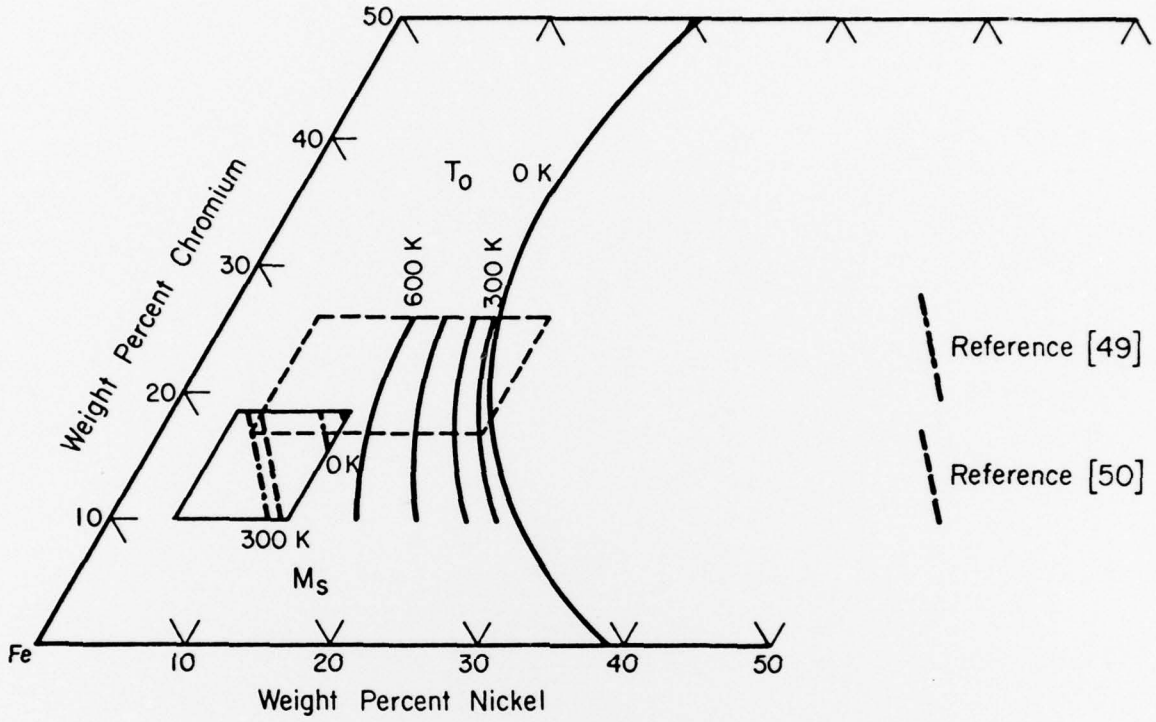

FIGURE 5. PLOTS OF THE COMPOSITIONAL DEPENDENCES OF T_0 AT SEVERAL TEMPERATURES BASED ON THE ANALYSES OF WARNES AND KING [43]. Also shown are the regimes of validity of the Eichelman and Hull [49] and Monkman, Cuff and Grant [50] relationships.

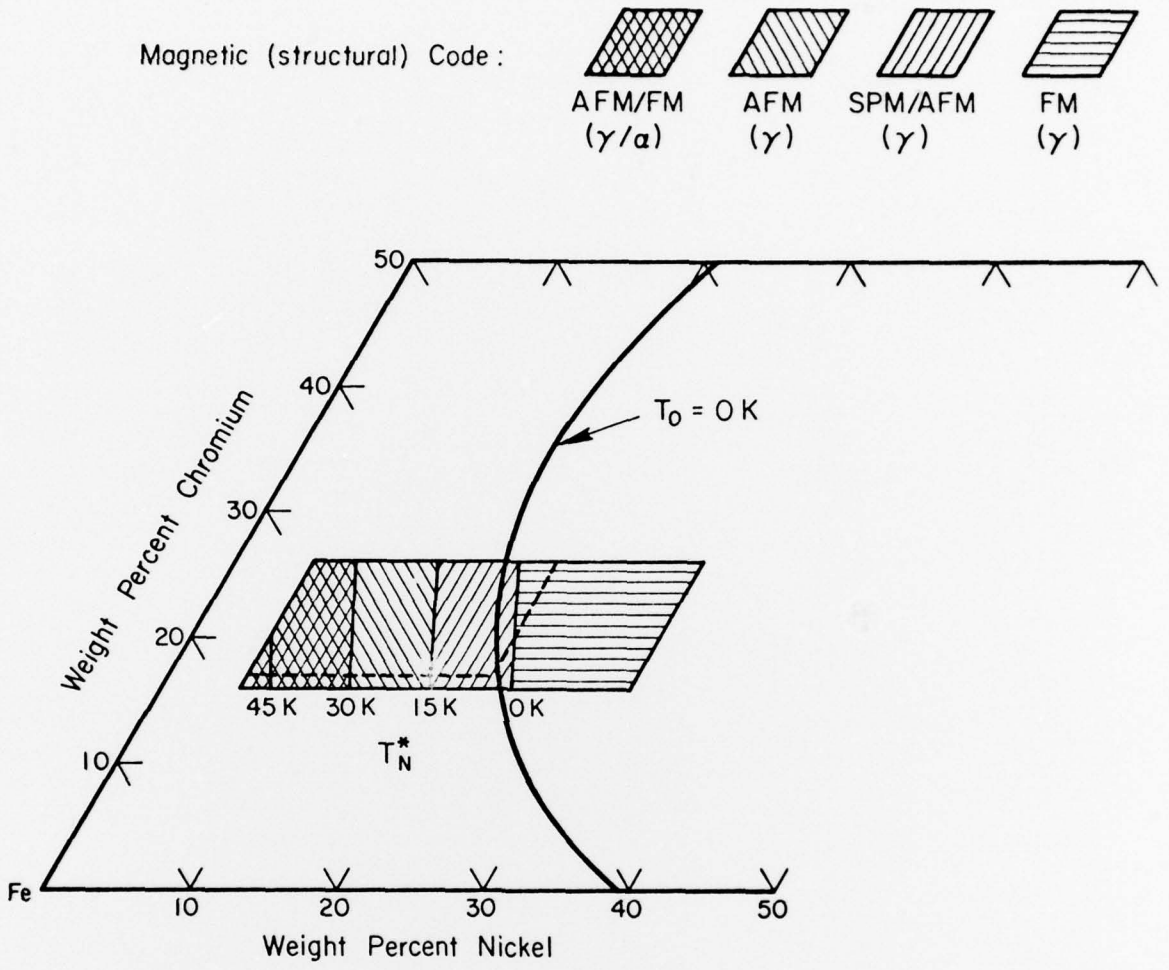

FIGURE 6. PORTION OF A MAGNETIC PHASE DIAGRAM FOR Fe-Cr-Ni ALLOYS.

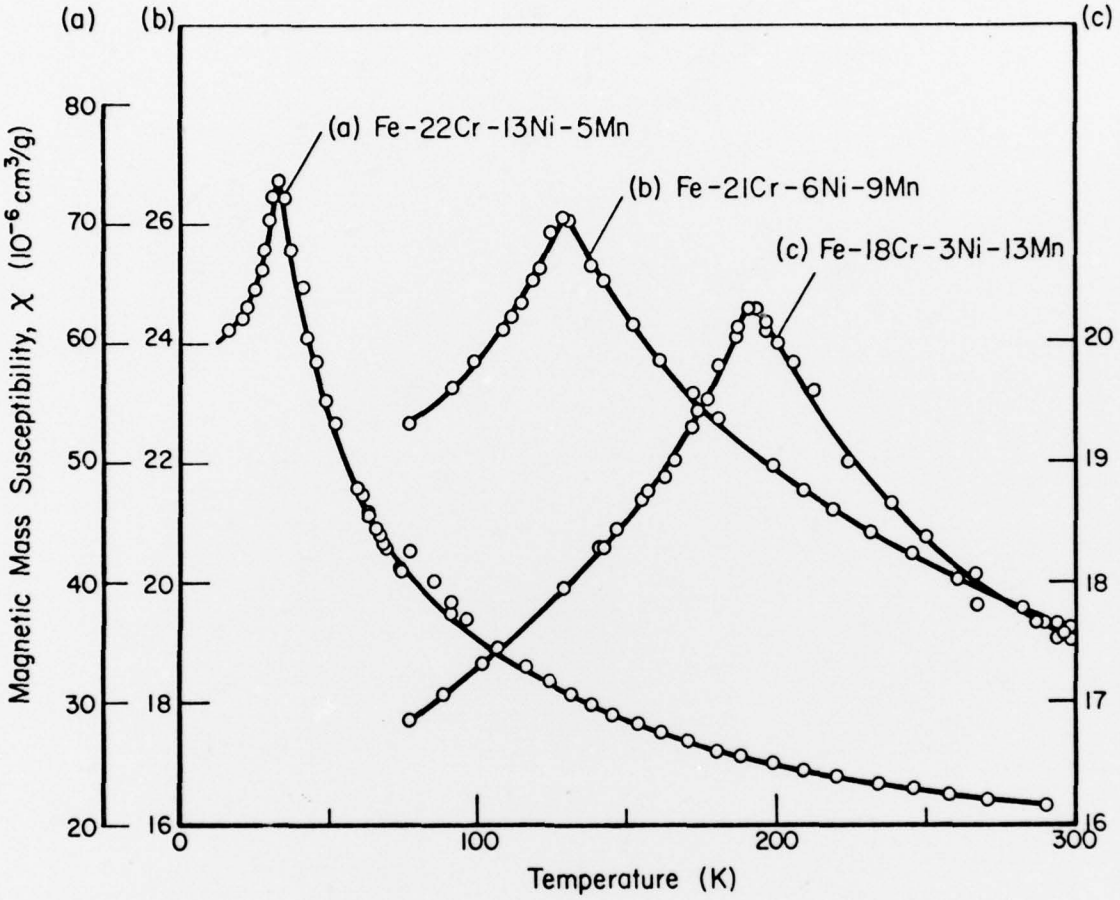

FIGURE 7. MAGNETIC SUSCEPTIBILITY TEMPERATURE DEPENDENCES OF A SERIES OF Fe-Cr-Ni-Mn ALLOYS (KNOWN COMMERCIALLY (a) NITRONIC 50, (b) NITRONIC 40, AND (c) NITRONIC 33, RESPECTIVELY). Apart from the fact that the temperature of a sharp antiferromagnetic-like transition increases as the Mn content increases, and that the magnetic properties are evidently quite different from those of the Mn-free stainless steels (e.g., Figure 4(b)), nothing is known about the magnetic properties or structures of these alloys.